CM chondrite aqueous alteration examined by geochemical modelling and laboratory experiments

Thesis submitted in fulfilment of the requirements for the degree of

PhD in Earth Science

by

Robin L. I. Haller

School of Geographical and Earth Sciences

College of Science and Engineering

October 2025

Revised version September 2026

Abstract

Mighei-like (CM) meteorites are the most abundant group of carbonaceous chondrites and have been aqueously altered on their parent body/bodies to various degrees. As such, their study is key to understanding the evolution of the early Solar System and the delivery of water to Earth. However, the CM chondrites in our collection still sample only a small portion of the asteroids in our Solar System and questions such as under what conditions CM chondrites have been altered or how long did the aqueous alteration require are difficult to answer through meteoritical studies alone. Hence, this thesis was created to complement and expand on knowledge about the aqueous alteration of CM chondrites through geochemical modelling and laboratory experiments. As there is to date relatively little mineralogical information available on unaltered CM chondrites of petrologic type 3 (CM3s), the pristine CO3.00 Dominion Range 08006 was chosen as starting composition and was reacted with an aqueous fluid with additional CO_2, NH_3 and HCl based on cometary abundances and other modelling studies. Equilibrium models with variations in temperature, water/rock (W/R) ratio (by mass), CO_2 concentration and other parameters such as pressure were built to provide an overview of possible alteration conditions in CM chondrites. Based on the results of these models, kinetic models were built to simulate the evolution of aqueous alteration with the trade-off of fewer parameters (fixed CO_2 concentration in the aqueous fluid) and a simplified mineralogy. The models suggest that CM chondrites could form for a wide range of temperature, W/R ratio and CO_2 concentration with more altered CM1 chondrites forming generally at higher temperatures than CM2s. All CM chondrites could have formed in different areas of a single parent after several years of aqueous alteration, although the exact duration depends heavily on the temperature. The laboratory experiments simulated a parent body alteration of DOM 08006 chips for which significant amounts of calcite formed after 30 days with a carbonated fluid but not with pure water, suggesting that the formation of early calcite in CM chondrites likely required the accretion of C-bearing ice, meaning that the CM parent body/bodies likely accreted beyond the CO_2 snowline.

Terrestrially altered CM chondrites usually build little rust due to their low abundance of iron metal; nonetheless, terrestrial weathering can still have a profound impact on the mineralogy and isotopic composition, as shown by previous studies and experiments with pristine samples returned form asteroids Ryugu and Bennu. To evaluate the effect of terrestrial weathering on CM chondrites of different petrologic type, laboratory experiments were conducted with chips of Chwichiya 002 (a C3.00-ung but with similarities to CM chondrites), Murchison, Kolang and LaPaz Icefield 02277 reacting with artificial rainwater under oxidising conditions. The reacted chips, together with complementary kinetic models, suggest that Fe-sulphides, calcite and unknown Na-K chlorides are highly susceptible to terrestrial weathering and can potentially dissolve within less than 30 days. In less altered CM chondrites, metal and amorphous silicates also alter very quickly. Oxidising conditions result mainly in goethite and talc whereas under more reducing conditions, alteration products bear similarities to parent

body alteration. Especially for CM3 chondrites, this style of alteration could decrease their petrologic type and could be the reason for the scarcity of CM3 chondrites in meteorite collections. Better models and broader and more sophisticated laboratory experiments are needed to better study and understand the aqueous alteration of CM chondrites.

Acknowledgment

I would like to sincerely thank my family, whose support was invaluable for the completion of this thesis. Thank you for giving me this opportunity. My supervisor enabled me an insight into academic research and without his guidance, I would have never been able to do this work. I would also like to thank the GES for giving me the opportunity to teach at the school, where I had the privilege to meet and teach many bright students. Throughout my PhD, I had the privilege to attend multiple conferences which would not have been possible without the support of travel grants from the Meteoritical Society, the Lunar and Planetary Institute and the University of Glasgow. A research grant from the Meteoritical Society enabled me also to carry out experiments on meteorites, which helped to shape and improve my PhD project greatly. Finally, I would like to thank my viva convener and examiners for organising my viva and evaluating my thesis; their feedback substantially improved this final thesis version.

Author's declaration

I declare that this dissertation is the result of my own work and has not been submitted for any other degree at the University of Glasgow or any other institution.

Robin Haller

Table of Contents

1. Introduction

1.1 Asteroids and their link to meteorites

Asteroids are the first celestial bodies to form in the solar nebula during the early solar system (Burbine, 2017). Based on their reflectance spectra, they are classified into S-complex (Q, S, Sq, Sr and Sv), C-complex (B, C, Cb, Ch and Cgh), X-complex (X, T, Xc, Xe, Xk and Xn) and D-, L-, K-, A-, Sa- and V-type asteroids (e.g., DeMeo et al., 2022). In the solar system, there are over 1 million asteroids larger than 1 km (DeMeo et al., 2022) although their current position and forms differ from the early solar system (Walsh et al., 2011; Desch et al., 2018; Greenwood et al., 2020) (see Figure 1.1 for the current distribution of asteroids). The evolution and distribution of asteroids in the early solar system has been described by several modelling studies; notably, Walsh et al. (2011) created the "grand tack" model that explains the scattering of asteroids due to the formation and migration of Jupiter and Saturn and Desch et al. (2018) created a hydrodynamical model that shows where asteroids could have been distributed before the "grand tack". Due to processes in the early solar system such as asteroid collisions or gas pressure disruption (Wilson et al., 1999), most current asteroids differ in composition and shape compared to the first asteroid generation (Greenwood et al., 2020). One surviving primary asteroid could be asteroid Ceres, which shows evidence for recent activity of liquid water (e.g., McCord et al., 2022). As such, it has been the target of NASA's Dawn mission (Russel et al., 2011) as well as detailed spectroscopic and modelling studies (e.g., DeSanctis et al., 2016; Zolotov, 2016; Carrozzo et al., 2018; McSween et al., 2018; Travis et al., 2018; DeSanctis et al., 2020; Takir et al., 2023). On the other hand, asteroids Ryugu and Bennu, which have been the target of sample return missions Hayabusa2 (e.g., Tsuda et al., 2019) and OSIRIS-REx (Lauretta et al., 2017), respectively, are labelled as rubble-pile asteroids that have formed from a previous generation of asteroids. Ryugu and Bennu are labelled as C-type and B-type (Tsuda et al., 2019; Lauretta et al., 2017); in other words, based on spectroscopy, the two asteroids were believed to be compositionally different. However, analysis of returned samples (e.g., Nakamura et al., 2022; Lauretta et al., 2024) showed little difference and material from both asteroids was suggested to be similar to the Ivuna-like (CI) meteorites. As a result, whereas spectroscopic observations are useful to broadly classify asteroids, returned samples are needed to understand the origin and evolution of asteroids in more detail.

A different source of material from our solar system are meteorites. With a few exceptions, meteorites are believed to originate from asteroids (Burbine, 2017). Meteorites are classified into different groups, usually based on their mineralogy, isotopic composition or abundance of objects like chondrules and matrix (see e.g., Weisberg et al., 2006 and Figure 1.2). Furthermore, meteorites are classified as "fall" or "find", depending on whether the meteorite fall has been observed or not. The official classification and description of all known meteorites can be found in the Meteoritical Bulletin. The term CC-NC dichotomy was coined based on isotopic differences between carbonaceous chondrites (CCs) and non-

carbonaceous chondrites (NCs); the dichotomy likely reflects differences in heliocentric distance with parent bodies of CCs having accreted in the outer and NCs in the inner solar system (see e.g., Palme and Mezger, 2024). CCs are further divided traditionally into the CI, Mighei-like (CM), Ornans-like (CO), Vigarano-like (CV), Renazzo-like (CR), Karoonda-like (CK) as well as CH and CB meteorite groups (e.g., Weisberg et al., 2006) (see Figure 1.3 for an example of a CM chondrite). With further research, additional groups were suggested such as the Yamato-like (CY) (King et al., 2019), the Loongana-like (CL) (Metzler et al., 2021) or the Asuka-like (CA) meteorites (Kimura et al., 2022), although those groups have yet to be officially recognised by the Meteoritical Bulletin. Each meteorite group likely originated from a different parent body, although some groups like the CMs and COs could have originated from the same parent body (e.g. Zhu et al., 2021). On the other hand, there is also evidence for multiple parent bodies required for one CC group (see e.g., Lee et al., 2019a) and additional complexity arises from clasts of meteorites found in a different meteorite (e.g., CM-like clasts in HED meteorites) (Patzek et al., 2020). In addition to meteorites, other extraterrestrial materials of interest are most notably micrometeorites (e.g., Suttle et al., 2019) or interplanetary dust particles (IDPs) (e.g., Noguchi et al., 2024) that have comets instead of asteroids as possible parent bodies (Noguchi et al., 2024). So far, only few groups and individual meteorites have been linked confidently with an asteroid (Greenwood et al., 2020). Based on spectroscopy, groups of meteorites can be matched with spectral types of asteroids although matches are often not unique (e.g., Jenniskens et al., 2018; De Meo et al., 2022).

1.2 Aqueously altered meteorites

The main focus of the thesis is the study of the aqueous alteration in CM chondrites because CMs are one of the most abundant groups of carbonaceous chondrites (The Meteoritical Bulletin) and span the entire range of aqueous alteration (Zolensky et al., 1997). As such, the focus of this section is to describe a broader picture of aqueous alteration in meteorites (cf. sections 2.1 and 3.1 for more detail on CM chondrites).

Aqueously altered extraterrestrial material is of particular interest to planetary science, as Earth most likely derived its water from collisions with asteroids and comets (Morbidelli et al., 2000). Accreted water ice in asteroids most likely melted through the decay of short-lived radionuclides, most importantly ^{26}Al (Brearley, 2006; Lee et al., 2025). With this heat source, aqueous alteration could have started ~450,000 y after the accretion of the asteroid (Palguta et al., 2010), although the exact timeframe depends on the time of accretion and asteroid size. Modelling studies such as Young et al. (1999), Young (2001) or Palguta et al. (2010) favour an open system with convection of an aqueous fluid to explain the mineralogy and isotopic composition of aqueously altered CCs. On the other hand, the broadly isochemical nature and low permeability of aqueously altered CCs is more compatible with a closed system with no or very little fluid flow (Bland et al., 2009). Information on when aqueous alteration

took place mainly stems from radiometric dating of minerals, such as $^{53}Mn/^{53}Cr$ of carbonates (e.g., Fujiya et al., 2012) and $^{129}I/^{129}Xe$ of magnetite (e.g., Pravdivtseva et al., 2018). Different ages could reflect differences in precipitation sequences or variations between meteorite groups and individual meteorites but could also be caused by differences in analytical methods (see e.g., Visser et al., 2020 for a discussion).

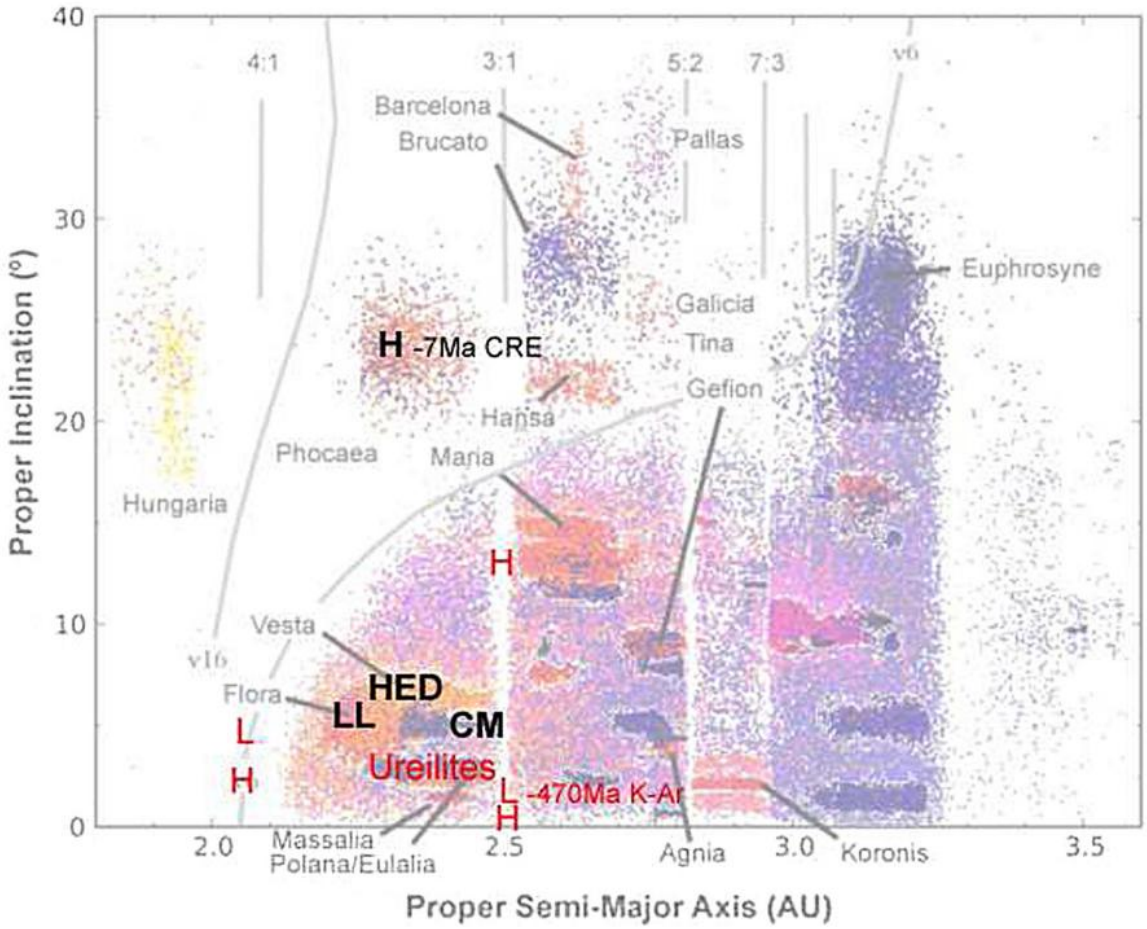

Figure 1.1. Asteroid distribution in the solar system with potential parent bodies labelled (Jenniskens et al., 2018) (image and labels).

Except for amorphous silicates that could have been hydrated in the solar nebula (Marrocchi et al., 2023), aqueous alteration of meteorites has likely taken place on their parent bodies (e.g., Brearley, 2006). Among the meteorite groups, only the CI, CM and CR chondrites display extensive aqueous alteration, although products of limited alteration are also observed among other groups (e.g., CO and CV chondrites). In addition to meteorites, aqueous alteration has also been studied in other extraterrestrial material; e.g., Dobrica et al. (2022) discovered dolomite and ankerite in a micrometeorite. Other meteorite groups, notably CO, CK and CV chondrites experienced metasomatism at high temperatures and low W/R ratios (e.g., Brearley and Krot, 2012; Jiang et al., 2021; Krot et al., 2024. Products of metasomatism have also been observed in the CM2 MET 01075 (Lee et al., 2019b), which raises the question whether aqueous alteration erased metasomatism products in other CM chondrites or if metasomatism required specific conditions that were only met by very few

CM chondrites. Some ungrouped meteorites, notably Flensburg, Sutter's Mill, Tarda and Tagish Lake are also aqueously altered and are of great interest as they could represent aqueous alteration conditions intermediate between CI, CM and CR chondrites or originate from different asteroid types (e.g., Fujiya et al., 2019; Bischoff et al., 2021; Holt and Herd, 2022; Schrader et al., 2024).

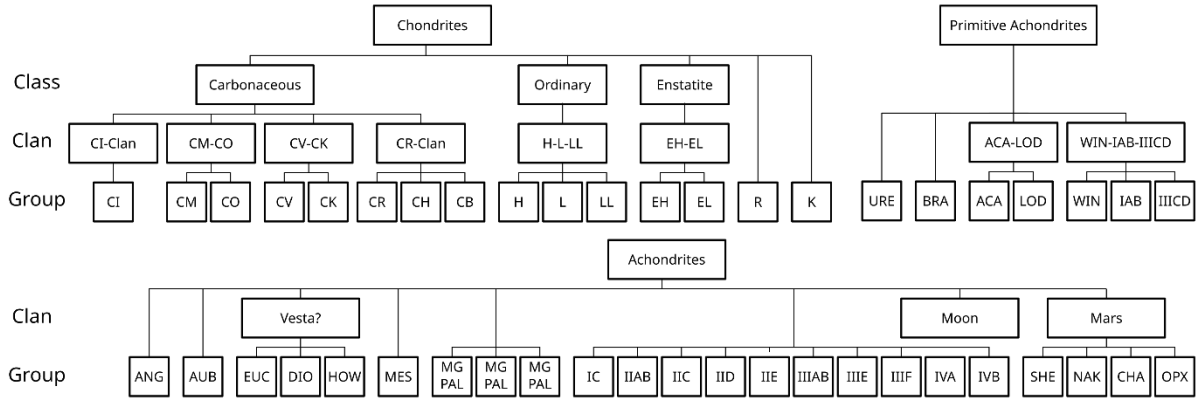

Figure 1.2. Classification of meteorites (after Weisberg et al., 2006).

Figure 1.3. Images of the CM2 Winchcombe (King et al., 2022).

The effect of aqueous alteration on a meteorite has been quantified with a scale from 3 (unaltered) to 1 (completely altered) (Van Schmus and Wood, 1967). A more detailed distinction between differently altered meteorites was made with scales established by Browning et al. (1996), Rubin et al. (2007), Alexander et al. (2013) and Howard et al. (2011, 2015). Other possibilities to determine and classify degrees of alteration involve K abundances and $\delta^{41}K$ (Hu et al., 2024), pentlandite vs. pyrrhotite abundances (Singerling et al., 2024), magnetite abundances (Sridhar et al., 2021) or visible and near-infrared spectroscopy (Takir et al., 2013). The reasons why some meteorites from the same group are more altered than others are likely either elevated temperature, W/R ratio or duration of alteration or a combination of these parameters (see e.g., King et al., 2017). The CM chondrites are a particularly valuable CC group to study differences in aqueous alteration as they span the entire range from petrologic type 3 to 1 (Zolensky et al., 1997; Kimura et al., 2020). CM chondrites are also the most abundant group of CCs with currently 21 falls and 751 finds listed in the Meteoritical Bulletin. Meteorites of petrologic type 3.0 are rare, as most meteorites experienced at least some degrees of aqueous alteration or metamorphism or a combination of both, and are currently only represented by

L/LL, CO, CM and CR chondrites (Kimura et al. 2024). Among these meteorites, the CO3 DOM 08006 and the CM3 Asuka 12169 are of particular interest, as they represent some of the most pristine extraterrestrial material on Earth (Davidson et al., 2019; Kimura et al., 2020; Noguchi et al., 2021; Xu et al., 2022). Some ungrouped meteorites, notably the C2-ung Acfer 094 (Newton et al., 1995; Greshake, 1997; Hopp and Vollmer, 2018; Matsumoto et al., 2019, 2022; Vaccaro et al., 2023) and the C3.00-ung Chwichiya 002 (Ruggiu et al. 2022) are also known to be highly pristine meteorites and valuable to study the effects of incipient aqueous alteration. However, whether meteorites of petrologic type 3 are representative of originally accreted material or rather represent regions of the parent body unaffected by aqueous and thermal alteration is not clear. A further unknown factor is the composition of the aqueous fluid, as fluid inclusions have rarely been found in extraterrestrial material (Zolensky et al., 2017; Tsuchiyama et al., 2021; Nakamura et al., 2022), although some minerals like apatite can also be used to constrain the fluid composition (e.g., Piralla et al., 2021; Dobrică et al., 2022; Che et al., 2023); however, those inferred compositions represent conditions during the precipitation of specific minerals and are likely different from the initial fluid. Geochemical models as well as laboratory experiments are needed to further study the aqueous alteration in meteorites within the context of the evolution of the early solar system, which has been the focus of this thesis.

1.3 Connection of CM chondrites to other celestial bodies and derived meteorites in our solar system

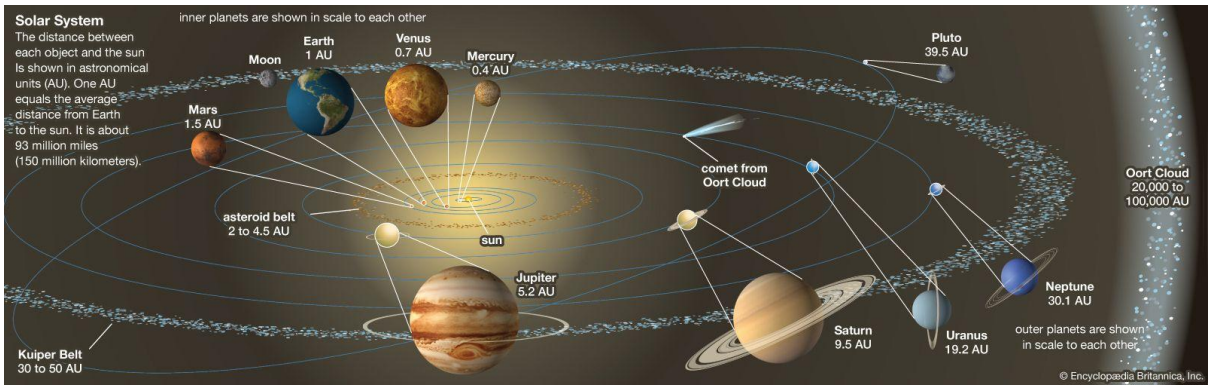

Figure 1.4. Distribution of celestial bodies in our solar system (not to scale) (Britannica).

This chapter aims to briefly provide a more comprehensive overview of our solar system and how its objects are related to the CM chondrites. Starting from the Inner Solar system, the innermost planets Mercury and Venus (cf. Figure 1.4) are chemically differentiated and show little similarity to the chemically primitive CM chondrites (see e.g., Lauretta and McSween, 2006). Earth, while also differentiated, was subjected to a large flux of meteors; some of them were hydrated and potentially similar to CM chondrites, although overall, Earth is isotopically more similar to enstatite chondrites. Mars, while appearing dry, used to have a substantial amount of surface water based on geomorphological features and its oxidised mineralogy. The next two planets, Jupiter and Saturn, consist of mainly hydrogen and helium, whereas the outmost two planets, Uranus and Neptune, have a

silicate-rich core which might have some similarities to CM chondrites. Particularly the outer planets can have dozens of moons, many of which like Saturn's moon Titan are bigger than the largest asteroid, Ceres. The moons in our solar system vary greatly in composition. Some moons, mainly from Jupiter and Saturn, have subsurface liquid oceans in addition to rocky cores and icy mantles. While the largest moons like Ganymede and Callisto are too differentiated to resemble CM chondrites, smaller moons like Neptune's Larissa could be fairly similar to CM chondrites due to the lack of metamorphic heating and differentiation occurring in larger moons.

In addition to the aforementioned asteroids, the solar system is also populated by other small objects which do not orbit a specific planet. Comets are mainly located in the Kuiper Belt and Oort Cloud but some of them were scattered further inwards and could have delivered water to Earth (Mumma and Charnley, 2011). They are a mixture of rocky dust and water ice; the Stardust mission returned dust from comet 81P/Wild 2 and the volatile composition of comets is well known through spectroscopic studies. While comets were traditionally regarded as being distinct from asteroids, the sample return mission and more recent studies revealed that a continuum exists between comets and asteroids (Nuth et al., 2017). The dusty part of comets, similarly to asteroids, is also composed of CAIs, olivine, pyroxene and presolar grains. Some samples returned from 81P/Wild 2 also suggest the presence of limited aqueous alteration through the presence of magnetite and sulphides, although phyllosilicates so far have not been detected. Overall, comets likely accreted at greater heliocentric distances which would explain their differences in stable isotopes and their more volatile composition compared to asteroids. Nonetheless, it is possible that the parent bodies of hydrated carbonaceous chondrites like CMs accreted further away from the Sun so that the accreted ice was a mixture of water ice with other volatiles found in comets, most notably CO_2 ice. This possible accretion of "exotic ices" is explored in the geochemical models of this thesis. The asteroid-comet continuum is further highlighted through the existence of the centaurs, celestial bodies similar in size to asteroids, with orbits between Jupiter and Neptune. Those objects likely originate beyond the orbit of Neptune in the Kuiper Belt and have been scattered inward. The Kuiper Belt is populated the Kuiper Belt objects (KBOs), also called trans-Neptunian objects (TNOs); however, most of its current population has been scattered outwards from its original region due to the outward migration of Neptune (see e.g., Gladman and Volk, 2021). While most KBOs are located within 30 and 50 AU, some KBOs with very elliptic orbits can be found beyond 50 AU. KBOs are mainly composed of volatiles, although similar to comets, they also consist of rocky material which is compositionally similar to chondrites.

1.4 A brief introduction to geochemical modelling with PHREEQC

The geochemical modelling undertaken in this thesis was done with the help of the software PHREEQC (Parkhurst, 1995; Parkhurst and Appelo, 1999, 2013). This section aims to give only a brief overview of the modelling tools used in this thesis; a full description of the software is described in the PHREEQC

v3 user guide (Parkhurst and Appelo, 2013). PHREEQC requires two files to function; an input file which is a script based on keywords describing the model parameters and a geochemical database in which the modelled solid, aqueous and gaseous phases and species are described in more detail. Geochemical databases used by PHREEQC are usually sourced from the US Geological Survey and related institutions and their data are derived mainly from experimental studies. Other databases have been created by carefully merging thermodynamic data (mainly mineralogical) from different databases (e.g., *core10.dat* from Neveu et al., 2017) or by using thermodynamic software like SUPCRTBL (Zhang et al., 2020). A database contains information about solute species (e.g., Mg^{2+}, $MgHCO_3^+$), solid phases for equilibrium calculations (e.g., albite), gases (e.g., H_2) and sometimes also rate expressions of a smaller number of phases for kinetic calculations (e.g., pyrite). PHREEQC utilises the law of mass action to calculate saturation indices of minerals and calculates solute activities mainly through ion-association (i.e., the Debye-Hückel equation), although other options exist for more saline solutions.

In the input file for equilibrium modelling (section 2), the first line is specifying the database used for the calculation. The next line usually specifies the composition of the aqueous solution, as the primary goal of PHREEQC is the simulation of chemical reactions in aqueous solutions (Parkhurst and Appelo, 2013). For this thesis, the amount (mass) of water varied to represent different water/rock ratios and additional elements (C, N, S and Cl) were added to the solution to simulate the accretion of cometary ices on the CM parent body. The temperature and pressure of the system was also changed through the solution keyword. By default, PHREEQC only calculates the saturation index of solid phases so a list of potential precipitates needs to be specified in the input file to quantify any precipitation. The same keyword also specifies the solid input composition, i.e., mineralogy, of the carbonaceous chondrite. The amount of each mineral (in moles) was calculated from mineralogies in the literature to represent a total of 1 kg of rock. A separate gas phase was allowed to form for most simulations (cf. section 2) and was specified with a separate keyword. Running a PHREEQC input file generates a customisable output file; notably, it quantifies precipitated minerals (or remaining primary minerals) as well as the fluid chemistry (total dissolved elements, molality of aqueous species as well as quantification of gases and pH and pe of the system). Postprocessing of the output involved the transformation of absolute mineral quantities (mol) to volume percentages to allow for comparisons with meteorite mineralogies in the literature.

Based on the results of the equilibrium models, the kinetic models quantify the temporal evolution of the modelled mineralogy and fluid composition. An additional keyword is needed in the input file to specify the solid phases affected by kinetic dissolution (described by the rate expression in the database). In addition, the number and duration of timesteps needs to be specified so that at each timestep, PHREEQC generates a snapshot of the modelled water-rock interaction. The sequence of all modelled timesteps for a specific combination of temperature and W/R ratio can then be assembled to

temporally describe the aqueous alteration of a CM chondrite on its parent body (cf. section 3) or in a terrestrial environment (cf. section 4).

1.5 Thesis aims and objectives

This thesis is structured in three main chapters, written as publications for *Geochimica et Cosmochimica Acta* and *Meteoritics & Planetary Science* (cf. sections 2.1, 3.1 and 4.1 for their aims). The overall aim of this thesis is to improve the understanding of aqueous alteration of CM chondrites in past (parent body settings) and present (terrestrial environment) times. The bulk of the work involves geochemical models in PHREEQC (Parkhurst, 1995; Parkhurst and Appelo, 1999, 2013) in which the interaction of a chondritic rock with an aqueous fluid was modelled in equilibrium (cf. section 2) or considering kinetics (cf. section 3 and 4). Modelling of aqueous alteration of meteorites with PHREEQC has been done previously (e.g., Neveu et al., 2017); however, the models in this thesis aim to provide new constraints on the conditions and timeframes of alteration of CM chondrites. Complementary to the models, laboratory experiments to simulate aqueous alteration on a parent body (cf. section 3) or terrestrial weathering (cf. section 4) were carried out using chondritic meteorite chips (cf. sections 3.2 and 4.2). Overall, the thesis aimed to provide answers to the following questions:

1. Under which conditions (temperature, W/R ratio, CO_2 concentration) have CM chondrites been altered on their parent body/bodies? (section 2)
2. What factors cause differences in petrologic type across CM chondrites? (sections 2 and 3)
3. How quickly did aqueous alteration take place on the CM chondrite parent body/bodies? (section 3)
4. Have minerals in CM chondrites formed over time from a single fluid? Or did some minerals require a secondary fluid or different parent body to form? (section 3)
5. How quickly do terrestrial weathering products form in CM chondrites? Is there any difference between CMs of different petrologic type? (section 4)
6. Could the petrologic type of some CM chondrites have been influenced by terrestrial weathering? (section 4)

2 Controls on the petrologic type of CM carbonaceous chondrites evaluated by geochemical equilibrium modelling

Robin L. Haller*, Martin R. Lee

School of Geographical and Earth Sciences, University of Glasgow, Glasgow G12 8QQ, UK

*Corresponding author: *E-mail address:* robin.haller123@gmail.com

This chapter represents a revised manuscript submitted to *Geochimica et Cosmochimica Acta* with minor adaptions and differs from the published paper (https://doi.org/10.1016/j.gca.2025.10.034)

2.0 Abstract

The most abundant group of carbonaceous chondrites are the Mighei-like (CM) meteorites, and they span petrologic types ranging from almost unaltered (CM3) to heavily aqueously processed (CM1). The factors that controlled the extent of aqueous alteration that CM chondrites experienced on their parent body/bodies are debated and remain poorly constrained. Geochemical models, and equilibrium models in particular, are powerful tools for emulating water-rock (W/R) interactions as a function of different parameters and conditions. In order to investigate possible CM chondrite alteration conditions and evaluate controlling factor(s) on petrologic type we modelled the interaction of a CM3 proxy, the CO3.0 chondrite Dominion Range 08006, with a fluid under different temperatures (1–150°C), W/R ratios (by mass) (0.2–5) and solute concentrations (0.2–2 mol/kg CO_2, 0.02–0.2 m NH_3, 0.01–0.1 m H_2S and 0.001–0.01 m HCl). Five additional scenarios that use the same parameter space but with differences in properties including pressure and redox conditions were also created to further investigate the controls on petrologic type. Systems that are CM chondrite-like from their close similarity to the mineralogy of CM meteorites as determined by sample analysis can form under a wide range of temperatures (1–140°C), W/R ratios (by mass) (0.3 – 5), solute concentrations (0.2 – 2 m CO_2), pH (8.5 – 12.6) and pe (-10.8 – -6.6). Across the different scenarios CM2-like systems are most abundant followed by CM1-like, whereas CM1/2-like systems are rare. Differences in petrologic type can be mainly attributed to variations in temperature, with CM1s overall being formed by alteration at higher temperatures (80–140°C) than CM2s (1–105°C). CM1/2 chondrites might be produced by elevated W/R ratios (by mass) and/or solute concentrations. From a mineralogical perspective, CM chondrites of different petrologic type might have originated from contrasting regions of a singular, thermally stratified parent body. Some differences between model results and CM chondrite samples could be addressed by more sophisticated tools like kinetic modelling.

Keywords: CM chondrites, equilibrium modelling, CM parent body, CM petrologic type, aqueous alteration

2.1 Introduction

Infrared spectra of C-complex asteroids (B- C-, Cb, Cg, Ch- and Cgh-type) reveal adsorption features typically associated with aqueous alteration (e.g., DeMeo et al., 2022). Whereas hydration is commonly observed at their surfaces, the only asteroid-derived meteorites that contain notable abundances of water are some groups of carbonaceous chondrites and related ungrouped meteorites. Among the hydrated carbonaceous chondrites, the Mighei-like (CM) group is of particular interest due to its high abundance comprising ~770 meteorite records (including 21 falls) out of 3085 carbonaceous chondrites in total (The Meteoritical Bulletin, April 30, 2025). The CMs also display different degrees of aqueous processing, ranging from the nearly unaltered (Asuka 12169, Kimura et al., 2020) to almost completely hydrated (e.g., Scott Glacier 06043, Howard et al., 2011). The nature and extent of aqueous alteration of CM chondrites has been examined in detail by numerous studies (e.g., McSween, 1979; Browning et al., 1996; Rubin et al., 2007; Alexander et al. 2013; Lentfort et al., 2021). While most CM chondrites are broadly classified as petrologic type 2 (Van Schmus and Wood, 1967), the group can be more finely divided into 'subtypes' using properties including the abundance and chemical composition of secondary minerals and the preservation of chondrule silicates (Rubin et al., 2007). Other proxies of the degree of alteration include the progressive replacement of anhydrous silicates by phyllosilicates as determined by bulk X-ray diffraction (XRD) (Howard et al., 2015) and the water/OH content of bulk samples (Alexander et al. 2013). The mineralogy of CMs of petrologic type 2 (CM2) as described by XRD is characterised by a mixture, roughly in order of decreasing abundance, of: phyllosilicates (predominantly serpentine), anhydrous silicates (olivine and pyroxene), tochilinite-cronstedtite intergrowths (TCIs), Fe-Ni sulphides, Fe-oxides (mainly magnetite) and carbonates (mainly calcite) (Howard et al., 2015). Also present, but usually not identified by XRD is organic matter (insoluble and soluble) and Ca- and Al-rich minerals in calcium-aluminium inclusions (CAIs) and amoeboid olivine aggregates (AOAs), such as spinel, perovskite and hibonite (Rubin and Ma, 2021). Fe,Ni metal (kamacite and taenite) is rarely found in mildly altered CMs like Murchison (e.g., Howard et al., 2011), whereas only the least altered CMs contain amorphous silicates that are likely the precursors of phyllosilicates (Leroux et al., 2015; Kimura et al., 2020). In contrast, the CM1s have only minor quantities of anhydrous silicates remaining, little to no TCI, and typically contain phyllosilicates, magnetite, sulphides and dolomite (King et al., 2017).

Parameters that are believed to be the most important controls of the extent of aqueous alteration of CM chondrites are temperature, water-rock (W/R) ratio (by mass), duration of alteration, and composition of the fluid (chemical composition, pH, Eh) (Zolensky et al., 1993; Brearley, 2006; Marrocchi et al., 2018; Suttle et al., 2021). Higher temperatures would have characterised parent bodies that were larger and that accreted early so that ^{26}Al was more abundant, and would have also been generated during more advanced stages of alteration (i.e., a higher fraction of anhydrous silicates reacting exothermally to phyllosilicates) (Grimm and McSween, 1989). In such environments the rates of dissolution and

precipitation of minerals would have been greatly accelerated yielding CM chondrites of lower petrologic type for a given duration of alteration. The extent of aqueous alteration would have been restricted by limiting the W/R ratio (by mass), thus preventing the complete reaction of anhydrous silicates to phyllosilicates. Other carbonaceous chondrite groups (COs and CVs) show evidence of incipient aqueous alteration reflecting very low W/R ratios (by mass) (Brearley, 2006) whereas higher W/R ratios (by mass) are inferred for CM chondrites (Zolensky et al., 1993; Marrocchi et al., 2018; Suttle et al., 2021). Potentially of significance to the extent of alteration might also be different timescales (e.g., King et al., 2017), one cause of which could be loss of the fluid phase due to overpressure of gas formed during aqueous alteration causing fracturing and maybe also catastrophic disruption of the parent body (Wilson et al., 1999). Finally, alteration by fluids of different composition might be responsible in contrasts in mineralogy and extent of alteration observed across CM chondrite samples. For instance, CO_2 ice might have accreted heterogeneously on the parent body/bodies, leading to differences in pH and aqueous carbon concentrations. Experimental studies of mineral dissolution (Palandri and Kharaka, 2004) have demonstrated that most minerals dissolve faster in acidic fluids, and elevated dissolved inorganic carbon concentrations could trigger the precipitation of more carbonates.

Carbonates, while only being a volumetrically minor phase, are particularly useful for studying the conditions of aqueous alteration in CM chondrites in terms of fluid composition, microenvironments of dissolution-precipitation reactions, temperatures of alteration, and chronology of W/R interaction using the $^{53}Mn/^{53}Cr$ system. Fluid composition, particularly the aqueous Mg/Ca ratio, can be inferred from the composition of the carbonate: almost pure calcite suggests a Ca-rich fluid poor in trace elements whereas the occurrence of aragonite in less altered CM chondrites points to a higher aqueous Mg/Ca ratio (Riciputi et al., 1994; Lee et al., 2014). Carbon and oxygen stable isotopes provide further information on the nature and extent of interaction of water with the host rock (Alexander et al., 2015; Vacher et al., 2017; Vacher et al., 2018). Oxygen isotopes can also be used to determine temperatures of carbonate precipitation via several methods including clumped isotope thermometry (Guo and Eiler, 2007; Clog et al., 2024), with the caveat that the values obtained provide only a snapshot of the thermal history of the parent body during aqueous alteration. Multiple generations of calcite have been reported in CM chondrites based on petrographic and isotopic evidence indicating that carbonates could be both among the first and the last secondary phases that form by aqueous alteration of CM chondrites (e.g., Tyra et al., 2012; Lee et al. 2014; Tyra et al., 2016). Finally, traces of Mn that commonly occur in carbonates allows the application of radiometric $^{53}Mn/^{53}Cr$ dating. The low abundance and small sizes of carbonates in CM chondrites, as well as the lack of suitable matrix-matched standards, poses a challenge to radiometric dating. Carbonates examined by Fujiya et al. (2012) in four different CM chondrites suggest rather late precipitation (4,563.4+0.4/-0.5 million years ago, relative to the LEW 06100 angrite (Lugmair and Shukolyukov, 1998) with no difference (within error) across calcite and dolomite. Whether different generations (types) of calcite are also similar in age remains to be seen. In

summary, the aforementioned applications of carbonates highlights their importance to deconvolute the alteration conditions and histories of CM chondrites.

In addition to sample analysis, environments of aqueous alteration of CM chondrites can be explored by modelling. Thermal models (e.g., Young et al., 1999; Palguta et al., 2010) have examined aqueous alteration on the CM chondrite parent body in an open system regarding water flow, supported by oxygen isotopic evidence (Young et al., 1999). However, the transport of fluid-mobile elements in CM chondrites seems to be limited to spatial scales of no more than a few 100 µm due to the high abundance of very fine-grained matrix material, creating environments of low permeability (Bland et al., 2009). Whether aqueous alteration occurred in a closed or open system regarding water flow is still unresolved, although recent studies of new CM chondrite falls (e.g. Winchcombe (King et al., 2022)) show differences in degree of alteration in close spatial proximity, further supporting a closed system. A closed system with little to no fluid flow can be represented by an equilibrium model that calculates the abundance of solid phases and aqueous species based on the law of mass action or a minimisation of the Gibbs free energy (see Leal et al. (2017) for an overview). Previous equilibrium models (e.g., Zolensky et al., 1989; Rosenberg et al., 2001) focused on constraining the formation conditions of CM chondrites (mainly from variations in temperature, W/R ratio (by mass) or fluid composition). Although these studies in combination with the aforementioned analytical work help to understand the overall alteration conditions of CM group, the causes for differences in the extent of alteration between CM lithologies of different petrologic type are still debated. Furthermore, most CM chondrite aqueous alteration models so far have either used an initial mineralogy based on anhydrous minerals in Murchison (e.g., Zolensky et al., 1989; Rosenberg et al., 2001; Neveu et al., 2017) or started with an elemental instead of mineralogical input (e.g., Schulte and Shock, 2004; Shibuya et al., 2024) due to the lack of suitable CM3s or CM3 proxies. For water-bearing meteorites like CI chondrites, an anhydrous starting composition can be achieved by subtracting H and O from the elemental composition (see e.g., Zolotov et al., 2012). An additional limitation of previous models arises from the restricted number of phases in thermodynamical databases that are needed for equilibrium models, especially for minerals that are more common in meteoritical rather than terrestrial environments like cronstedtite and tochilinite. A more recent study from (Neveu et al., 2017) that examined the distribution of antifreezes and radionuclides through chondritic W/R interaction considered a more sophisticated thermodynamic database and examined an extensive range of different parameters (temperature, pressure, oxygen fugacity and W/R ratio (by mass)); however, to our knowledge, no study has to date attempted to examine the reasons for differences in petrologic type of CM chondrites with equilibrium models. In addition to CM chondrites, equilibrium modelling has been more commonly used for CI chondrites, related asteroids like Bennu or icy worlds (e.g., Zolotov and Shock, 2004; Zolotov, 2007, 2009, 2012, 2014, 2017, 2020; Castillo-Rogez et al., 2018; Nakamura et al., 2022).

Here we aim to use a series of equilibrium models in PHREEQC (Parkhurst, 1995; Parkhurst and Appelo, 1999, 2013) to explain the aqueous alteration conditions of CM chondrites, and possible reasons for differences in their extent of hydration by simulating the interaction of an unaltered carbonaceous chondrite (CM3 proxy) with an aqueous fluid. The examined parameters are temperature, W/R ratio (by mass) and concentration of solutes in the fluid (CO_2, NH_3, H_2S and HCl). We further expand the range of different aqueous alteration conditions by examining additional scenarios that explore differences in: gas formation conditions, ratios of aqueous CO_2/NH_3, pressure, and initial mineralogy. Based on the initial compositions of solid material and aqueous phase of the modelled systems, we infer possible alteration conditions of CM chondrites and examine the influence of the modelled parameters and scenarios on the extent of alteration observed in different CM chondrites. We then discuss the structure of a possible CM chondrite parent body as constrained by the conditions of alteration or whether multiple parent bodies are required to account for the diversity of CM chondrites.

2.2 Methods

Chemical equilibria were calculated that simulate the interaction of accreted rock ("CM chondrite precursor") with a parent body fluid. Meteorites of petrologic type 3.0 show very little or no evidence of aqueous and/or thermal alteration. Among the currently known meteorites only one CM chondrite, Asuka 12169 (Kimura et al., 2020), is classified as a CM 3.0, although little information is available regarding its composition and especially its modal mineralogy. In contrast, the CO chondrite Dominion Range (DOM) 08006 has been examined in several publications (Davidson et al., 2019; Patzer et al., 2021) and is arguably the most pristine CO chondrite, being assigned a petrologic subtype 3.00 by (Alexander et al., 2018), although DOM 08006 also has magnetite rims around metal grains, indicating some aqueous alteration. Astrophysical models (Desch et al., 2018) show that CO and CM chondrites likely accreted on parent bodies in close proximity, and from similar properties like CAI abundance, chondrule composition, and chondrule size (e.g. Greenwood et al., 2023; Floyd et al., 2024). CO chondrites might even represent CM chondrites that have largely escaped aqueous alteration on their parent body. Regardless of whether or not CO chondrites are indeed unaltered precursors of CM chondrites, they are deemed to be a suitable proxy from a modelling perspective and regarding their mineralogy and chemical composition.

The equilibrium models were built in the geochemical software PHREEQC (Parkhurst, 1995) in a closed aqueous Al, C, Ca, Co, Cl, Cr, Fe, H, K, Mg, Mn, N, Na, O, P, S, Si system (no gain or loss of gas or water) at a pressure of 10 bar.. In PHREEQC, the starting material was entered as phases in moles and as a first step we converted the modal mineralogy of DOM 08006 determined by (Alexander et al., 2018) into moles. However, modal mineralogies by XRD generally only include mineral phases with an abundance of >1 vol.%. Therefore, we attempted to also match the chemical composition of DOM 08006 as determined by (Patzer et al., 2021), by including more minerals (mostly phases present in

CAIs like melilite) and slightly adjusting the abundance of some minerals like olivine. For example, the abundance of forsterite was lowered from 45 to 38.2 vol.% and the abundance of fayalite increased from 6 to 11 vol.%. Some amorphous silicates were modelled as $Fe(OH)_2$, as Marrocchi et al. (2023) found strong evidence for hydration of amorphous silica in the molecular cloud prior to the onset of aqueous alteration on the parent body. As an Antarctic find, DOM 08006 has been affected by terrestrial weathering and has been assigned a weathering grade A/B (Meteoritical Bulletin). To what extent weathering affects modal mineralogies is poorly understood; however, Alexander et al. (2018) notably detected magnetite and chrysotile in DOM 08006 by XRD. Those minerals, especially chrysotile, are likely the product of terrestrial weathering and so they were replaced by metallic iron, Fe-sulphides and olivine in the input file (see Table S2.1).

The input mineralogy did not include any carbon- or chloride-bearing phases; instead, those elements were introduced as CO_2 and HCl in the solution block of the input file (CO was omitted, as CO ice condensates at much lower temperatures (e.g., Sandford and Allamandola,1988) than CO_2 ice (e.g., Kasting, 1991)).CM chondrites typically contain carbon in the form of carbonates and organic matter (e.g., Schmitt-Kopplin et al., 2010; Alexander et al., 2015; Suttle et al., 2021). Organic matter in meteorites is present as a complex mixture of insoluble and soluble phases (Schmitt-Kopplin et al., 2010), many of which are fairly inert; hence, as a simplification, we did not attempt to include organic matter in our models and all C is sourced by melting of CO_2 ice. Other volatile compounds, primarily NH_3 and H_2S (Kurokawa et al., 2021) and also HCl condense at temperatures only slightly lower than H_2O (Sandford and Allamandola, 1993; Zolotov and Mironenko, 2007; Fedoseev et al., 2015) and it is therefore possible that the CM chondrite parent body accreted a mixture of different ices, potentially similar to comets (Mumma and Charnley, 2011). In order to test the influence on the models of accretion of different volatile ices, CO_2, NH_3, H_2S and HCl were included in the input in different concentrations to simulate a dilute cometary fluid. The proportions (based on hydration and hydroxylation) were kept constant and roughly represent their abundance in cometary volatiles (Mumma and Charnley, 2011). In addition to solute concentration, other parameters of interest are temperature and W/R ratio (by mass).A range of 1 to 150°C is included in the models to account for most previous estimates by clumped isotope geothermometers (Guo and Eiler, 2007; Clog et al., 2024) and geochemical models (e.g., Rosenberg et al., 2001) and to address uncertainty about at which point (or points) in the thermal history of the CM parent body that aqueous alteration took place. Higher W/R ratios (by mass or volume) have also been proposed to produce more altered CM chondrites (e.g., Verdier-Paoletti et al., 2017). The water content of CM chondrites can be translated to a bulk W/R ratio (by mass) of around 0.2 on the parent body (Howard et al., 2015). However, the low permeability of CM chondrites would likely result in environments of heterogeneous amounts of water and the amount of water available to react with the CM chondrite precursor might also have changed over time. The potential for higher W/R ratios (by

mass) has been included in the models with a range of 0.2 to 5 (see Table 2.1 for an overview of the input parameters).

In PHREEQC, the input file, which mainly contains information about the composition of the initial fluid and rock, has to be combined with a database that stores the geochemical data needed to calculate output, e.g. the fluid composition and saturation indices of minerals (see e.g., Leal et al. (2017) for a discussion). Many databases exist and are compatible with PHREEQC although their usage is limited by their applicable range of temperature and pressure and/or number of phases. Recently, (Zhang et al., 2020) generated customed databases with the software SUPPHREEQC that are applicable over a broad range of temperature and pressure. Among those, we chose the database *diagenesis.dat* that follows the framework of the *phreeqc.dat* database (inclusion of molar volumes for pressure correction up to ~1000 bar (see (Appelo, 2015)), Davies equation for activity coefficients for aqueous species and Peng-Robinson fugacity coefficients but includes a much larger number of species. Another database, *core10.dat* (Neveu et al., 2017), contains additional phases of interest like saponite, and we created a modified version of *diagenesis.dat* (it can be accessed at doi:10.17632/vf9n9f2z9z.1) that includes additional phases (mostly sulphides and phyllosilicates) from *core10.dat*. The output of the models in the form of the modal abundance of minerals (calculated from the number of moles of equilibrium phases), pH, pe, fluid composition (activity and concentration of solutes) and gases is presented in section 2.3.

Table 2.1
Range of parameters examined in the default scenario.

Parameter (units)	Minimum	Maximum
Temperature (°C)	1	150
W/R ratio (by mass)	0.2	5
Solute concentration (mol/kg water)	0.2 CO_2, 0.02 NH_3, 0.01 H_2S, 0.001 HCl	5 CO_2, 0.5 NH_3, 0.25 H_2S, 0.025 HCl

The aforementioned models examine only a small subset of possible environments for aqueous alteration. An overview of deviations from these standard models (or "default scenario") is described in Table 2.2. It is possible that the strength of the CM parent body was sufficiently high to prevent the escape of gas; this possibility is addressed by deleting the gas phase block in the input file. Castillo-Rogez et al. (2018) modelled varying abundances of accreted CO_2 and NH_3 to interact with a dry CI chondrite and average CM chondrite, and showed that elevated concentrations of NH_3 could stabilise the alkaline conditions needed for the precipitation of carbonates and serpentine over saponite. To account for possible accretion of more NH_3- relative to CO_2-ice, we created a third scenario in which the concentration of those compounds in solution is reversed. Thermal and hydrodynamical models generally simulate the CM chondrite parent body as a rather small planetesimal (<50 km radius) (e.g., Travis and Schubert, 2005; Palguta et al., 2010), which corresponds to a maximum lithostatic pressure of around 50 bar in their core. Preliminary models showed little effect of pressure variations below 50

bar; in contrast, Neveu et al. (2017) demonstrated that an increase from 1 to 200 bar can result in substantial changes in the equilibrium mineralogy; see also Zolotov et al. (2006) and Zolotov (2012) for a discussion on the effect of pressure in chondritic systems. Hence, in a fourth scenario, we explored the possibility of aqueous alteration in the core of a parent body of ~100 km radius, which produces ~200 bar lithostatic pressure. The fifth and last scenario examines the effect of a different starting mineralogy. The elemental abundance of the CM3.0 Asuka 12169 has recently been determined (Patzer et al., 2023) and in this scenario, we adapted the starting mineralogy in order to fit the elemental composition of Asuka 12169. Instead of examining an alternative environment of alteration, this last scenario aims to justify the choice of the CO3.0 DOM 08006 as a suitable starting material for CM chondrites.

Table 2.2
Overview of modelled alternative scenarios.

Scenario	Difference to scenario 1
Scenario 1: default scenario with separate gas phase	-
Scenario 2: no formation of gas phase	No equilibrium gas phase
Scenario 3: accretion of more NH_3 ice	Reversed concentrations of CO_2 and NH_3
Scenario 4: alteration in centre of a large parent body	200 bar instead of 10 bar pressure
Scenario 5: Asuka 12169 as starting material	Mineralogy adjusted to elemental composition of Asuka 12169

2.2.1 Model validation

The database used for this study, *diagenesis_equi.dat*, was validated by running the PHREEQC input file in Neveu et al. (2017, Supplementary data 9) which was used by Neveu et al. (2017) to model the interaction of a CM-like starting composition with a cometary fluid. The input file was run with both the original database *core10.dat* and the newly created database for four different temperatures (1, 50, 100 and 150°) at a W/R ratio (by mass) of 1 and pressure of 1 bar. Running the input file with the newly created database required some adjustments to the starting composition, as organics like kerogen and trace elements like Eu or Cu were not considered in *diagenesis_equi.dat*. Table 2.3 lists a selection of the results from both databases, focusing on solid phases, aqueous solutes and gases of importance to this study. Whereas a good fit exists between phases like Mg-serpentine or polydymite, major differences between aqueous HCO_3^- or also aqueous HS^- could be caused by the lack of organics in *diagenesis_equi.dat*. Despite those discrepancies, we believe that the new database is of sufficient quality to be used for this study.

2.3 Results

2.3.1 Default scenario: overview of results

The chosen parameterisation of temperature, W/R ratio (by mass) and solute concentration resulted in a total of 3720 systems (including 620 systems that simulate aqueous alteration with pure water for reference). A total of 44 different solid phases occur under the modelled conditions, spanning a range

of mainly different phyllosilicates and carbonates, oxides like magnetite and sulphides (Fe- and Ni-bearing). A list of all minerals forming in the modelled systems is in Table 2.4. Calcite is a diagnostic mineral in CM chondrites (see section 2.1) and systems containing calcite could therefore be indicative of equivalent alteration conditions to the CM chondrite parent body, provided also that the abundance of other minerals like phyllosilicates can be matched with samples of CM chondrites. Calcite occurs in 510 different systems as a minor phase with an abundance of up to 1.9 vol.%. It occurs for the entire range of modelled solute concentrations (0.2–2 mol/kg CO_2) and temperature (1–150°C).

Table 2.3
Validation of created database *diagenesis_equi.dat* (d) by comparing it with *core10.dat* (c) (Neveu et al., 2017) across four different temperatures. Selected result from running the PHREEQC input file from Neveu et al. (2017), supplementary data 9. Solid phases and gases are in mol, solute concentrations are in mol/kg.

Temperature (°C)	1	50	100	150
Mg-serpentine (c)	1.60E+00	9.99E-02	6.98E-02	2.10E-02
Mg-serpentine (d)	1.71E-01	1.71E-01	1.71E-01	1.71E-01
Polydymite (c)	6.67E-02	6.67E-02	6.67E-02	6.67E-02
Polydymite (d)	6.67E-02	6.67E-02	6.67E-02	6.67E-02
pH (c)	9.49	7.70	6.21	5.19
pH (d)	9.81	8.34	7.24	6.40
pe (c)	-7.52	-5.70	-4.18	-3.09
pe (d)	-10.00	-7.96	-6.40	-5.10
HCO_3^- (c)	1.81E-06	1.56E-05	3.47E-05	7.95E-05
HCO_3^- (d)	2.13E-23	8.24E-18	1.11E-13	4.49E-10
HS^- (c)	6.48E-08	3.19E-07	6.04E-07	9.34E-07
HS^- (d)	4.05E-02	3.78E-02	2.06E-02	2.77E-03
H2(g) (c)	9.37E-06	1.24E-04	9.59E-04	5.92E-03
H2,g (d)	1.73E-01	1.74E-01	1.74E-01	1.74E-01
H2O(g) (c)	1.81E-03	3.81E-02	3.69E-01	3.07E+00
H2O,g (d)	2.10E-03	3.83E-02	3.47E-01	2.76E+00

Whereas calcite can exist at all modelled temperatures, dolomite only starts precipitating at 105°C or higher; at temperatures below that, the carbonate is ankerite. Dolomite is present in 424 systems and can reach higher abundances than calcite (up to 3.5%); it can exist at a W/R ratio range (by mass) of 0.2–2 (mainly 0.5–2). Calcite can coexist with dolomite and ankerite but does so for only a very limited range of W/R ratios (by mass) whose values depend on the solute concentration. A total of 43 calcite-dolomite systems are predicted, requiring combinations of either high W/R ratios (by mass) and low solute concentrations (e.g., 5 and 0.2 M) or vice versa (e.g., 0.6 and 2 M). Temperatures for those systems are restricted to the minimum formation temperature of dolomite or higher (>105°C). More common are systems with both calcite and ankerite; those require, compared to calcite-dolomite systems, similar combinations of W/R ratios (by mass) and fluid compositions but exist over a larger temperature range (usually 1–105°C). Other carbonates that are predicted to form are magnesite, siderite and rhodochrosite. Magnesite and siderite can reach very high abundances but require combinations of both moderate to high W/R ratios (by mass) and solute concentrations, and rarely coexist with calcite. Rhodochrosite, on the other hand, is fairly common (found in 1738 systems) but usually of low abundance (~0.2%). It can coexist with all other carbonates; sometimes, it forms together with calcite

(311 cases) and almost always accompanies dolomite (422 cases). Rhodochrosite requires slightly higher W/R ratios (by mass) to form, compared to calcite, especially at 40°C or higher.

An additional mineral group of interest in CM chondrites are Fe,Ni sulphides. In the modelled systems, they mostly appear as troilite, pyrrhotite, heazlewoodite or polydymite. The Fe- and Ni-sulphides appear in a fairly similar number of systems and usually form mutually exclusively (i.e., most systems only have one type of Fe- or Ni-sulphide), although heazlewoodite and polydymite coexist in 116 systems. Calcite forms together with pyrrhotite and polydymite but not with troilite and heazlewoodite. Pyrrhotite abundances in most systems are around 1%, but with increasing W/R ratio (by mass) and solute concentration abundances of up to 2.1% can be reached. Other modelled sulphides of minor abundance are Co-sulphides (linnaeite (3038 systems but only 0.09% max abundance) and cattierite (228 systems, 0.09% max abundance) and the oxidised Ni-sulphide vaesite (10 systems, 1.36% max abundance). No sulphates or iron metal appear in any systems and nickel metal is only stable in a few systems with pure water.

Table 2.4
List of solid phases appearing in systems (broadly sorted by mineral group).

Mineral name (adapted from database)	Chemical formula	Mineral name (adapted from database)	Chemical formula
Lizardite	$Mg_3Si_2O_9H_4$	Polydymite	Ni_3S_4
Greenalite	$Fe_3Si_2O_9H_4$	Troilite	FeS
Clinochlore	$Mg_5Al_2Si_3O_{18}H_8$	Pyrrhotite	$Fe_{0.875}S_1$
Mg-saponite	$Mg_{3.175}Al_{0.35}Si_{3.65}O_{10}(OH)_2$	Heazlewoodite	Ni_3S_2
Fe-rich saponite	$Mg_{0.175}Fe_3Al_{0.35}Si_{3.65}O_{10}(OH)_2$	Linnaeite	Co_3S_4
Cronstedtite	$Fe_2Fe_2SiO_5(OH)_4$	Cattierite	CoS_2
Talc	$Mg3Si_4O_{12}H_2$	Vaesite	NiS_2
Na-bearing saponite	$Na_{0.35}Mg_3Al_{0.35}Si_{3.65}O_{10}(OH)_2$	Alabandite	MnS
K-bearing saponite	$K_{0.35}Mg_3Al_{0.35}Si_{3.65}O_{10}(OH)_2$	Magnesite	$MgCO_3$
Mg-Nontronite	$Mg_{0.165}Fe_2Al_{0.33}Si_{3.67}O_{12}H_2$	Siderite	$FeCO_3$
NH_4 Muscovite	$NH_4Al_3Si_3O_{10}(OH)_2$	Ankerite	$CaFe(CO_3)_2$
Phlogopite	$KMg_3AlSi_3O_{12}H_2$	Dolomite	$CaMg(CO_3)_2$
Sodaphlogopite	$NaMg_3AlSi_3O_{12}H_2$	Calcite	$CaCO_3$
Illite	$K_{0.6}Mg_{0.25}Al_{1.8}Al_{0.5}Si_{3.5}O_{10}(OH)_2$	Rhodochrosite	$MnCO_3$
Fe-Beidellite	$Fe_{0.175}Al_{2.35}Si_{3.65}O_{10}(OH)_2$	Native cobalt	Co
Fe-saponite	$Fe_{3.175}Al_{0.35}Si_{3.65}O_{10}(OH)_2$	Native nickel	Ni
Andradite	$Ca_3Fe_2Si_3O_{12}$	Native iron	Fe
NH_4 Feldspar	$NH_4AlSi_3O_8$	Magnetite	Fe_3O_4
Amorphous SiO_2	SiO_2	Chromite	$FeCr_2O_4$
Tephroite	Mn_2SiO_4	Amorphous $Mn(OH)_2$	$Mn(OH)_2$
Enstatite	$Mg_2Si_2O_6$	Manganosite	MnO
Rhodonite	$MnSiO_3$	Ferropericlase	FeO
Microcline	$KAlSi_3O_8$	Goethite	FeOOH
Acmite	$NaFeSi_2O_6$	Hydroxyapatite	$Ca_5(PO_4)_3OH$
Diopside	$CaMgSi_2O_6$	Scacchite	$MnCl_2$
Albite	$NaAlSi_3O_8$		

Phyllosilicates, in addition to cronstedtite, that appear in the systems are mainly serpentine (lizardite and greenalite), saponite (Mg-, Fe-, Na- and K-varieties) and chlorite (clinochlore) with occasional and minor nontronite, NH_4-muscovite (tobelite), phlogopite, illite and beidellite. Those minor phyllosilicates usually require either pure water or very high solute concentrations and do not appear together with calcite. An exception is K- and Na-bearing saponite which often forms as a minor phase (~1%) together with serpentine.

Other minor to trace minerals of <~1% abundance but almost ubiquitously present are apatite (specifically hydroxyapatite) and chromite, as they are the only stable P- and Cr-phases that appear in the systems. No halides like halite or sylvite form in the modelled systems but there is rare scacchite ($MnCl_2$, 29 systems, 1.5% max abundance), although this mineral is only stable at the highest modelled solute concentration and does not coexist with calcite. Mn-phases other than rhodochrosite appearing in the models are tephroite and more rarely amorphous $Mn(OH)_2$, rhodonite and manganosite; Calcite-bearing systems with no rhodochrosite would often have tephroite (198 systems) instead. Calcite also only coexists with linnaeite (509 systems) but not with the more reduced (native cobalt) or more oxidised (cattierite) Co-phase and in terms of N-phases, it occurs with NH_4-feldspar (65 systems) but not with the rarer NH_4-muscovite.

2.3.1.1 Mineralogy of calcite-bearing and CM-like systems

Calcite-bearing systems can be further subdivided based on their similarity to CM chondrites. For the purpose of the equilibrium models and as a first approximation, CM2-like systems are defined to require calcite, lizardite, greenalite, cronstedtite, pyrrhotite but less than 10% magnetite, less than 2% talc and Mg-saponite, less than 0.5% ankerite and no dolomite (primary minerals like olivine and pyroxene, despite being present in CM2s, are not included in this definition as they usually don't form in equilibrium models). CM1/2-like systems follow similar criteria but also need to have dolomite, whereas CM1-like systems require magnetite but should not have cronstedtite (and dolomite is optional). 232 of the modelled systems meet the CM2 definition, 49 resemble CM1 but only 5 are CM1/2-like. The CM2-like systems typically consist of (in vol%): 50 lizardite, 25 greenalite, 10 clinochlore (as Al-phase) and cronstedtite, 1 calcite, polydymite and saponite (K- and/or Na-bearing), 0.5 hydroxyapatite, pyrrhotite and chromite and minor and/or occasional NH_4-feldspar, ankerite, andradite, rhodochrosite, tephroite and linnaeite. The CM1/2s have around 48 vol% lizardite, 22 greenalite, 10 clinochlore and cronstedtite, 3 Na-bearing saponite, 2 dolomite, 1 K-bearing saponite, polydymite and calcite, 0.5 hydroxyapatite, pyrrhotite and chromite and minor rhodochrosite. Finally, the CM1s contain around 50 vol.% lizardite, 25 greenalite, 10 clinochlore, 3 magnetite and Na-bearing saponite, 1.5 calcite, 1 K-bearing saponite and polydymite, 0.5 hydroxyapatite, pyrrhotite and chromite and minor and/or occasional Mg-saponite, andradite, tephroite, rhodochrosite and linnaeite.

2.3.1.2 Aqueous fluid and gaseous phase

The modelled systems, on average, contain fluids rich in Na and N with substantial amounts of C and K; S, Si, Cl, P, and Fe can occasionally also reach concentrations of 0.01 m or higher (see Table 2.5). Dissolved species are predominantly Na^+, NH_3, NaOH, N_2, K^+ and HCO_3^-; depending on the system parameters, HS^-, CO_3^{2-} and $NaHSiO_3$ can also be of notable concentration (0.1 m or higher). Major elements like Mg and Al are also present in the fluid but are of only minor concentrations. Sulphur is predominantly reduced (mainly as HS^- with minor H_2S); oxidised S is rare (<10^{-8} m). The pH of the aqueous fluid after interacting with the chondritic rock ranges from 6.2 to 14.9 and the pe from -15.7 to -3.8. Calcite-bearing systems require a more narrow range of pH (8.2 to 12.5) and have generally lower concentrations of dissolved solutes with most notably less Fe, K and Na but C concentrations are on average slightly higher with elevated levels of aqueous CO_3^{2-} and CH_4 but lower CO_2 and HCO_3^-. The modelled CM2s fluid has even higher DIC concentrations whereas, compared to the CM2s, the CM1/2s and CM1s fluid has less C (more comparable to the overall average) and other elements are also generally less concentrated. Overall, modelled CM2s formed from more concentrated fluids and CM1/2s and especially CM1s from more diluted ones. It is also notable that CM1/2s and CM1s on average form at lower pH and higher pe values compared to CM2s; CM1/2s in particular require only slightly alkaline pH and fairly oxidising conditions.

Table 2.5
Mean aqueous fluid composition (default scenario) across different systems (selected elements and species) as well as range and mean values (in brackets) for pH and pe at 10 bar pressure.

Feature	All systems	Calcite systems	CM2-like systems	CM1/2-like systems	CM1-like systems
pH	6.22–14.9 (10.3)	8.17–12.52 (9.94)	8.74–12.5 (10.69)	8.63–8.76 (8.71)	8.66–10.0 (9.52)
pe	-15.7–-3.78 (-9.04)	-10.6–-6.12 (-7.97)	-10.6–-6.71 (-8.76)	-6.72–-6.58 (-6.66)	-8.19–-6.63 (-7.65)
Total C (mol/kg)	2.45E-02	3.73E-02	4.91E-02	2.46E-02	1.57E-02
Total Ca (mol/kg)	2.81E-06	7.32E-06	8.04E-06	6.73E-06	6.07E-06
Total Cl (mol/kg)	6.06E-03	5.98E-03	5.65E-03	6.72E-03	5.66E-03
Total Fe (mol/kg)	2.33E-04	1.57E-07	2.36E-07	3.30E-08	2.60E-07
Total K (mol/kg)	1.72E-02	3.71E-04	5.04E-04	2.45E-04	2.32E-04
Total N (mol/kg)	1.09E-01	1.04E-01	9.31E-02	1.34E-01	1.13E-01
Total Na (mol/kg)	1.75E-01	5.50E-02	7.92E-02	2.31E-02	2.28E-02
Total P (mol/kg)	1.25E-03	1.10E-05	1.11E-05	4.09E-06	1.23E-06
Total S (mol/kg)	6.68E-03	8.79E-04	9.14E-04	3.07E-04	2.08E-03
Total Si (mol/kg)	3.67E-03	1.28E-03	2.08E-03	3.48E-04	9.26E-04
Aqueous CO_2 (mol/kg)	8.13E-04	2.81E-05	3.92E-06	6.62E-05	4.48E-06
Aqueous HCO_3^- (mol/kg)	1.26E-02	8.19E-03	6.45E-03	1.57E-02	4.49E-03
Aqueous CO_3^{2-} (mol/kg)	4.54E-03	1.90E-02	3.10E-02	1.18E-03	3.65E-03
Aqueous CH_4 (mol/kg)	6.55E-03	1.01E-02	1.17E-02	7.57E-03	7.51E-03

Aqueous alteration in all modelled systems results in a separate gas phase. Gas volumes range from 0.71 to 24.7 mol and are predominantly a mixture of H_2 and CH_4 across all systems but CO_2 and H_2O (water vapour) can also be of high abundance in some systems. For the modelled calcite and CM-like systems, however, average gas volumes are slightly lower with CH_4 and H_2O as dominant phases and

less abundant H_2. The average gas volumes for CM1/2s and CM1s are slightly higher compared to CM2s.

In the following subsections the effect of the modelled parameters (temperature, W/R ratio (by mass) and solute concentration) is further explored.

2.3.1.3 Influence of temperature

Calculated minerals in equilibria assemblages are fairly temperature insensitive but there are notable exceptions. In addition to the aforementioned dolomite (requiring 105°C or higher temperature), another mineral of interest that only forms at elevated temperatures is troilite (minimum 145°C),. In contrast, minerals that are only stable at lower temperatures are cronstedtite (maximum 125°C) and ankerite (maximum 125°C).

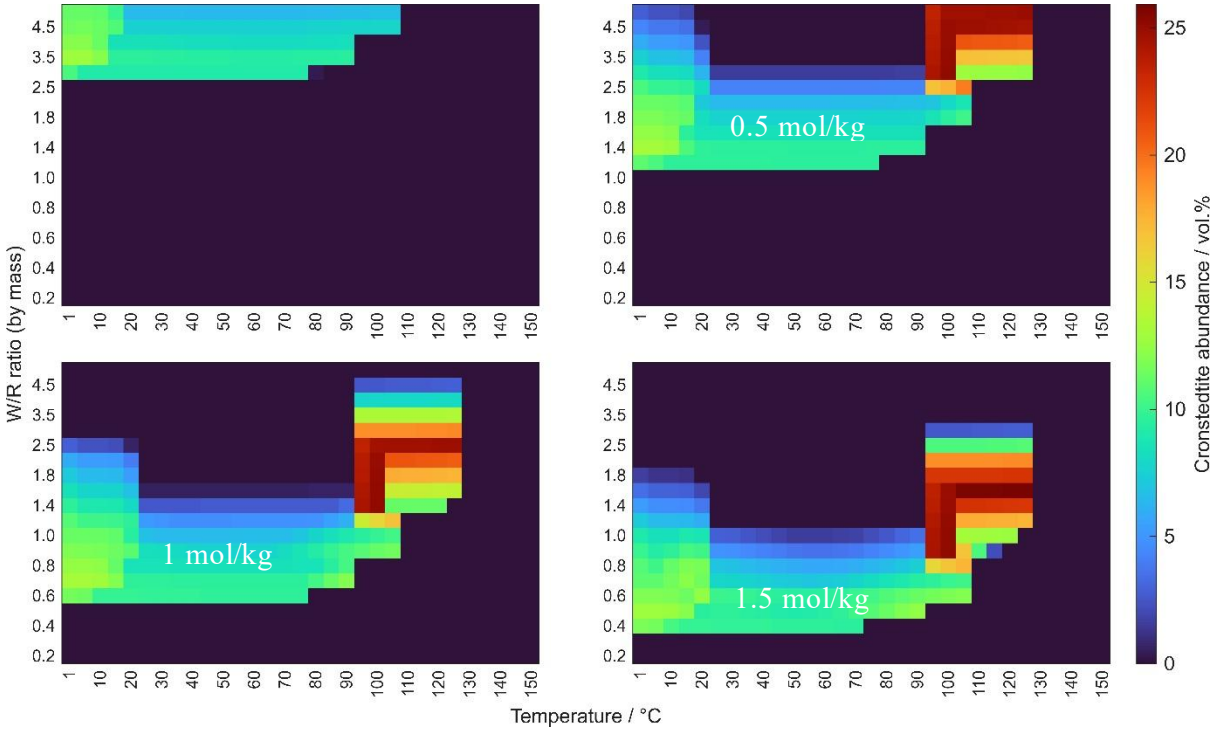

Fig. 2.1. Cronstedtite abundance heatmaps as a function of temperature and W/R ratio (by mass) at 10 bar pressure. The four tiles have constant initial CO_2 abundances of 0.2 (top left), 0.5 (top right), 1 (bottom left) and 1.5 (bottom right) mol/kg.

Temperature also affects the abundance of some minerals. Notable cases are cronstedtite with increased concentrations between 95 and 125°C (increase of max. concentration from 15 to 30 vol.%) (see Figure 2.1) and magnetite (significantly higher concentrations at 125°C or above). Minerals of interest with fewer but still significant variations are calcite (slightly elevated abundances between 110 and 120°C), lizardite (almost linear mean abundance decrease between 1 and 150°C (from 46 to 33 vol.%), greenalite (drop in mean concentrations at 95°C and higher temperature), pyrrhotite (~20% increase with temperature) and Mg-saponite (significant increase in abundance at 105°C and higher temperature). Lizardite and greenalite co-occur in most systems; lizardite is generally more abundant, resulting in an average Mg# of serpentine of 0.63 across all systems. Below 95°C, Mg# don't reach

higher values than 0.73 but Mg# of 1 (pure Mg-serpentine) can be reached at 95°C or higher for specific combinations of W/R ratio (by mass) and solute concentration.

Whereas calcite can form for all modelled temperatures, the modelled CM-like systems (i.e., where calcite is accompanied by other minerals including serpentine) require a more restricted range of temperature. The CM2s can form between 1 and 105°C (mean temperature of 49°C), the CM1s between 95 and 120°C (mean 108°C) and the CM1/2s only at 105°C. None of the modelled CM1s contain dolomite and none of the CM2s and CM1/2s have magnetite. Calcite is of similar abundance in CM2s and CM1s (up to 1.8%, 1.2% on average); in contrast, the CM1/2s predominantly contain dolomite (up to 2.2%, mean of 1.6%) with only 0.85% calcite on average. CM1s have on average 4% magnetite and, on average, less rhodochrosite compared to the other CM-like systems. Whereas calcite-bearing systems can have serpentine of Mg#1, the serpentine in CM-like systems reaches max Mg# of 0.74 and average Mg# are also slightly lower. Relatively little difference in average Mg# is observed across the various CM-like systems but CM1s tend to have a slightly lower or higher Mg# (0.65 compared to 0.69/0.61) than CM2s, depending on whether cronstedtite is included in the definition of serpentine Mg# or not.

2.3.1.4 Influence of W/R ratio (by mass)

In contrast to temperature, the modelled W/R ratio (by mass) has a significant effect on the stability and abundance of most minerals. Saponite (except Na-bearing) and cronstedtite require W/R ratios (by mass) of 0.3 or higher, and with increasing W/R ratios (by mass), mean abundances of serpentine (especially lizardite) decrease and saponite increase. Systems with pure greenalite (serpentine with Mg#0) exist for W/R ratios (by mass) of 0.8 or higher in combination with elevated solute concentrations (1 m CO_2 or higher) (see Figure 2.2); combinations of 3.5 W/R ratios (by mass) or higher and 1.5 m CO_2 or higher result in systems with only saponite instead of serpentine. No carbonates are stable at 0.2 W/R ratios (by mass) but calcite and rhodochrosite can form at 0.3 W/R ratios (by mass), whereas ankerite and dolomite, magnesite, and siderite require higher ratios (0.5, 0.6 and 2.5, respectively). An increase in W/R ratios (by mass) does not significantly change the abundance of calcite or rhodochrosite but leads to an increase in dolomite and ankerite and most notably in siderite and magnesite abundances. On average, oxidised sulphides (pyrrhotite and polydymite) become more abundant than reduced ones (troilite and heazlewoodite) at W/R ratios (by mass) of 0.8 to 1.2 and pyrrhotite abundances increase slightly with increasing W/R ratios (by mass) (see Figure 2.3). With increasing W/R ratios (by mass) magnetite exists in fewer systems but its mean abundance increases before reaching a plateau at a ratio of 0.6. Some uncommon minerals only exist at very high W/R (by mass) (e.g., amorphous silica or microcline) or at very specific values (e.g., scacchite or illite, W/R ratio (by mass) of 0.8).

CM-like systems exist over a slightly narrower range of W/R ratios (by mass) (0.4 to 4.5 for CM2 and CM1 and 0.5 to 5 for CM1/2) compared to calcite-bearing systems in general. Mean W/R ratios (by

mass) are fairly similar across all petrologic types (1.75, 1.85 and 1.65 for CM2, CM1/2 and CM1, respectively).

2.3.1.5 Influence of the initial concentration of species in melted ice

In general, an increase in solute concentration (higher CO_2, NH_3, H_2S and HCl) has a similar effect as increasing W/R ratio (by mass), albeit with some differences. Many of the modelled minerals require a minimum concentration of the modelled solutes (i.e., 0.2 m CO_2 or higher); the more important minerals are Mg-saponite, cronstedtite, ankerite, polydymite, pyrrhotite, dolomite, calcite and rhodochrosite (all 0.2 m or higher), Fe-rich saponite, magnesite and talc (0.5 m or higher) and siderite (1 m or higher). Other minerals like scacchite or vaesite only form at the highest modelled solute concentration (2 m CO_2). Similarly to increasing W/R ratios (by mass), the maximum abundance of carbonates increases with higher solute concentrations, with exception of calcite and rhodochrosite.

CM-like systems span the entire range of solute concentrations (except pure water). However, calcite and serpentine exist in fewer systems with high solute concentrations (1.5 and 2 m CO_2) and calcite and cronstedtite form most commonly between 0.5 and 1 m CO_2 whereas dolomite is most common in systems with initial 2 m CO_2. Mean solute concentrations are fairly similar across different petrologic types - 0.84 m CO_2 for CM2s and CM1s and 1.05 m CO_2 for CM1/2s.

2.3.2 Effect of different scenarios

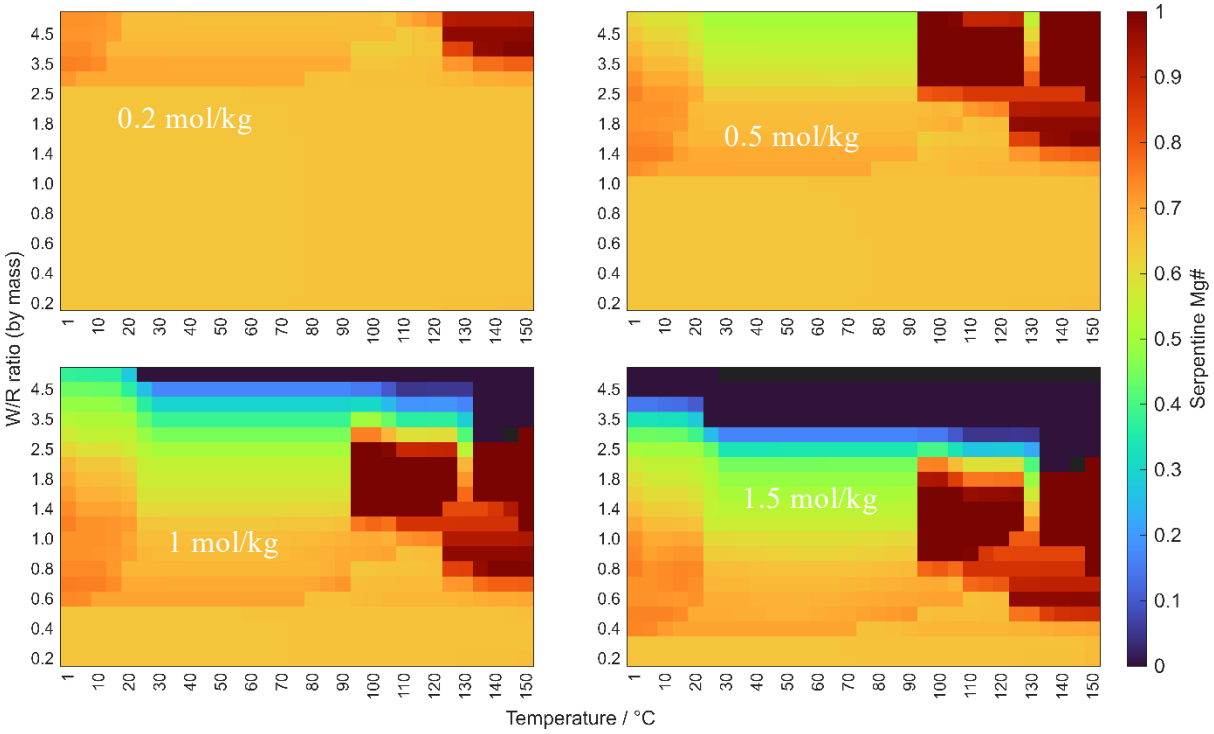

Fig. 2.2. Mg# of serpentine (lizardite+greenalite) heatmaps as a function of temperature and W/R ratio (by mass) at 10 bar pressure. The four tiles have constant initial CO_2 abundances of 0.2 (top left), 0.5 (top right), 1 (bottom left) and 1.5 (bottom right) mol/kg.

If not specified otherwise, the different scenarios were modelled with the same range of temperature, W/R ratio (by mass) and solute concentration. The main purpose of having different scenarios is to establish the impact of a specific change (for example, a different starting composition) in the modelled system/scenario on the occurrence and abundance of minerals discussed in section 2.3.1. Hence, the presented results will be less detailed and aim to mainly focus on a comparison to the default scenario. An overview of characteristics of CM-like systems across different scenarios is illustrated in Table 2.6 (CM2-like), Table 2.7 (CM1/2-like) and Table 2.8 (CM1-like). Differences in mineralogy across different petrologic types and scenarios are shown in Table 2.9.

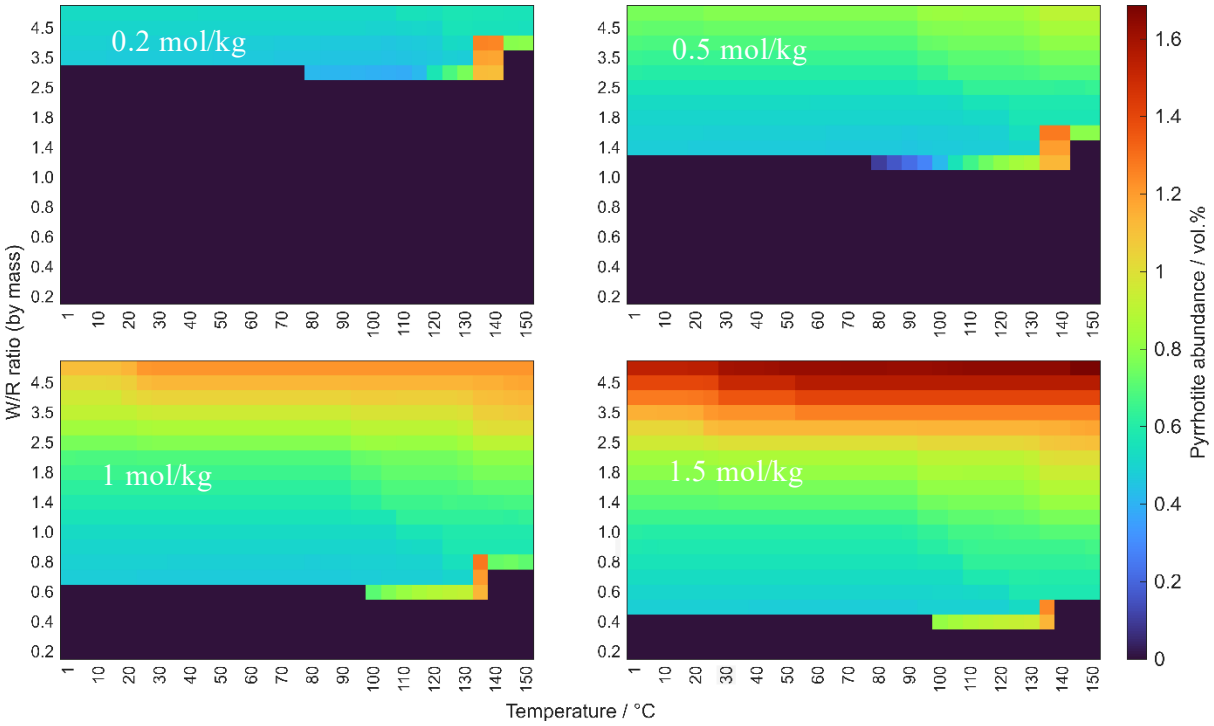

Fig. 2.3. Pyrrhotite abundance heatmaps as a function of temperature and W/R ratio (by mass) at 10 bar pressure. The four tiles have constant initial CO_2 abundances of 0.2 (top left), 0.5 (top right), 1 (bottom left) and 1.5 (bottom right) mol/kg.

Table 2.6
CM2-like characteristics across different scenarios (numbers in brackets denote mean values).

Feature/Scenario	Default (10 bar)	NoGas (10 bar)	More NH_3 (10 bar)	HighP (200 bar)	Asuka 12169 (10 bar)
Number of systems	232	104	256	216	164
Temperature range (°C)	1–105 (49)	1–90 (38)	20–100 (57)	1–95 (43)	1–90 (46)
W/R ratio range	0.4–4.5 (1.74)	0.6–4.5 (2.64)	0.4–5 (1.81)	0.4–4.5 (1.74)	0.3–3 (1.16)
Initial CO_2 concentration range (mol/kg))	0.2–2 (0.85)	0.2–1.5 (0.50)	0.2–2 (0.94)	0.2–2 (0.84)	0.2–2 (0.84)
pH range	8.74–12.52 (10.69)	9.12–12.46 (10.86)	8.96–11.66 (10.60)	8.99–12.53 (10.89)	10.03–12.63 (11.14)
pe range	-10.62–-6.71 (-8.76)	-10.77–-7.25 (-9.07)	-9.78–-6.91 (-8.65)	-10.81–-7.12 (-9.13)	-10.74–-8.15 (-9.27)
Serpentine Mg# range	0.66–0.74 (0.69)	0.65–0.73 (0.68)	0.66–0.98 (0.68)	0.65–0.75 (0.68)	0.62–0.72 (0.65)
Serpentine+cronstedtite Mg# range	0.60–0.63 (0.61)	0.60–0.63 (0.61)	0.60–0.69 (0.61)	0.60–0.63 (0.61)	0.61–0.63 (0.62)

Table 2.7
CM1/2-like characteristics across different scenarios (numbers in brackets denote mean values).

Feature/Scenario	Default (10 bar)	NoGas (10 bar)	More NH_3 (10 bar)	HighP (200 bar)	Asuka 12169 (10 bar)
Number of systems	5	0	6	0	8
Temperature range (°C)	105–105 (105)	N/A	105–105 (105)	N/A	105–105 (105)
W/R ratio range	0.5–5 (1.84)	N/A	0.8–3 (1.60)	N/A	0.4–4 (1.62)
Initial CO_2 concentration range (mol/kg)	0.2–2 (1.04)	N/A	0.5–2 (1.17)	N/A	0.2–2 (0.86)
pH range	8.63–8.76 (8.71)	N/A	8.77–8.80 (8.79)	N/A	8.68–8.77 (8.74)
pe range	-6.72–-6.58 (-6.66)	N/A	-6.75–-6.73 (-6.74)	N/A	-6.73–-6.64 (-6.70)
Serpentine Mg# range	0.65–0.69 (0.67)	N/A	0.64–0.69 (0.67)	N/A	0.61–0.68 (0.65)
Serpentine+cronstedtite Mg# range	0.59–0.59 (0.59)	N/A	0.59–0.60 (0.59)	N/A	0.60–0.61 (0.60)

2.3.2.1 Effect of dissolved gas (no equilibrium gas phase) (NoGas scenario)

This scenario prevents the formation of a separate gas phase and instead any gas generated stays in solution. On the parent body, this scenario might be part of a high pressure environment or it considers the possibility that formation of gas phases like CH_4 is inhibited. Overall, there is relatively little change in the type of stable minerals across all systems compared to the default scenario. However, notable differences are in the abundance and occurrence of more reduced phases: native nickel occurs across 1487 systems (compared to just one in the default scenario) and native iron is present in 1109 systems. Both phases are stable across the entire temperature range but require a combination of low W/R ratios (by mass) and solute concentrations. More oxidised sulphides (pyrrhotite and polydymite) occur in fewer systems than more reduced ones (troilite and heazlewoodite), although differences to the default system are fairly small (~10%). All carbonates are present in slightly more systems (~5-10%, reflected by a broader stability range of W/R ratios (by mass)) but with similar maximum abundances. Magnetite occurs in fewer systems (1416 compared to 2135) and mean and max abundances are also lowered. Cronstedtite follows a similar trend; notably, for this scenario, the mineral preferably forms at lower temperatures (absent at temperature >100°C) but in return it can also exist at lower W/R ratios (by mass).

Table 2.8
CM1-like characteristics across different scenarios (numbers in brackets denote mean values).

Feature/Scenario	Default (10 bar)	NoGas (10 bar)	More NH_3 (10 bar)	HighP (200 bar)	Asuka 12169 (10 bar)
Number of systems	49	107	87	144	60
Temperature range (°C)	95–120 (108)	80–135 (114)	90–120 (106)	85–140 (113)	95–120 (108)
W/R ratio range	0.4–4.5 (1.67)	0.4–5 (2.08)	0.5–5 (1.80)	0.3–5 (1.64)	0.3–3 (1.07)
Initial CO_2 concentration range (mol/kg)	0.2–2 (0.85)	0.2–2 (0.79)	0.2–2 (0.95)	0.2–2 (0.89)	0.2–2 (0.89)
pH range	8.66–10.05 (9.52)	8.52–10.29 (9.28)	8.77–10.19 (9.52)	8.48–10.54 (9.45)	8.67–10.06 (9.49)

pe range	-8.19–-6.63 (-7.65)	-8.63–-6.64 (-7.55)	-8.33–-6.72 (-7.64)	-8.87–-6.63 (-7.74)	-8.20–-6.77 (-7.61)
Serpentine Mg# range	0.63–0.67 (0.65)	0.61–0.67 (0.63)	0.63–0.67 (0.65)	0.61–0.67 (0.64)	0.61–0.67 (0.65)
Serpentine+cronstedtite Mg# range	0.63–0.67 (0.65)	0.61–0.67 (0.63)	0.63–0.67 (0.65)	0.61–0.67 (0.64)	0.61–0.67 (0.65)

Calcite coexists with similar minerals compared to the default scenario but instead of pyrrhotite and polydymite ~40% of the systems contain troilite and heazlewoodite instead (but none of the calcite systems have native iron or nickel). Magnetite is also encountered more often than cronstedtite, which is reflected by a decrease in CM2-like systems but increase in CM1-like systems. No modelled system met the criteria for a CM1/2. The CM2s form over a narrower range of temperature, W/R ratio (by mass) and solute concentration (1–90°C, 0.6–4.5 and 0.2–1.5 m, respectively) with a slightly higher mean W/R ratio (by mass) (2.6(+0.9)). The CM1s, on the other hand, have a broader range of temperature and W/R ratio (by mass) (80–135°C and 0.4–5); however, the mean solute concentration is slightly lower. In contrast to the default scenario, some (48 out of 107) modelled CM1s also contain dolomite (max 2.8%, mean (excluding zeros) of 1.4%) in addition to calcite (max 1.8%, mean of 1.2%). Within those systems, higher dolomite abundances (>1%) are accompanied by lower calcite abundances (<1%) and vice versa, in contrast to CM1/2s from the default scenario in which dolomite is consistently more abundant than calcite. Whereas rhodochrosite was only present in one CM1-like system in the default scenario, 75 of the CM1-like systems of the NoGas scenario contain rhodochrosite. The fluid for the CM2s is, on average, slightly more alkaline and reduced for the CM2s but slightly more acidic and oxidised for the CM1s, resulting in a wider gap in pH and pe space between CM2s and CM1s compared to the default scenario. Serpentine in CM-like systems is slightly more Fe-rich compared to the default scenario.

2.3.2.2 Effect of elevated NH_3 concentration (more NH_3 scenario)

The original concept of this scenario was to reverse the concentrations of NH_3 and CO_2 in the fluid, following a similar approach as Castillo-Rogez et al. (2022). However, many of the systems failed to equilibrate, with only 9 systems containing calcite and none of the systems met the CM criteria. To address the scarcity of calcite and carbonates in general, the scenario was rearranged to have equal concentrations of NH_3 and CO_2. The scenario yields the same major phases as in the default scenario but there are some differences in minor phase occurrence, such as the disappearance of native nickel, scacchite and NH_4-bearing muscovite; on the other hand, goethite is stable in 14 systems at high solute concentrations and low temperature, and alabandite exists in 53 systems at low temperature. Compared to the default scenario, calcite occurs in slightly more systems but all other carbonates have more limited occurrences; notably, dolomite occurs in only 176 instead of 422 systems. In addition to its high-temperature (105°C and higher) occurrence, dolomite is also predicted to be stable between 1 and 10°C (up to 3% abundance) for a limited range of W/R ratios (by mass) and solute concentrations. Calcite

occurs at slightly higher W/R ratios (by mass) compared to the default scenario; concentrations can vary considerably (between 0.2 and 2%) but without any clear correlation with temperature, W/R ratio (by mass) or solute concentration. Cronstedtite notably yields high concentrations either at low (1–25°C) or high temperature (95–120°C), although appearances at high temperature are rare. Lizardite and greenalite are stable for all combinations of W/R ratio (by mass) and solute concentration but serpentine is present in fewer systems and is more unstable at high temperature when combined with high W/R ratio (by mass) and solute concentration. Overall, temperature has a larger influence on mineral abundance and occurrence than W/R ratio (by mass) or solute concentration.

Compared to the default scenario, there are more CM-like systems: 256 resemble CM2s, 87 CM1s and 8 CM1/2s. Four of the CM2-like systems contain magnetite and fewer systems contain ankerite. Mg# of serpentine on average are similar but some systems have Mg# of up to 0.98 (0.68 when accounting for cronstedtite) (see Table 2.6). The temperature interval is narrower (20–100°C) with slightly higher average temperature (57°C compared to 49°C). Other differences are a slightly higher max W/R ratio (by mass) (5) and average solute concentration (0.9), whereas the max pH is slightly lower (11.7). The CM1/2-like systems are very similar to the default scenario with exception of a narrower W/R ratio (by mass) range (0.8-3) and a lower mean (1.6) and a minimum CO_2 concentration of 0.5 m is also required. Another difference is calcite being more abundant than dolomite in two systems. Finally, most CM1-like systems have no dolomite except one, in which dolomite is of similar abundance compared to calcite (1.2%). The minimum temperature required is slightly lower (90°C), and the minimum, maximum and also average W/R ratios (by mass) as well as average solute concentrations are slightly higher.

2.3.2.3 Effect of elevated pressure (HighP scenario)

This scenario consists of a total of 3940 instead of 3720 systems due to having additional modelled temperatures (175°C and 200°C) facilitated by the higher pressure (200 bar). When comparing mineral occurrences to other scenarios, this difference is accounted for by a scaling factor of 6%. Phases that occur more often at 175°C or higher are talc, Fe-rich saponite, troilite, ferropericlase, heazlewoodite, phlogopite and native Ni, whereas lizardite, greenalite, siderite, amorphous silica, pyrrhotite, and polydymite occur less often. Native Ni and, to a lesser degree, iron exist in a few systems but only at low solute concentrations and are not coexisting with calcite. Compared to the default scenario, calcite occurs in slightly more systems (581) and requires slightly lower W/R ratios (by mass) (1-2 units); dolomite also has a slightly higher occurrence (505 systems) with a similar behaviour to calcite in terms of W/R ratio (by mass) and requires 110°C or higher temperatures to form. Cronstedtite, on the other hand, forms only at 105°C or lower temperatures at low W/R ratios (by mass) or solute concentrations and is only abundant at low temperatures (1-15°C) and/or low W/R ratios (by mass). Magnetite shows a trend of increasing abundance with temperature with highest concentrations (~15%) yielded at 200°C for moderate W/R ratios (by mass) and solute concentrations.

Whereas only minor differences are notable when comparing phases across all systems, changes in abundance and mineralogy of CM-like systems are more prominent. CM2-like systems are slightly rarer (216), with four of them containing additional magnetite (up to 2%); ankerite and NH_4-feldspar are rarer and rhodochrosite occurs in fewer systems than tephroite. Mean and maximum temperature are slightly lower and the average pe is slightly more reducing. CM1-like systems are more numerous (144) compared to the default system. A few systems contain heazlewoodite, dolomite and ankerite in which dolomite, similarly to section 2.3.2.2, is either of lower or higher abundance than calcite. It is also noteworthy that the only Mn-phase forming with dolomite is rhodochrosite, whereas dolomite-free CM1s would usually have tephroite as Mn-phase. The temperature and W/R ratio (by mass) intervals are wider (85–140°C and 0.3–5, respectively), the max pH is higher (10.5) and the min pe slightly lower (-8.7). No CM1/2-like systems formed in this scenario.

2.3.2.4 Effect of different starting composition (Asuka (12169) scenario)

Relative to DOM 08006, Asuka 12169 has higher concentrations of Na, S, Mn, Al, K and P, and is slightly depleted in Ca and Fe (see Table S2.2). These compositional differences primarily affect the abundances of minerals but also have an influence on their occurrence and on fluid composition. Carbonates, apart from magnesite and rhodochrosite, have lower maximum abundances even though they occur, with the exception of calcite, in more systems. On the other hand, sulphides reach higher abundances and pyrrhotite and polydymite occur in more systems whereas troilite and heazlewoodite are rarer. Greenalite and lizardite are slightly less abundant and in return, Fe-rich saponite and talc appear in more systems. No metals are stable in this scenario and in general, reduced phases are rarer compared to the default scenario. In W/R ratio (by mass) and solute concentration space, calcite stability is shifted to lower values and it is also notable that for combinations of higher W/R ratios (by mass) and solute concentration, calcite would only form at ~110°C or higher temperature with a trend of increasing abundance with increasing temperature. In contrast, the dolomite stability is expanded to higher W/R ratios (by mass) and dolomite is also more abundant at 0.2 m CO_2. The stability of cronstedtite is shifted to slightly lower W/R ratios (by mass) and for combinations of higher W/R ratios (by mass) and solute concentrations, cronstedtite only forms at higher temperatures (95°C or more). Magnetite is absent below 50°C and abundances of >0.14% are only reached at 80°C or more; it also only appears in 800 systems compared to the 2135 systems in the default scenario.

In terms of CM-like systems, there are more CM1 and CM1/2-like systems but fewer are CM2-like, compared to the default scenario. All CM-like systems are characterised by a lower minimum, maximum and mean W/R ratios (by mass). Other characteristics vary between different petrologic types. The CM2s have a slightly elevated minimum and mean pH and slightly decreased maximum temperature, maximum and mean pe and minimum and maximum Mg# of serpentine. Cronstedtite abundances are fairly low and vary between 1 and 10%. Compared to the default system, the CM1/2s have a slightly lower mean solute concentration and mean Mg# of serpentine. Finally, the CM1s in this

scenario form under fairly similar conditions with the only differences being in the abundance and occurrence of some minerals like calcite (lower max and mean abundance) or rhodochrosite (higher occurrence).

Table 2.9
Differences in mineralogy (vol.%) (mean excluding zeros) across different petrologic types (numbers in row 2) and scenarios.

	Default (10 bar)			NoGas (10 bar)			More NH_3 (10 bar)			HighP (200 bar)			Asuka 12169 (10 bar)		
Mineral/petrologic type	2	1/2	1	2	1/2	1	2	1/2	1	2	1/2	1	2	1/2	1
Lizardite	51	48	50	51	-	50	51	48	50	51	-	50	49	45	47
Greenalite	23	23	27	25	-	29	24	24	27	24	-	28	26	24	25
Cronstedtite	9.6	9.4	0	8.5	-	0	9.0	9.2	0	8.7	-	0	4.0	5.5	0
Magnetite	0	0	4.0	0	-	2.9	0.97	0	3.9	0	-	3.3	0	0	2.8
Calcite	1.2	0.84	1.2	1.3	-	1.2	1.3	0.84	1.2	1.2	-	1.1	0.89	0.46	0.86
Dolomite	0	1.6	0	0	-	1.4	0	1.6	1.2	0	-	1.3	0	1.5	0
Pyrrhotite	0.49	0.53	0.48	0.49	-	0.61	0.51	0.60	0.52	0.49	-	0.69	1.8	1.8	1.8
Polydymite	1.2	1.2	1.2	1.2	-	0.77	1.2	1.2	1.2	1.2	-	1.1	1.1	1.1	1.2
Clinochlore	9.8	9.3	9.5	10	-	10	10	9.3	9.5	10	-	9.9	11	10	9.9
Andradite	0.94	0	0.79	0.90	-	0.96	1.1	0	1.1	0.87	-	0.96	0.82	0	1.2
Mg-saponite	0	0	1.9	0	-	0	0	0	0.53	0	-	1.6	0	0	0
Na-bearing saponite	2.1	4.2	4.3	0	-	3.3	1.7	3.4	4.2	0	-	3.9	4.9	6.9	8.3
K-bearing saponite	1.2	1.2	1.2	0.66	-	1.1	1.1	1.2	1.2	0.92	-	1.1	1.6	1.6	1.6
Hydroxyapatite	0.61	0.61	0.62	0.61	-	0.62	0.61	0.61	0.62	0.61	-	0.62	0.79	0.79	0.81
NH_4 feldspar	1.7	0	0	1.6	-	0	5.5	0	0	1.7	-	0	1.2	0	0
Chromite	0.35	0.35	0.36	0.35	-	0.35	0.35	0.35	0.36	0.35	-	0.35	0.34	0.35	0.35
Rhodochrosite	0.22	0.22	0.22	0.22	-	0.22	0.21	0.22	0.20	0.22	-	0.22	0.19	0.26	0.08
Linnaeite	0.08	0.08	0.08	0.08	-	0.08	0.08	0.08	0.08	0.08	-	0.08	0.08	0.08	0.08
Tephroite	0.17	0	0.18	0.17	-	0.16	0.16	0	0.17	0.17	-	0.17	0.15	0	0.18
Troilite	0	0	0	0.17	-	0.67	0	0	0	0	-	0	0	0	0
Heazlewoodite	0	0	0	0	-	0.65	0	0	0	0	-	0	0	0	0
Ankerite	0.21	0	0	0.38	-	0.41	0.22	0	0	0.38	-	0.41	0	0	0

2.4 Discussion

2.4.1 Possible alteration conditions of CM chondrites (default scenario)

One of the main aims of producing these equilibrium models was to evaluate the alteration conditions on the CM chondrite parent body/bodies and the factors causing differences in petrologic type. Based on mineralogical studies of CM chondrites (e.g., Howard et al., 2011), a filter was applied to the results to sample only systems that resemble CM chondrites (see section 2.3.1). Across all systems, modelled CM chondrites could form over a wide range of temperatures (1–120°C), W/R ratios (by mass) (0.4–5) and solute concentrations (0.2–2 m CO_2), and even higher values might be possible for the latter two parameters. However, the aforementioned CM chondrite criteria only serve as a first approximation and it is crucial to further evaluate the mineralogy in CM chondrite-like systems.

Howard et al. (2011, 2015) quantified the mineralogy of a suite of CM chondrites by XRD; CM2 chondrites (n = 22) had 22–83% Mg,Fe- serpentine, 0–50% cronstedtite, 6–34% anhydrous silicates (predominantly olivine with lesser orthopyroxene), 0.6–8.4% magnetite, 0.6–5.4% sulphides, 0–4.2% calcite and 0–0.2% Fe,Ni metal. No primary anhydrous silicates are found in the models but instead, more phyllosilicates are present (96% on average as a consequence of the equilibrium approach of the model). Mg-chlorite and saponite of various composition (Mg-, Fe-, Na- or K-bearing) that are formed in addition to Mg- and Fe-serpentine and ferroan serpentine (cronstedtite) could either be the result of the more extensive modelled alteration that would release Al, Na and K to the solution, or due to those elements being found as trace elements in other minerals like serpentine and not forming their own secondary phases. The range of calcite abundance (0–1.8%) is in good agreement with measured abundances but sulphides (pyrrhotite+polydymite) only reach 1.7% and magnetite does not form in any of the CM2-like systems of the default scenario. Magnetite especially differs strongly from the mineralogy of meteorites determined by sample analysis and could further indicate that CM2 chondrites did not form in equilibrium but could for example have experienced a short period at high temperature (~110°C or higher) that would allow for an incomplete reaction of cronstedtite to magnetite. Mg# in modelled CM2 serpentine is fairly constant; however, mineralogical studies like Howard et al. (2011) noted an increase in serpentine Mg# with decreasing petrologic subtype. A potential explanation for those differences could be a combination of temperature and duration of aqueous alteration. The CM2-like systems form over a wide range of temperatures (1–105°C); the slower aqueous alteration at lower temperatures could produce more Fe-rich serpentine, owing to faster reaction of Fe-rich olivine (modelled as fayalite) compared to forsterite (Palandri and Kharaka, 2004). Considering that aqueous alteration ended before all primary silicates had been consumed, only alteration at higher temperature would have been able to dissolve significant amounts of Mg-rich olivine and produce more Mg-rich serpentine. In summary, different temperatures and durations of aqueous alteration could have been responsible for CM2 chondrites of different petrologic subtype, although it cannot be excluded that differences in W/R ratio (by mass) and/or solute concentration had an additional effect.

CM1 chondrites are much rarer than CM2 chondrites and so far no CM1 fall has been documented, although the recent falls Mukundpura and Winchcombe contain CM1 lithologies (Potin et al., 2020; King et al., 2022). King et al. (2017) determined the mineralogy of six different CM1 finds by XRD; they have 84–91% phyllosilicates (52–72% Mg-serpentine and 16–32% Fe-cronstedtite), 3.6–8% olivine, 1.9–3.3% magnetite, 0.1–4.4% sulphides and 0.4–1.7% calcite; tochilinite is rare (<1%) or absent. Most modelled CM1 systems show higher abundances of magnetite, although some systems have less than 3%, which is more consistent with measured quantities. In common with the CM2s, there is a narrow range of modelled sulphide abundances (1.6–1.7%), indicating that the much broader range observed in the meteorites likely reflects a redistribution of sulphides, either through terrestrial or parent body alteration, although differences in sourced sulphur (heterogeneous S accretion or different parent bodies) are also a possibility. Modelled calcite abundances (0.6–1.8%) are in good agreement with measured abundances but like the CM2s, there are more different modelled phyllosilicate phases than determined by XRD. Since CM1s are extensively altered (Zolensky et al., 1997; King et al., 2017), Al, Na and K are unlikely to be found in primary phases but instead the absence of those elements in analysed secondary phases could perhaps be attributed to a lack of precision in the sample analysis or other phases like phyllosilicates incorporating Al, Na and K as trace elements. Alternatively, at least some of those elements are leached from the system and transported elsewhere; indeed, the more extensively altered lithology of the Paris meteorite has lower bulk abundances of Al, Na and K compared to the less altered one (Hewins et al., 2014). On average, the modelled CM1s form under fairly similar W/R ratios (by mass) and solute concentrations as CM2s but average temperatures are significantly higher (108°C compared to 49°C), which suggests that elevated temperatures could be the primary driving force to form a CM1 rather than a CM2 from an unaltered CM3.

Some CMs are considered to be more altered than CM2s but less than CM1s and are labelled as CM1/2s. Five CM1/2s finds analysed by King et al. (2017) (XRD) contain 7–24 vol. % anhydrous silicates (olivine and pyroxene), 71–88% phyllosilicates (36–68% Mg-serpentine and 18–37% Fe-cronstedtite), 1.6–2.9% magnetite, 1.1–2.3% sulphides and 0.7–1% calcite. Despite not detected by King et al. (2017), dolomite has been found in various CM chondrites of lower petrologic subtype (Lee et al., 2014). Carbonate precipitation sequences are difficult to establish but dolomite is suggested to form after aragonite and early types of calcite but before type 2 calcite. Hence, dolomite can be expected to be mostly found in CM1/2s whereas type 2 calcite in CM1s is observed to replace dolomite (Lee et al., 2014). Modelled CM1/2-like systems are rare (5 out of 3720 total systems) and notably only from at 105°C, which is likely the temperature required for coexisting dolomite and cronstedtite. None of the systems contain magnetite, which is attributed to the fact that no systems contain magnetite, cronstedtite, dolomite and calcite in equilibrium. Dolomite is present in an abundance of up to 2.2%, which is in good agreement with the highest quantity of dolomite in CM chondrites (2.3% in ALH 83001 (Lee et al., 2014)). Modelled calcite abundances (0.5–1 vol%) are in excellent agreement with

(King et al., 2017) (0.7–1 vol%) but slightly lower than reported in ALH 83001 (1.5 vol%) (Lee et al., 2014). Sulphides (1.7 vol%) are also within the range of abundances reported by King et al. (2017) (1.1–2.3 vol%) but do not reach the high abundances in some of the CM1/2s. Contrary to the modelled CM2- and CM1-like systems, all the modelled CM1/2 have rhodochrosite instead of tephroite as a Mn-phase. Whereas the temperature is fairly similar to CM1s, average W/R ratios (by mass) and especially solute concentrations are slightly higher, likely due to the greater initial CO_2 abundances required by dolomite, which also favours the formation of rhodochrosite over tephroite. (Telus et al., 2019) observed that early forms of calcite in CM chondrites are Mn-poor whereas later calcite that precipitates at similar times to dolomite at ~125°C is more Mn-rich. Overall, modelled CM1/2s appear distinct from CM2s and CM1s as they require differences in W/R ratio (by mass) and/or solute concentration and also a specific temperature (105°C) to form. Considering the scarcity of modelled CM1/2s compared to documented CM1/2 meteorites, it is likely that further factors are required for CM1/2 meteorites such as an early termination of aqueous alteration or incomplete equilibration of the system, which would enable coexisting cronstedtite, dolomite and magnetite.

Overall, the equilibrium models are able to replicate CM chondrite mineralogies fairly well with aqueous alteration predicted over a broad range of temperature, W/R ratios (by mass) and solute concentrations with pH values between 8.6 and 12.5 and pe values between -10.6 and -6.6. However, especially the number of CM1/2- and CM1-like systems is limited, and some minerals reported from meteorites such like magnetite in CM2s are missing in the systems of this scenario. The lack of magnetite is likely coupled to the high abundance of cronstedtite at low temperatures, preventing the formation of magnetite.

2.4.2 Are CM chondrites more or less likely to form under different scenarios?

A potential way to address the limitations of the default scenario is by modelling CM chondrite alteration under different conditions/scenarios. As described in section 2.3, all five modelled scenarios yield CM chondrite-like systems, albeit with differences in the number of systems and mineralogy, and in the predominance of different CM petrologic types. Notably, only three of the scenarios (default, more NH_3 and Asuka) created a small number of CM1/2-like systems. The absence of this petrologic type in the NoGas and HighP scenario is likely the result of cronstedtite forming only at lower temperature, perhaps due to more stable magnetite at higher temperature, whereas dolomite in general requires 105°C or a higher temperature. CM1-like systems are, with the exception of the NoGas scenario, rarer than CM2s but more abundant compared to the default system.

The lack of a coexisting gas phase in the NoGas scenario is responsible for more reducing conditions overall, which would explain the abundance of fewer oxidised phases like magnetite and more reduced phases like troilite and metal. In the default scenario, the dominant gaseous species is CH_4 followed by H_2O, suggesting that the absence of a gas phase increases the abundance of C in solution which in turn

could be responsible for the lower average solute concentration required for CM-like systems. On the other hand, the more reduced conditions caused by more dissolved CH_4 are likely the reason for the higher W/R ratios (by mass) for CM-like systems in this scenario. Especially for the CM2 chondrites, those values are on average unrealistically high compared to literature values (e.g., Verdier-Paoletti et al., 2019; Alexander et al., 2019) and make this scenario rather unsuitable to represent CM chondrites. On the other hand, the occurrence of dolomite in some CM1-like systems is more realistic than the default scenario. Whereas Zolensky et al. (1997) and King et al. (2017) found no dolomite in CM1 chondrites, Lee et al. (2014) reported some dolomite in CM2.0s (CM1s) Meteorite Hills 01070 and Scott Glacier 06043, suggesting that dolomite in some CM1s has escaped replacement by calcite. Overall, CM1-like systems in this scenario appear to be more akin to CM1 meteorites whereas modelled CM2s are less realistic.

The more NH_3 scenario resulted in high numbers of both CM2- and CM1-like systems and is also the only scenario to have some modelled CM2s with magnetite in realistic abundance. Other factors that make this scenario more favourable for CM chondrite formation are more occurrences of rhodochrosite in CM1s and fewer occurrences of andradite overall as well as additional dolomite in one CM1-like system. This scenario is also notable in yielding low temperature dolomite, although it does not occur in any CM-like system. Nonetheless, the occurrence at dolomite between 1-10°C is surprising and could perhaps be associated with research about terrestrial dolomite formation conditions. For example, Chang et al. (2020) suggest that dolomite could precipitate at lower temperatures (<60°C) and Kim et al. (2023) also proposed that dolomite could form at lower temperature through cycles of super- and undersaturation. Another favourable aspect of this scenario is the greater influence of temperature on mineral stability and abundance (notably calcite abundances) which might explain the formation of different meteorites as function of temperature alone. On the other hand, the higher concentration of aqueous NH_3 creates a more reducing and more alkaline fluid which is likely responsible for the overall higher W/R ratio (by mass) and solute concentration required for the CM-like systems.

The highP scenario bears similarities to the NoGas and more NH_3 scenarios in having more reduced phases, as also noted by e.g., Zolotov (2012), which is likely the result of a smaller amount of gas generated due to the higher pressure. In common with the NoGas scenario, the instability of cronstedtite at higher temperatures prevents the formation of CM1/2-like systems. Instead, this scenario yields the highest number of CM1-like systems that also have the widest interval of temperature, W/R ratio (by mass), solute concentration, pH and pe across all scenarios. CM2-like systems, on the other hand, are more akin to the default scenario with no additional magnetite. Temperatures beyond 150°C that are possible with this scenario are not represented in any CM-like system due to the overabundance of magnetite and occurrence of atypical phases, such as talc and ferropericlase.

Finally, the Asuka scenario shows that differences in the starting composition do not have a major influence on the modelled systems, as also observed by Zolotov et al. (2012), because the mineralogy

of its CM-like systems is identical to the default scenario. However, the scenario appears to be less favourable overall for the formation of CM chondrites as the number of CM-like systems is reduced and calcite, dolomite and cronstedtite are less abundant, which is likely caused by the lower abundance of Ca and Fe in Asuka 12169 than in DOM 08006. One positive aspect of this scenario, however, is the more oxidised starting mineralogy that requires less water for CM-like alteration, resulting in W/R ratios (by mass) that are, on average, more comparable to W/R ratios (by mass or volume) suggested by, for example, oxygen isotopes (e.g., Verdier-Paoletti et al., 2019). Also notable is that sulphides are more abundant and especially the higher abundance of pyrrhotite compared to pentlandite is more typical for a CM chondrite.

Overall, perhaps apart from Asuka, the different scenarios result in systems that are a better match for CM chondrites than the default scenario. The more NH_3 is arguably the best scenario, as it results in both more realistic CM2 (with magnetite) and CM1 chondrites (with dolomite), while also yielding some CM1/2-like systems. However, none of the scenarios fully reflect CM chondrite mineralogies and inferred alteration conditions; especially average W/R ratios (by mass) are too high, most modelled CM2 chondrites lack magnetite and most CM1 chondrites lack dolomite. The different scenarios are not necessarily mutually exclusive, however, and a combination of, e.g., highP, default and more NH_3 scenarios on a single, fairly large parent body might be possible, where the highP environment with CM1 chondrites would be in the core and heterogeneous accretion of NH_3 and CO_2 ices might result in the more NH_3 scenario.

The high abundance of CM1-like systems in the highP and NoGas scenario might provide a further explanation for why CM1 chondrites are more altered than CM2s because a lack of gas or a smaller gas volume could prevent an early escape of gaseous H_2 and H_2O that would terminate further alteration of a CM chondrite. Dolomite is particularly abundant in CM1-like systems of the NoGas scenario which is probably caused by the higher concentration of aqueous DIC that could facilitate dolomite formation, and in reality might prevent replacement of dolomite by calcite caused by lower concentrations of carbonate species. Across all scenarios and petrologic types, CM chondrites could form within 1–140°C, W/R ratios (by mass) of 0.3–5, solute concentrations of 0.2–2 m CO_2, pH between 8.5 and 12.6 and pe between -10.8 and -6.6. Figure 2.4 shows a simple model of a CM parent body where CM chondrites of different petrologic type are located in different regions. Direct comparisons with other geochemical modelling studies are difficult, as most of their objectives and results differ significantly from this model. Results are in fairly good agreement with Neveu et al. (2017) in terms of mineralogy and pH values and are also broadly consistent with other modelling studies of carbonaceous chondrite alteration such as Shibuya et al. (2024).

2.4.3 Limitations and applicability of the models

Equilibrium modelling and geochemical modelling usually consider terrestrial settings, such as shale-CO_2 interactions (Fatah et al., 2022) or reaction of basaltic rocks with seawater (Marieni et al., 2020). Hence, databases for geochemical modelling are typically tailored towards terrestrially relevant phases, whereas some minerals of importance in CM chondrites, such as pentlandite and tochilinite, are missing, likely due to a lack of experimental data. Tochilinite as its Mg-endmember has been implemented as a mixture of brucite and troilite by (Neveu and Desch, 2015) for geochemical modelling of Ceres' surface. Earlier forms of the models in our study also implemented tochilinite as a mixture of brucite and troilite

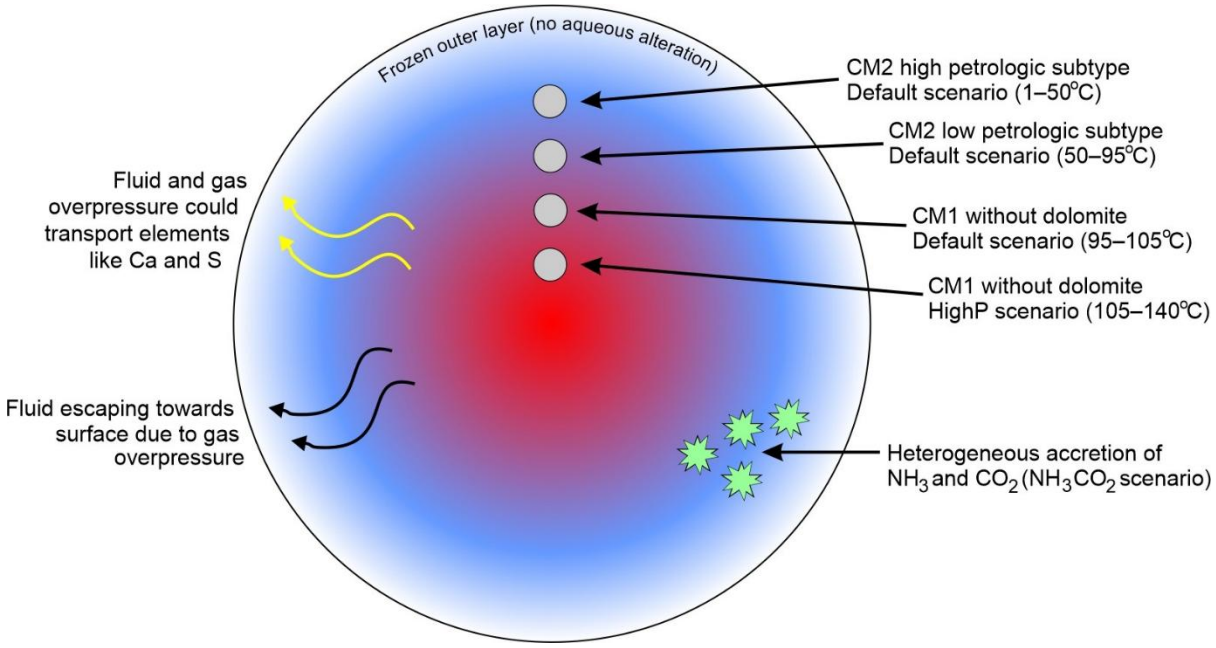

Fig. 2.4. Schematic illustration of a possible CM chondrite parent body characterised by a stratified temperature. Higher temperatures in the core generate CM1 chondrites with or without dolomite, depending on the pressure. Cooler conditions closer to the surface result in CM2s of different petrologic subtype, depending on the temperature. Gas generated from aqueous alteration can redistribute mobile elements like Ca or S to more shallow areas or can terminate aqueous alteration due to fluid escaping to space. CM1/2s could also form close to the core but also require elevated W/R ratios and/or fluid concentrations. Heterogeneous accretion of ice or dust could further influence aqueous alteration conditions.

but tochilinite was too abundant and formed at unrealistically high temperatures. Hence, it seemed more suitable to instead consider co-occurring cronstedtite and pyrrhotite/troilite as a proxy for tochilinite intergrown with cronstedtite (TCI).

Another limitation of the models arises from not implementing organic carbon in the starting material or precipitate. Consequently, carbonate formation requires dissolved CO_2 in the fluid, whereas other studies (e.g., Neveu et al., 2017) that included organic carbon in the starting material found that carbonates can form in systems with initial pure water. A lack of organic carbon in secondary phases could also be responsible for an overabundance of carbonates and methane gas, especially for higher solute concentrations, meaning that the modelled carbonate values likely represent upper values. Having organic carbon instead of dissolved CO_2, however, would also result in a more reducing fluid. Assuming that the formation of CM chondrites is mainly controlled by a suitable range of pH and pe, modelled

W/R ratios (by mass) might be shifted to higher values as more of the more acidic fluid is required to neutralise the alkalinity produced by the aqueous alteration. However, considering that the modelled W/R ratios (by mass) are already higher than suggested by petrological studies (e.g., Verdier-Paoletti et al., 2019), implementing organic matter in the model would likely have a negative impact on estimated aqueous alteration conditions. The formation of methane, contrary to other studies such as Zolotov (2012, 2014) was also not suppressed, which could pose a further limitation to our models. A major limitation is also the lack of solid solutions in the models. Furthermore, PHREEQC requires sufficient water for equilibrium calculations, W/R ratios (by mass) lower than 0.2 were not possible in the models. As no calculations with a W/R ratio of 0.2 showed a CM-like mineralogy, it seems unlikely that lower W/R ratio values are of interest, even though some software like GEOCHEQ (see e.g., Zolotov et al., 2006) are capable of carrying out calculations with insufficient water for equilibration.

Most simulations with a W/R ratio (by mass) of 1 or lower yield ionic strengths (I) that exceed the limit of the extended Debye-Hückel equation of I≤0.1 mol/kg and values of >1 mol/kg are obtained for simulations with 0.2 W/R ratio (by mass). Systems with 0.2 W/R ratios (by mass) should therefore be only qualitatively analysed, and the systems with ionic strengths between 0.1 and 1 mol/kg should be cautiously interpreted. While there are databases for PHREEQC that allow for modelling of higher ionic strengths with specific ion interaction theory or pitzser equations (e.g., *sit.dat* and *pitzser.dat*), we deemed those databases too limited in their number of phases and species. However, a sensitivity analysis with the *sit.dat* database for a simplified serpentine system showed that results are fairly similar to the customised database that uses the extended Debye-Hückel equation, even for >1 molal ionic strengths.

Some chemical elements like Ti or Cu were included in other modelling studies (e.g., Neveu et al., 2017) but were disregarded in the present study. As mentioned in section 2.2, the starting composition was based on the chemical composition of DOM 08006 analysed by Patzer et al. (2021) who focused on major and minor elements but not on trace elements like Cu. Although Ti was included in their analysis, geochemical information about Ti-minerals in databases is limited (Zhang et al., 2020) and therefore, no Ti phases were included in our models. In general, inclusion of elements present at <1 wt.% is of rather limited benefit to the model results, as in reality, those elements would either partition as trace elements in other minerals like carbonates or form separate phases whose abundance is too low to be detected by XRD; in addition, there is also little information available on the form in which those elements would be present in the starting material.

Despite supressing minerals like zeolites and most anhydrous silicates from precipitating by excluding them from the models, many systems still contain minerals that are not or only rarely found in CM chondrites. The most notable example is andradite which appears in ~50% of the CM-like systems (more commonly in the default and more rarely in the NoGas scenario). Its abundance appears to be coupled to calcite: systems with abundant calcite have little or no andradite and vice versa. In reality,

Ca could be present in traces or forming solid solutions with phyllosilicates, or the dissolution of Ca-bearing primary minerals may be inhibited, which would lower the amount of Ca available to form secondary minerals. A similar mineral, hydroandradite, has been detected in the CM falls Kolang and Shidian (Jenkins et al., 2024). Alternatively, Ca might be able to leave or enter a system, which could be supported by the fact that some meteorites contain more calcite than yielded from DOM 08006 (e.g. 2.3% in LON 94101 (Lee et al., 2014; Alexander et al., 2015)), whereas CM1s are often reported to have fewer carbonates than CM2s (King et al., 2017). Evidence for the mobility of Ca could also be metre long bright veins on asteroid Bennu which were interpreted to be mainly calcite (Kaplan et al., 2020). Assuming that CM1s could be genetically related to CM2s, Ca could be leached from the former and transported to the latter in a fashion that could resemble the H_2 transport model from (Shibuya et al., 2024). Aqueous alteration would start in the centre of the CM chondrite parent body where high temperatures of ~100°C can be sustained long enough for extensive aqueous alteration that would leach mobile elements like Na and Cl and perhaps also less mobile elements like Ca and S. As described in the previous section, most systems generate a separate gas phase whose pressure might be high enough to facilitate fracturing through which a fluid could be transported outwards, as also suggested by Lee et al. (2013). That fluid, together with freshly molten ice, would interact with yet unaltered CM3 material to make CM2s with similar values of W/R ratios (by mass) and solute concentrations compared to CM1s. However, conditions might have been slightly colder, either due to less available radiogenic energy, more heat loss due to alteration taking place closer to the asteroid surface or aqueous alteration was terminated early before peak temperatures could be reached. The latter could be caused by fracturing due to gas overpressure, similar to the CM1s or due to fractures caused by collisions on the parent body, which would facilitate the transport of liquid water and gas to the asteroid surface and terminate water-rock interaction.

2.4.4 Could CI chondrites be from a similar starting material as CMs but altered under different conditions?

CI chondrites typically contain 81–84% mixed serpentine and saponite, 6–10% magnetite and 4–7% sulphides with some meteorites also containing 2–3% dolomite and 3% olivine (in vol%, by XRD) and some sulphates (King et al., 2015). Analysis of returned samples from CI-like asteroids Ryugu and Bennu reveal additional minor and rare phases (breunnerite, hydroxyapatite, chlorite, Mg-Na phosphates, Ca-carbonate, chromite, ilmenite, spinel, zincblende, cubanite and daubréelite (Nakamura et al., 2022; Lauretta et al., 2024). As well as their mineralogy, CI chondrites also differ from CM chondrites in having no chondrules, although small objects that are likely microchondrules have been found in Ryugu samples (Nakamura et al., 2022). Past modelling studies explored the possibility of a common CM-CI parent body. For example, Palguta et al. (2010) simulated aqueous alteration with a reactive transport model and found that CI chondrites could originate from the core, and CM chondrites from more shallow depths of the same parent body. However, this study used a fairly simplified

mineralogy with serpentinization of forsterite being the only reaction caused by aqueous alteration. Considering that many of the modelled systems of this study yield saponites, dolomite and abundant magnetite it might be suitable to test whether both CM and CI chondrites could originate from a similar starting material (i.e., a CM3 or CO3 like DOM 08006). In other words, even though CI chondrites were not the focus of the models, it can be discussed whether aqueous alteration of a CM-like starting composition can result in CI-like chondrites (which has already been showed by e.g., Palguta et al. (2010)) and how the alteration conditions differ from CM chondrites.

Based on the aforementioned mineralogy of CI chondrites, modelled CI-like systems should have more than 5% saponite (combined Mg-saponite and Fe-rich saponite), more than 5% Mg-serpentine, nonzero magnetite, dolomite and pyrrhotite but less than 0.5% calcite and magnesite. The different scenarios yield between 10 (more NH_3 scenario) and 40 (default) CI-like systems (more than CM1/2 but less than CM2 and CM1). The average mineralogy depends on the scenario but appears to be fairly similar to CI chondrite samples; the CI-like systems from the default scenario contain on average 41% Mg-saponite (no Fe-rich saponite), 28% lizardite, 12% magnetite, 3% dolomite, Na-bearing saponite, cronstedtite and talc, 2% greenalite, 1.3% polydymite and K-bearing saponite, 0.7% pyrrhotite and hydroxyapatite, 0.4% chromite, 0.25% rhodochrosite and <0.1% clinochlore, magnesite, calcite and linnaeite (see Table 2.10 for scenario-specific mineralogies. The high abundance of dolomite and magnetite is likely responsible for the scarcity of calcite and greenalite, respectively. For most systems saponite is more abundant than serpentine, although some systems contain fairly equal abundances. Average W/R ratios (by mass) (1.12) and solute concentrations (1.51 mol/kg CO_2) are quite similar to CM-like systems but W/R ratios (by mass) have a narrower range (0.5–3) (Table 2.10), probably caused by the combined effect of Mg-saponite that requires elevated W/R ratios (by mass) and lizardite that disappears at high W/R ratios (by mass). Thermochemical models of Ryugu samples yielded slightly lower W/R ratio values (by mass) (0.2–0.9) (Nakamura et al., 2022). Average formation temperatures are around 130°C with minimal and maximum values of 105°C and 150°C or higher, respectively, whereas CM chondrite formation temperatures are capped at lower values in the models. In short, CI chondrites could form with similar W/R ratios (by mass) and solute concentrations, although temperatures on average were likely higher compared to CM chondrites. However, sulphides in the modelled CI-like systems are present in lower concentrations (~2%) compared to CI samples and are also Ni-rich, indicating that CI chondrites either originated from a more S-rich starting composition than DOM 08006 (more accreted sulphides or S-bearing ice) or sulphur was redistributed from a different part of the parent body and transported to the CI chondrite alteration zone. Some CM2s that were examined by Howard et al. (2011) have less than 1% sulphides, although all those meteorites are finds and a sulphide deficit might be attributed to terrestrial weathering rather than leaching of sulphur on the parent body. Additional factors that differentiate CI from CM chondrites like lower abundance of chondrule or their pseudomorphs, higher abundance of volatile elements and oxygen isotopes make it unlikely that CI and CM chondrites

could originate from the same parent body. However, it is notable that minerals like saponite and magnesite do not require a different starting composition but are rather likely the product of aqueous alteration at higher temperatures. In other words, there might be some meteorites that have a CI-chondrite like mineralogy (mixed serpentine and saponite and abundant dolomite and magnetite) but are otherwise similar to CM chondrites in terms of oxygen isotopes, chondrule abundance etc; one of those meteorites might be the C2 Tagish Lake (Zolensky et al., 2002).

Table 2.10
CI-like characteristics across different scenarios (numbers in brackets denote mean values).

Feature/Scenario	Default (10 bar)	NoGas (10 bar)	More NH_3 (10 bar)	HighP (200 bar)	Asuka 12169 (10 bar)
Number of systems	40	29	10	36	39
Temperature range (°C)	105–150 (131)	120–150 (136)	105–150 (128)	120–200 (147)	105–150 (132)
W/R ratio range	0.7–3 (1.27)	0.6–2.5 (1.03)	1–2.5 (1.15)	0.6–3 (1.23)	0.5–2.5 (0.93)
Initial CO_2 concentration range (mol/kg))	0.5–2 (1.36)	0.5–2 (1.48)	1–2 (1.9)	0.5–2 (1.36)	0.5–2 (1.44)
pH range	7.56–8.52 (8.06)	7.85–8.51 (8.17)	7.55–8.52 (8.27)	7.19–8.39 (7.97)	7.70–8.60 (8.17)
pe range	-6.46–-5.41 (-8.06)	-6.75–-5.97 (-6.34)	-6.42–-5.39 (-6.18)	-6.55–-5.28 (-6.06)	-6.56–-5.55 (-6.08)
Mg-serpentine (vol.%)	23–31 (28)	29–39 (32)	24–30 (29)	23–40 (29)	22–32 (25)
Mg-saponite (vol.%)	34–45 (41)	18–43 (35)	37–45 (39)	17–46 (39)	24–51 (42)
Magnetite (vol.%)	5.9–16 (13)	7.4–13 (12)	8.4–15 (12)	7.2–16 (13)	0.94–14 (13)
Calcite (vol.%)	0–0.45 (0.013)	0–0.49 (0.066)	0	0–0.42 (0.012)	0–0.49 (0.16)
Dolomite (vol.%)	2.7–3.5 (3.4)	2.6–3.4 (3.3)	3.4–3.5 (3.4)	2.7–3.5 (3.4)	1.8–2.7 (2.4)

2.5 Conclusions

Equilibrium modelling of the interaction of a cometary fluid with the CM3 proxy DOM 08006 can be used to evaluate the conditions of aqueous alteration on the parent body/bodies and examine the factors controlling the formation of CM chondrites of different petrologic type. CM-like systems that resemble CM chondrite mineralogies were found across a wide range of temperature (1–140°C), W/R ratio (by mass) (0.3–5), solute concentration (0.2–2 m CO_2), pH (8.5–12.6) and pe (-10.8 – -6.6). The main factor differentiating between CM1 and CM2 chondrites is likely temperature, as the former require 80°C or more whereas latter are formed around 50°C. As the CM1-like systems are preferably formed by scenarios with little to no gas volume it is also likely that CM1 chondrites were produced deeper in the CM parent body in areas less prone to gas overpressure and temperature and duration of aqueous alteration could therefore be higher. The CM1/2 chondrites were rarely found in the models and could have formed due to slightly elevated W/R ratios (by mass) and/or solute concentrations and require very specific temperatures (105°C). CM and CI chondrites, whereas they are very unlikely to originate from the same parent body, could both have formed from similar primary materials but the latter likely experienced higher temperatures and solute concentrations. Hence, meteorites with chondrules and CM-like isotopic compositions but with CI-like minerals (saponite-serpentine, abundant magnetite and

dolomite etc.) are likely to exist. Finally, at least some differences between modelled and observed CM mineralogies can be attributed to non-equilibrated aqueous alteration that could be studied with kinetic modelling.

CRediT authorship contribution statement

Robin Haller: Conceptualization, Methodology, Software, Formal analysis, Investigation, Resources, Data curation, Funding acquisition, Writing – Original Draft Preparation, Writing – Review & Editing. Martin Lee: Conceptualization, Writing – Review & Editing, Supervision, Project administration

Data availability

Data are available through MendeleyData at doi:10.17632/vf9n9f2z9z.1.

Appendix A. Supplementary Material

Table S2.1 shows the mineralogy of DOM 08006 and Asuka 12169 inferred from their elemental composition. Table S2.2 shows the elemental composition (wt.%) of DOM 08006 (Patzer et al., 2021) and Asuka 12169 (Patzer et al., 2023).

Acknowledgments

This research was funded by the UK Science and Technology Facilities Council through grant ST/W001128/1. For the purpose of open access, the author(s) has applied a Creative Commons Attribution (CC BY) licence to any Author Accepted Manuscript version arising from this submission.

2.6 Supplementary Materials

Table S2.1
Mineralogy of DOM 08006 and Asuka 12169 calculated from their bulk elemental composition (see Table S2.2).Molar abundances are scaled to 1 kg of rock.

Mineral	DOM 08006 (vol.%)	Asuka 12169 (vol.%)	DOM 08006 (mol/kg rock)	Asuka 12169 (mol/kg rock)
Forsterite	38.2	37.08	2.413	2.382
Fayalite	11	10	0.656	0.606
Enstatite	18	18	1.592	1.619
Ferrosilite	3.5	3.5	0.294	0.299
Diopside	0.9	0.5	0.038	0.021
Anorthite	4.1	3	0.113	0.084
Iron	4.175	2.5	1.628	0.992
Nickel	0.55	0.52	0.231	0.222
Troilite	3	5.3	0.435	0.782
Millerite	0.17	0.17	0.028	0.028
Spinel	0.5	1	0.035	0.071
Gehlenite	1	0.5	0.031	0.016

Albite	2.57	4.05	0.071	0.114
Chromite	0.6	0.58	0.038	0.037
SiO2(am)	3.2	3.705	0.305	0.359
Tephroite	0.29	0.33	0.017	0.020
Fe(OH)2	5.65	6.15	0.591	0.655
CaAl-Pyroxene	0.4	0.8	0.017	0.035
Co-spinel	0.085	0.085	0.006	0.006
K-feldspar	0.56	0.71	0.014	0.018
Apatite	0.85	1.07	0.018	0.023
Ca-Perovskite	0.7	0.45	0.071	0.046

Table S2.2

Bulk elemental composition (wt.%) of DOM 08006 (Patzer et al., 2021) and Asuka 12169 (Patzer et al., 2023).

Element (wt.%)	DOM 08006	Asuka 12169
Na	0.19	0.3
Mg	14.23	13.89
Ca	1.58	1.31
Fe	24.84	23.54
Ni	1.56	1.49
Mn	0.19	0.22
Al	1.43	1.53
Cr	0.37	0.36
Si	15.94	15.91
O	38.02	37.26
S	1.13	3.68
Co	0.09	0.09
K	0.07	0.09
P	0.15	0.19

3 Timescales of CM carbonaceous chondrite aqueous alteration determined by kinetic modelling

Robin L. Haller[1,*], Martin R. Lee[1], Mark E. Hodson[2]

[1]*School of Geographical and Earth Sciences, University of Glasgow, Glasgow G12 8QQ, UK*

[2]*Environment Department, University of York, York YO10 5NG, UK*

*Corresponding author: *E-mail address:* robin.haller123@gmail.com

This chapter represents a first manuscript prepared for submission to *Geochimica et Cosmochimica Acta* with additional corrections and differs from the published paper (https://doi.org/10.1016/j.gca.2026.04.022)

3.0 Abstract

Mighei-like (CM) meteorites are the most abundant group of carbonaceous chondrites. They display a wide range of degrees of aqueous alteration, from very mild to near complete, as demonstrated by the relative abundances of phyllosilicates and surviving anhydrous silicates. The reasons for the range of alteration are debated, and must reflect variations within the parent body(ies) of one or more of water/rock ratio, temperature, and timescale. The least understood is timescale, and so to constrain the duration of aqueous alteration and to investigate precipitation conditions of key CM minerals, we created kinetic models with the software PHREEQC. These models simulated alteration of the CM3 proxy Dominion Range (DOM) 08006 by an aqueous fluid for different values of water/rock (W/R) ratio (by mass) and temperature over the timespan of 10^{-5}–10^{5} years with incremental time steps. Additional laboratory experiments in which chips of DOM 08006 were reacted with either pure water or a carbonated aqueous solution under reducing conditions were conducted to validate parts of the models and to evaluate formation conditions of calcite. The models suggest that regardless of their petrologic type, CM chondrites could have been altered over timescales ranging from months to ~10,000 years depending on temperature. The more highly altered CM chondrites that contain magnetite instead of cronstedtite would have needed temperatures of at least 100 °C but not necessarily different W/R ratios compared to less altered CM2s. Minimally altered CM chondrites like Asuka 12169 could have experienced aqueous alteration at ~1 °C and W/R ratios of ~3 or higher. Significant quantities of calcite only form in laboratory experiments with a carbonated solution, suggesting that at least for early formed calcite, aqueous carbonate was sourced from accreted C-bearing ice instead of intrinsic organic carbon. According to the models, a typical CM2 chondrite could have been altered within ~1,000 years at 50 °C and 0.8 W/R ratio.

Keywords: CM chondrites, kinetic modelling, CM parent body, CM petrologic type, aqueous alteration

3.1 Introduction

The Mighei-like (CM) meteorites are the most abundant group of carbonaceous chondrites and were aqueously altered on their parent body(ies) early in the history of the solar system (Brearley et al., 2006; Suttle et al., 2021; Lee et al., 2025). The extent of aqueous alteration ranges from nearly unaltered, as demonstrated by the CM3 Asuka 12169 (Kimura et al., 2020) to the extensively altered CM1s (see e.g., Zolensky et al., 1997; King et al., 2017) within which only few vol.% of primary solid phases remain. Most CM chondrite samples are classified as CM2s with moderate levels of alteration. With sufficient water and time, all primary anhydrous silicates (mainly olivine and pyroxene) should react to produce phyllosilicates (typically serpentine); hence, several mechanisms could have prevented a complete equilibration to explain the high abundance of CM2s. A possibility could be fracturing and disruption due to high internal gas pressures (Wilson et al., 1999); in that case, CM1s could have experienced higher temperatures than CM2s, leading to more extensive alteration. If aqueous alteration ended prematurely, the question remains when the terminating event occurred, or, in other words, how much time is needed for aqueous alteration of CM chondrites. It is also possible that the low permeability of CM chondrites (Bland et al., 2009) prevented a homogeneous distribution of water, which could have created environments with insufficient water for the complete reaction of anhydrous silicates to phyllosilicates.

In addition to anhydrous silicates, other indications of non-equilibrated aqueous alteration in CM chondrites are multiple generations of minerals (minerals forming during different stages of aqueous alteration), with one of the best examples being calcite (e.g., Tyra et al., 2012; Lee et al. 2014; Tyra et al., 2016). Different types of calcite are proposed based on their morphology and petrography (Tyra et al., 2012; Lee et al., 2014); one open question is whether those different types were caused by an evolving single fluid or by an external fluid derived from e.g., a collisional event (Rubin, 2012). $^{53}Mn/^{53}Cr$ ages of carbonates (calcite and dolomite) examined by (Fujiya et al., 2012) in four different CM chondrites suggest that calcite precipitation was relatively late (4,563.4+0.4/-0.5 million years ago, relative to the LEW 86010 angrite time anchor (Pb-Pb age of 4557.8 +/- 0.5 Ma)(Lugmair and Shukolyukov, 1998) and short-lived (within 1 Myr). Whether different types of calcite are also similar in age, however, is unclear.

Laboratory experiments can be useful to constrain the time required for aqueous alteration of different materials and to investigate early alteration products. Le Guillou et al. (2015) showed that amorphous silicates, which are present in unaltered carbonaceous chondrites such as Asuka 12169 (Kimura et al., 2020) and Paris (Leroux et al., 2015) can be altered within hours at 190 °C. Experiments on meteorite chips have also been carried out; Suttle et al. (2022) reacted samples of CO3.2 Kainsaz with water under elevated temperatures and pressures and Jones and Brearley (2006) used cubes of CV3 Allende for similar experiments at 100–200 °C and based on their results, estimated that 5,000–10,000 years are required for the formation of phyllosilicates at 25 °C. Igami et al. (2021) used a mixture of synthetic

amorphous olivine and enstatite for their hydrothermal experiments and a mixture of synthetic materials was also used by Fabre et al. (2024) to experimentally model the alteration of a CM3 and by Vacher et al. (2019) to investigate conditions of tochilinite and cronstedtite formation. Also relevant to CM parent body alteration are terrestrial serpentinization experiments carried out under reducing (e.g., McCollum et al., 2022) or even oxidising conditions (e.g., Fuhr et al., 2022). Details about the CM chondrite aqueous alteration history, however, are difficult to replicate with experimental studies; especially low temperature conditions might require timespans that are not feasible for laboratory experiments; based on forsterite hydration experiments from Martin and Fyfe (1970) and Wegner and Ernst (1983), Velbel et al. (2012) suggested that serpentinization could require timescales of ~120 days to ~15 years at room temperature.

With the help of geochemical modelling, longer timespans and a more detailed view of the mineralogy and aqueous chemistry are possible. Equilibrium models have been used to investigate various settings of aqueous alteration of CMs (e.g., Zolensky et al., 1989; Rosenberg et al., 2001), CI chondrites, and related asteroids and icy worlds (e.g., Zolotov and Shock, 2004; Zolotov, 2007, 2009, 2012, 2014, 2017, 2020; Castillo-Rogez et al., 2018; Nakamura et al., 2022). However, to investigate the evolution of aqueous alteration and model non-equilibrated mineral assemblages, kinetic models are preferable. While kinetic models have been used for different terrestrial systems like carbon sequestration (e.g., Fatah et al., 2022; Fuhr et al., 2022), to our knowledge they have rarely been applied to questions in planetary science (Kopp and Humayun, 2003). More commonly, reactive transport models were used to investigate the evolution of parent bodies (e.g., Palguta et al., 2010; Bland and Travis, 2017; Neumann et al., 2021); however, those models oftentimes lack the spatial and mineralogical detail seen in CM chondrite thin section.

The aims of this study are to provide new insights into how CM chondrites evolved during aqueous alteration and investigate the timescales and conditions necessary to produce CM chondrites of different petrologic type and mineralogy. Kinetic models in PHREEQC (Parkhurst, 1995; Parkhurst and Appelo, 1999, 2013), simulating the aqueous alteration of the CM3 proxy CO3.00 Dominion Range (DOM) 08006 were built to investigate formation conditions of key minerals in CM chondrites (i.e., calcite, dolomite, magnetite) as a function of time, temperature and W/R ratio (by mass). With the models, we also aim to test whether multiple generations of minerals like calcite can be produced by a homogeneous fluid solely due to differences in time (differences in solute concentrations during different times of aqueous alteration) and potentially also temperature and W/R ratio. With laboratory experiments utilising DOM 08006 chips, we can cross-validate modelling results but also test whether calcite/carbonate formation in CM chondrites requires an external C source like accreted CO_2 ice or whether the internal insoluble organic matter is sufficient to form carbonates within the duration of the experiments.

3.2 Methods

3.2.1 Kinetic Modelling

The interaction of a "CM chondrite precursor" with an aqueous fluid was simulated with kinetic models in a closed Al, C, Ca, Cl, Fe, H, Mg, Mn, N, Na, O, S, Si system (no loss or gain of water or gas) at a pressure of 10 bar using the geochemical software PHREEQC. Within the software, the solid component is represented with the keyword KINETICS which requires the amount of each solid phase (in mol) and its surface area (SA) (in m^2/kg water). The solid phases were added based on the mineralogy of the CO3.00 DOM 08006 (Alexander et al., 2018) (Table 3.1), which is deemed to be a suitable CM3 proxy due to its pristine nature (Davidson et al., 2019) and overall similarity of CO to CM chondrites (see e.g., Greenwood et al., 2023; Floyd et al., 2024). As modal mineralogies by XRD generally only include major phases (>1 vol.%), we added minor phases such as tephroite, anorthite, gehlenite to the models; their initial abundance was calculated based on the chemical composition of DOM 08006 (Patzer et al., 2021). Anorthite and gehlenite are commonly found in calcium-aluminium inclusions (CAIs) (e.g., Suttle et al., 2021), whereas tephroite was chosen to represent Mn-bearing olivine. The SA of a mineral can be approximated as a function of its grain size for a known grain shape, although the specific SA is mineral dependent and would ideally be evaluated by analysis of the sample using techniques such as 2D- or 3D-imaging (e.g., Beckingham et al., 2017) or gas adsorption (e.g., Brantley and Mellott, 2000). Reported specific SAs in the literature focus mostly on terrestrial rock-forming minerals and can show orders of magnitude differences depending on the study and analysis technique (e.g. Beckingham et al., 2017; Awolayo et al., 2022). Thus, as a first approximation, we calculated the specific SA of the initial phases based on a trimodal grain size distribution depending on whether the phase is predominantly present in chondrules (20 µm), as fine-grained material (fine-grained rims (FGRs) and matrix, 0.1 µm) or either in both of these materials or in refractory inclusions (RIs, 0.5 µm); using a formula described by (Brantley and Mellott, 2000) with parameters for quartz yielded specific SAs of 0.2, 50 and 10 m^2/g for the three grain sizes, respectively. The total specific SA of 3.74 g/m^2, obtained by multiplying the individual specific SAs with the modal abundances, is below values for phyllosilicate-rich carbonaceous chondrites like Tarda (72.5 g/m^2) or Aguas Zarcas (16.5 g/m^2) (Garvie et al., 2024) and could therefore be suitable for a CM precursor that has no phyllosilicates. To obtain SAs in m^2 for PHREEQC, the specific SAs were further multiplied by the molar mass and abundance (in moles) of the initial phases.

The SAs are required for the calculation of the dissolution and precipitation rate of the solid phases described by the KINETICS keyword. For PHREEQC, rate expressions are tabulated in the geochemical database specified in the input file. For our kinetic models, we used a customised database based on the database *diagenesis.dat* (Zhang et al., 2020) with additional solid phases from *core10.dat* (Neveu et al., 2017). Additional dissolution rates were derived from (Zhang et al., 2019); however, some

solid phases in the input file had no rate expressions and proxies (Table 3.1) based on similarities regarding chemistry and/or reactivity were chosen instead. Other solid phases in the database were allowed to precipitate in the models except for high P and/or high T phases like amphiboles.

The aqueous fluid was modelled as water with additional C, N, S and Cl to represent accretion of additional ices of CO_2, NH_3, H_2S and HCl. Solute concentrations of 1 m (mol/kg) CO_2, 0.1 m NH_3, 0.05 m H_2S and 0.005 m HCl are based on abundances in cometary volatiles (e.g., Mumma and Charnley, 2011) as well as in other modelling studies (Zolotov, 2012; Neveu et al., 2017; Kurokawa et al., 2021; Shibuya et al., 2024). The amount of initial solid phases were kept constant at 1 kg whereas the amount of aqueous fluid was changed to represent 20 different W/R ratio (by mass) values within a range of 0.2–5. Whereas other studies using e.g., four-component modelling (Alexander, 2019) or oxygen isotopes (Verdier-Paoletti et al., 2019) generally suggest W/R ratio values of <0.75 for CM chondrites, the amount of water available for the aqueous alteration could have been higher during the parent body history. Sixteen different temperatures (1–150°C) were chosen to investigate the effect of temperature on the aqueous alteration speed and mineralogy. The kinetic models included a total of 41 timesteps from 10^{-5} to 10^{5} years in 0.25 log unit intervals. To increase the speed and the stability of the calculations, the calculated output of each timestep was used as input of the subsequent timestep, which resulted in a total modelled time of 2.78×10^{5} years. The increased computational cost of kinetics also required the change from the default Runge-Kutta to the implicit CVODE method (Cohen et al., 1996) to integrate the kinetic rate expressions. A separate gas phase was allowed to form when the pressure of the total gas volume exceeded the pressure of the system (10 bar).

Table 3.1

Solid phases used in the input file.

Mineral	vol.%	SSA (m^2/g)	Correction factor	Dissolution rate proxy
Forsterite	38.2	0.1		
Fayalite	11	0.1		
Enstatite	18	0.1	10	
Ferrosilite	3.5	0.1	10	Enstatite
Diopside	0.9	5	10	
Anorthite	4.1	5		
Iron	4.175	5	10	Magnetite
Nickel	0.55	5	10	Magnetite
Troilite	3	5		Pyrrhotite
Millerite	0.17	5		Pyrite
Spinel	1.185	5		Magnetite
Gehlenite	1	5		Zoisite
SiO2 (am)	3.2	20	10	

Fe(OH)2	5.65	20		Goethite
CaAl pyroxene	0.4	5	10	Wollastonite
Ca-perovskite	1.55	5		Anorthite
Albite	3.13	5		
Tephroite	0.29	0.1		Fayalite

3.2.2 Laboratory Experiments

A ~1 g chip of DOM 08006 was acquired from ANSMET and broken down into four chips, each weighing ~150 mg (Table S3.1); meteorite chips of similar weight have been previously used in other laboratory experiments (Jones and Brearley, 2006; Lee et al., 2006; Suttle et al., 2022). Two of the chips were placed in glass vials with 20 g pure water whereas the other two (labelled with suffix C) reacted with 20 g 0.002 M $NaHCO_3$ aqueous solution for which 0.1677 g $NaHCO_3$ was added to 1 L deionised water. Preliminary equilibrium calculations showed that a concentration of 0.002 DIC is sufficient for calcite precipitation for W/R ratios (by mass) of 100–200. To simulate an oxygen-poor environment, the solutions were subjected to a constant stream of N_2 gas until oxygen concentrations, measured by an Orion Star A223 oxygen meter calibrated with deionised water and deionised water saturated with N_2 gas, were below 1%. The glass bottles were placed in a Grant OLS200 water bath at 50°C; two of the chips (labelled Ds and DsC) reacted for 30 days, whereas the other two chips (labelled Dl and DlC) were left in the water bath for 180 days. After the end of the reaction, the chips were extracted from the glass vials, rinsed with deionised water, placed in aluminium crucibles and dried in a Thermo Scientific oven overnight (around 15 h) at 50°C. The solution in the vials was passed through filter paper (Fisherbrand QT210) into 50 ml tubes and stored in a freezer until further analysis by inductively coupled plasma optical emission spectroscopy (ICP-OES) and ion chromatography (IC). The pH of the solutions was measured before and after the reaction with a ThermoOrion 420 A+ pH/ISE meter calibrated using three buffer solutions (pH 4.0, 7.0 and 10.0) and the oxygen concentration was also measured again after the experiment.

3.2.3 Analytical Methods

3.2.3.1 ICP-OES and IC

The reacted solutions were measured by ICP-OES for Al, Ba, Ca, Co, Cr, Cu, Fe, K, Mg, Mn, Na, Ni, P, S, Si, Sr and Zn, and by IC for Cl; those elements are fairly abundant in CCs (Lodders, 2021). ICP-OES analyses were carried out at the University of York (UoY) using a Thermo Scientific iCAP PRO. For most elements, a SupelCo ICP multi-element standard solution IV was used to produce calibration standards whereas for Si and S separate single-element Sigma-Aldrich and Specpure standards were used respectively. To ensure that most leachates were within the standard concentrations, they were 10x diluted with deionised water. Ten blank solutions (deionised water) were also analysed for determining

detection limits (Walsh, 1997). Detection limits for most elements were ~1 µg/L. The accuracies (measured concentration of reference standard divided by expected value) of measurements were generally around 100%. Duplicate measurements of leachates from three meteorites chips (~10% of all measured samples) allowed for the calculation of the precision (Gill and Ramsey, 1997). Precision values were generally around 1%. Values of detection limits, accuracy and precision are in Table S3.2.

Chlorine was measured by IC (Dionex ICS-2000). The detection limit was 0.026 mg/L, the accuracy was 113% and the precision (median of four leachate duplicates and 5 mg/L standard drift) was 0.79%.

3.2.3.2 SEM of altered meteorite chips and thin sections

The surfaces of the reacted chips were investigated with a Hitachi TM4000Plus Tabletop low-vacuum, 5-20 kV SEM equipped with an Oxford Instruments EDS and AZtecOne analysis software at the University of York. Due to the low vacuum operation conditions, no sample coating was needed. Mixed SE/BSE images were obtained at 15 kV accelerating voltage for different magnification levels. EDX analyses used 20 kV acceleration voltage and were used to obtain point spectra as well as some line spectra for regions of interest and X-ray maps. Count times were restricted to 60 s. Polished and carbon coated (~20 nm) thin sections of three meteorite chips (DsC, Dl and DlC) were further studied using a Zeiss Sigma VP Field-Emission SEM at the University of Glasgow (UoG).

3.2.4 Point counting of unaltered DOM 08006 thin sections

Two thin sections from an unreacted DOM 08006 sample (DOM 08006,131 and 08006,135) were carbon coated and examined by SEM at the UoG for mineral abundances and porosity by point counting. Point counting was undertaken at 1000x magnification with EDS analyses along a regular grid with 20 kV acceleration voltage and 9.0 mm working distance. The points counted for DOM 08006,131 and DOM 08006,135 were 200 and 1000, respectively.

3.3 Results

3.3.1 Modelling results

3.3.1.1 Evolution of mineralogy

The abundance of selected minerals for different timesteps is in Table 3.2, and Table S3.3 has a list of all secondary minerals appearing in the models. The abundances in Table 3.2 were averaged across the modelled temperatures and W/R ratios, and timesteps were grouped together for simplicity. The average abundance of some minerals of interest like serpentine and sulphides increases throughout time, whereas the average abundance of other minerals like calcite and magnetite reaches a maximum before the end of the modelled time. On average, Mg-serpentine is the slowest mineral of interest to precipitate, followed by greenalite, whereas rhodochrosite reaches its highest average abundance within hours. As different temperatures and in some cases also different W/R ratios significantly influence dissolution

and precipitation kinetics, heatmaps that show mineral abundances as a function of temperature and time are more illustrative. Examples of heatmaps for minerals of interest are in Figure 3.1 (calcite), Figure 3.2 (dolomite), Figure 3.3 (cronstedtite) and Figure 3.4 (Mg-serpentine). Additional minerals, namely magnetite, greenalite, and pyrrhotite in Figures S3.1–S3.3.

Calcite can precipitate at all modelled temperatures and W/R ratios except for a ratio of 5 (Figure 3.1). At lower W/R ratios, it generally precipitates within hours but dissolves after a few months whereas for higher ratios, calcite precipitates later and remains stable. Even when stable, abundances are often highest after some years to decades, and for some systems two or three abundance maxima are reached. For W/R ratios of 0.8–1.8, calcite is stable for specific modelled temperatures and metastable for all others. Compared to calcite, dolomite occurs in only few systems and requires a W/R ratio of 3 or higher to remain stable beyond a few days (Figure 3.2). For most systems, dolomite also requires a temperature of 90°C or higher although it can occur as metastable phase at modelled temperatures between 1–30°C and 70–90°C. Even for systems with stable dolomite, abundances reach a maximum after a few years to decades. Cronstedtite abundances and occurrences follow a less systematic pattern (Figure 3.3). In common with calcite, cronstedtite also requires a W/R ratio of 0.8 or higher to remain stable but precipitates only at specific temperatures. Maximum abundances are reached after a few years to decades. Mg-serpentine shows a strongly temperature-dependent and fairly W/R ratio-insensitive pattern (Figure 3.4). Abundances of >10 vol.% are reached after 1000 years for 1°C systems and after 2 days for systems at 150°C. High temperature- and high W/R ratio systems have lower abundances of Mg-serpentine and more Mg-saponite instead. Magnetite is ubiquitous in low W/R ratio systems and precipitates within minutes but becomes restricted to 110°C or higher temperatures for systems with W/R ratios of 3 or higher (Figure S3.1). Greenalite overall shows a fairly similar behaviour to Mg-serpentine, with the difference that a first generation precipitates earlier on (Figure S3.2). It is generally less abundant than Mg-serpentine, resulting in serpentine with Mg# of ~0.65. Finally, pyrrhotite abundances and occurrences are highly W/R ratio-dependent (Figure S3.3). At W/R ratios of 2 and higher, it forms two generations with complete dissolution between them.

Table3.2
Selected solid phase abundance (vol. %) averaged across different systems (selected elements and species).

Feature/time steps	1–8 (seconds–hours)	9–18 (days–months)	19–26 (years to decades)	27–34 (centuries to millennia)	35–41 (10,000–100,000 years)
Mg-serpentine	0.000376	8.16	26.7	40.5	45.4
Greenalite	1.79	5.71	14.0	18.6	21.4
Magnetite	0.339	1.37	2.31	1.57	1.08
Cronstedtite	0.243	0.250	1.31	1.56	1.03
Dolomite	0.193	0.464	0.550	0.566	0.537
Calcite	0.147	0.554	0.422	0.385	0.341
Pyrrhotite	0.461	0.148	0.100	0.356	0.445
Heazlewoodite	4.62E-05	0.167	0.350	0.392	0.432
Polydymite	0.00993	0.170	0.276	0.398	0.443
Secondary troilite	0.000371	0.00189	0.00127	0.159	0.622
Rhodochrosite	0.158	0.112	0.0793	0.0720	0.0719

The dissolution of primary phases is fairly W/R ratio-insensitive and temperature dependent, as expected from the Arrhenius equation. An example is shown with forsterite in Figure S3.4. Primary phases that dissolve quickly in the models are $Fe(OH)_2$, CaAl pyroxene, fayalite and diopside whereas tephroite, enstatite, ferrosilite, troilite and millerite are the most resilient phases to dissolution.

A more detailed view of a system with two or more generations of calcite, greenalite and cronstedtite is in Figure 3.5. Calcite precipitates when some primary Ca-phases dissolve but is quickly replaced by other carbonates (siderite and later ankerite). A second generation of calcite forms when more primary Ca-phases and ankerite start to dissolve and a third generation precipitates after the complete dissolution of Mg-Fe silicates. Cronstedtite forms earlier than greenalite and Mg-serpentine, and Mg-serpentine precipitates earlier than a second generation of greenalite, which itself forms when cronstedtite abundances decrease.

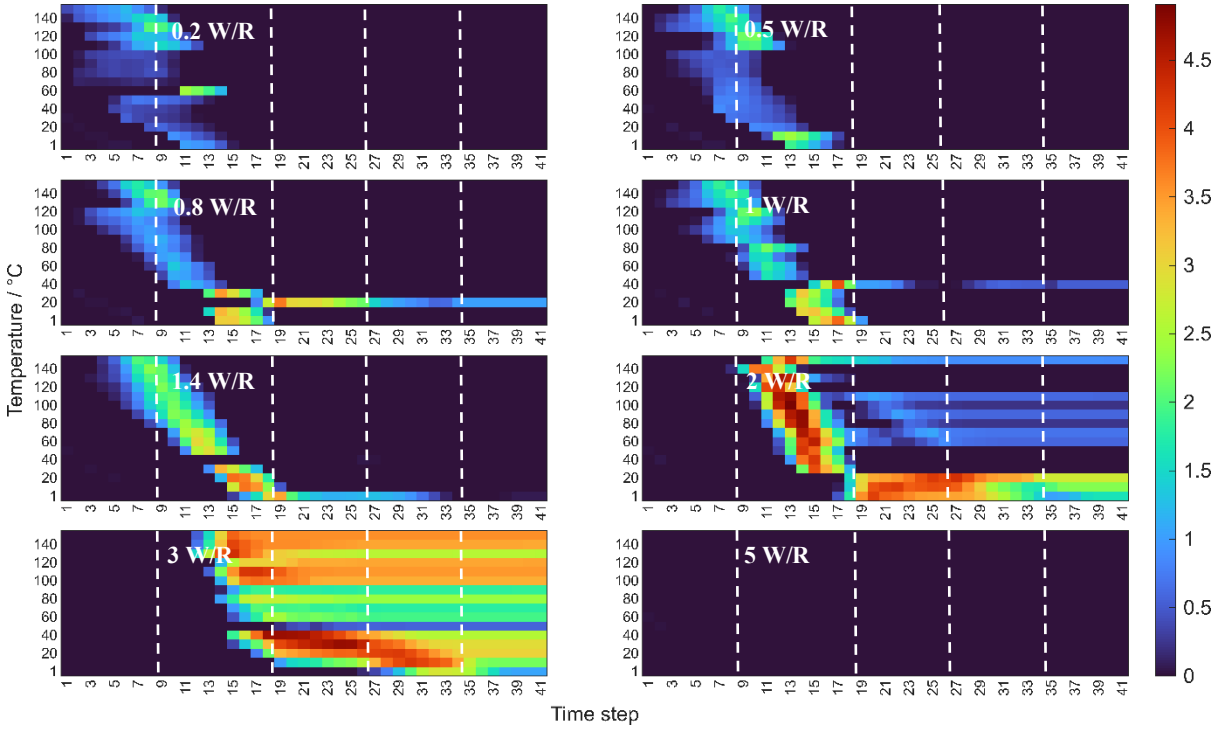

Figure 3.1. Heatmaps of calcite abundance as a function of temperature and time. The different panels denote different values of W/R ratio (by mass). Timesteps 1–8 represent time of the order of seconds to hours, timesteps 9–18 days to months, timesteps 19–26 years to decades, timesteps 27–34 centuries to millennia, timesteps 35–41 10,000 to 100,000 years (time groups are separated by white dashed lines).

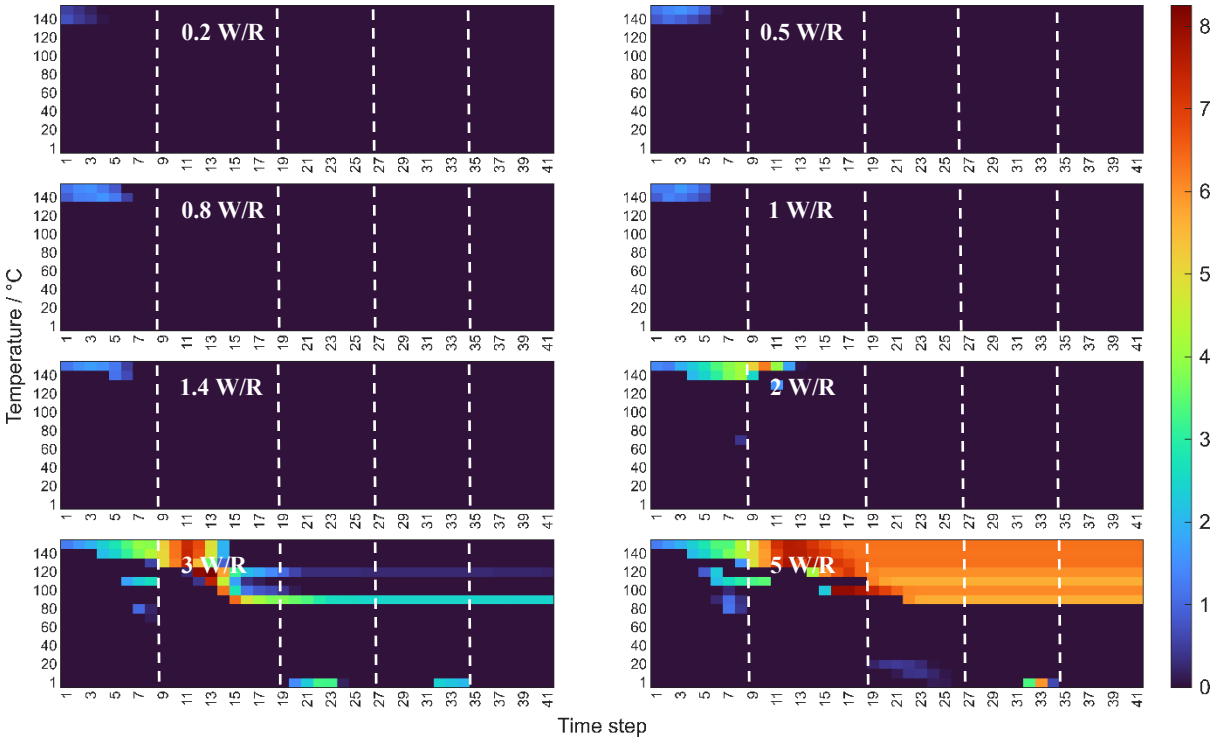

Figure 3.2. Heatmaps of dolomite abundance as a function of temperature and time. The different panels denote different values of W/R ratio (by mass). Timesteps are described similarly to Figure 2.

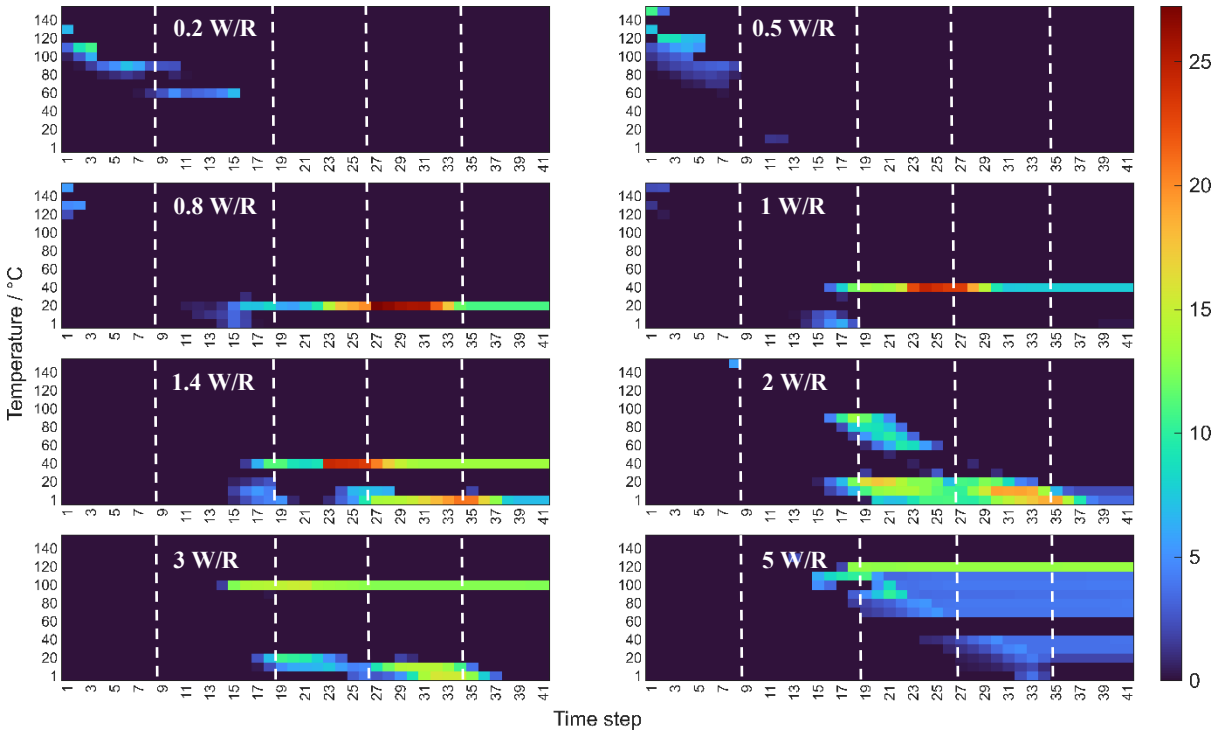

Figure 3.3. Heatmaps of cronstedtite abundance as a function of temperature and time. The different panels denote different values of W/R ratio (by mass). Timesteps are described similarly to Figure 2.

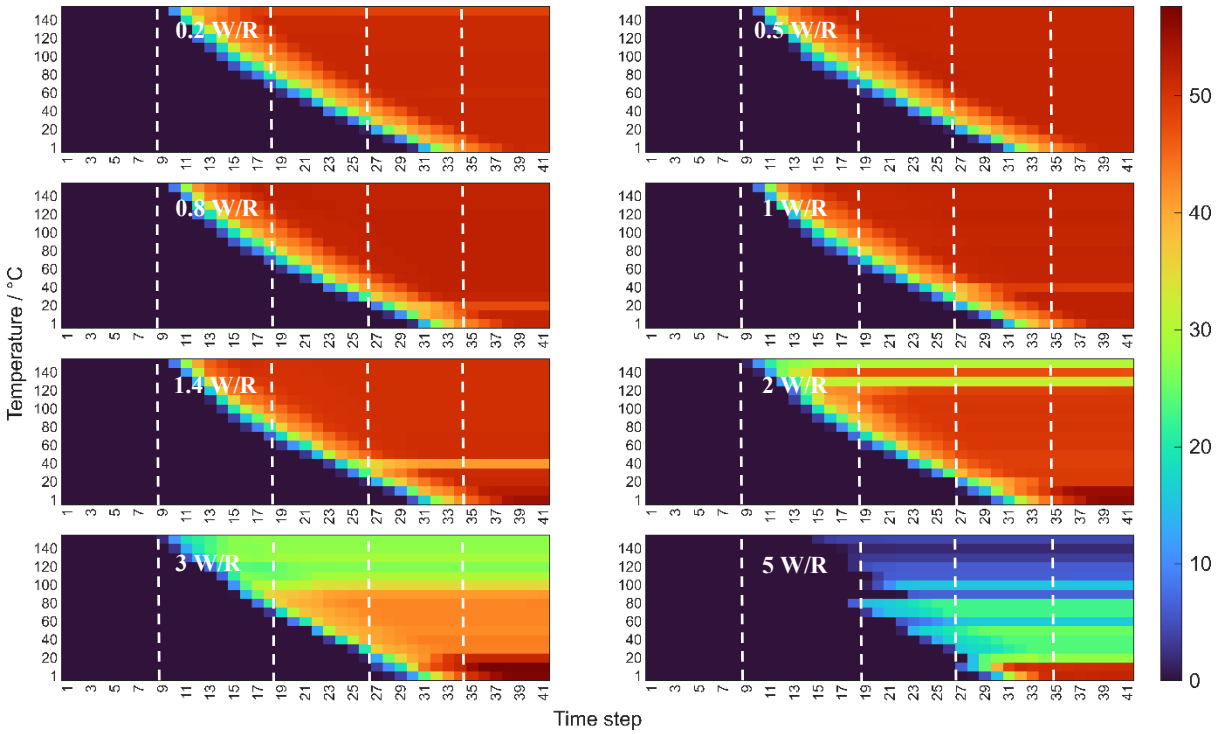

Figure 3.4. Heatmaps of Mg-serpentine abundance as a function of temperature and time. The different panels denote different values of W/R ratio (by mass). Timesteps are described similarly to Figure 2.

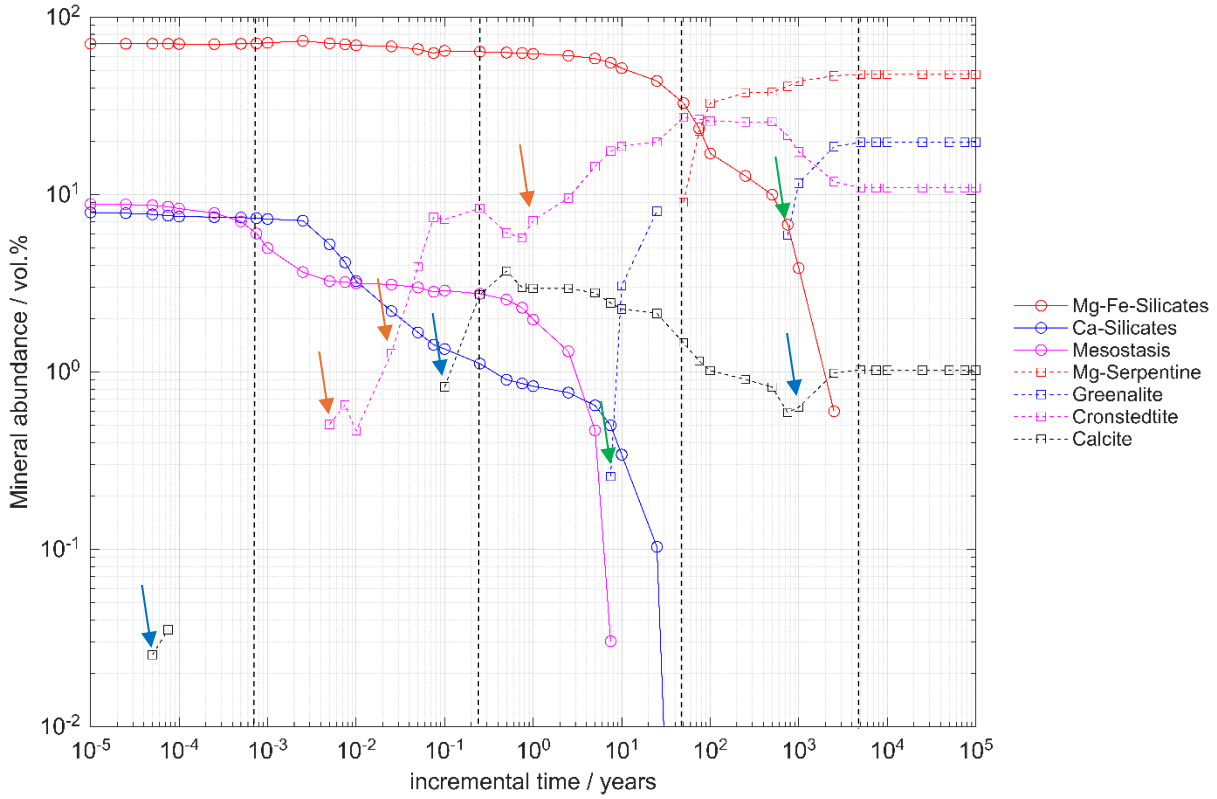

Figure 3.5. Abundance of minerals (vol. %) as a function of log10 time (years) for a system of 20°C and 0.8 W/R; the black dashed lines denote the same time groups as shown in Figures 2–5. Arrows show the begin of a mineral generation. Note the two generations of greenalite (green arrows) and three generations of cronstedtite (orange arrows) and calcite (blue arrows). A second or third generation was identified based on increasing following on decreasing abundances. For simplicity, only a selection of minerals is shown in the figure.

3.3.1.2 Evolution of aqueous fluid and gases

The concentration of total dissolved elements and selected aqueous species for different grouped time steps, averaged across all systems is shown in Table 3.3. During the earliest stages of alteration, the pH is slightly acidic and the pe only slightly negative due to the dissolved CO_2 in the initial solution. After days to months of alteration, the pH raises to ~9 and the pe drops to ~-7; the most abundant elements in solution are N and C (influenced by the initial solution) followed by Na. Average concentrations above 0.001 mol/kg are also reached for Cl and Si. With the continuation of aqueous alteration, Na becomes the most abundant element in solution. Except for S, however, the concentration of other elements stagnate or even decrease as in the case of Mg and Ca. The values of pH and pe continue to raise and drop slightly, respectively. Little change in average concentrations occurs until the end of the modelled timespan.

Gases that exsolve from solution due to elevated gas pressure in the models are mainly H_2, CH_4, H_2O and CO_2 (Table 3.3). During early stages of aqueous alteration (seconds to hours) the gas is mainly composed of CO_2 and becomes more concentrated in H_2 and CH_4 and less concentrated in CO_2. Gas quantities (in mol) do not increase significantly for the modelled timespan.

3.3.2 Point counting of polished thin sections DOM 08006,131 and DOM 08006,135

There is little difference in object abundance between thin sections DOM 08006,131 and ,135. (Table S3.5). Chondrules appeared to be mostly type I POP, some resembled BO chondrules and some chondrules were up to 500 µm large. Most chondrules had fine-grained rims which were counted as matrix for the point counting. Mineral abundances based on EDS point spectra are shown in Table S3.6. Thin section ,131 had more pyroxene and magnetite and less olivine, sulphides and metal than ,135. Notable were some minerals like Ca-sulphate and calcite.

Table3.3
Mean modelled aqueous fluid and gas characteristics (pH, pe, ionic strength and dissolved element and gas concentrations) across different systems (selected elements and species).

Feature/time steps	1–8 (seconds–hours)	9–18 (days–months)	19–26 (years to decades)	27–34 (centuries to millennia)	35–41 (10,000–100,000 years)
pH	6.61	9.05	10.80	10.86	10.83
pe	-3.94	-7.35	-9.95	-10.03	-9.98
Ionic strength (mol/kg)	0.0499	0.0683	0.137	0.167	0.182
Total C (mol/kg)	0.205	0.0754	0.0113	0.0102	0.0101
Total Ca (mol/kg)	0.00119	0.000306	6.46E-05	3.18E-06	3.46E-06
Total Cl (mol/kg)	0.00499	0.00533	0.00641	0.00712	0.00748
Total Fe (mol/kg)	2.71E-06	3.78E-05	0.000176	0.000229	0.000283
Total Mg (mol/kg)	0.000435	0.000864	0.000118	1.71E-06	1.80E-06
Total N (mol/kg)	0.0967	0.0901	0.119	0.136	0.143
Total Na (mol/kg)	0.00135	0.0539	0.154	0.199	0.223
Total S (mol/kg)	0.00200	0.000381	0.00119	0.00877	0.0101
Total Si (mol/kg)	0.00480	0.00417	0.00317	0.00444	0.00498
Aqueous CO_2 (mol/kg)	0.158	0.0503	0.000413	9.01E-05	8.96E-05
Aqueous HCO_3^- (mol/kg)	0.0431	0.0173	0.00392	0.00324	0.00325

Aqueous CO_3^{2-} (mol/kg)	0.000117	0.000913	0.00138	0.00140	0.00117
Aqueous CH_4 (mol/kg)	0.00294	0.00662	0.00556	0.00552	0.00562
Gas quantity (mol)	0.816	0.583	1.22	1.23	1.22
Gaseous CH_4 (mol)	0.0287	0.166	0.315	0.326	0.325
Gaseous CO_2 (mol)	0.677	0.111	0.00138	0.00118	0.00118
Gaseous H_2 (mol)	3.66E-05	0.205	0.733	0.728	0.711
Gaseous H_2O (mol)	0.109	0.101	0.174	0.179	0.179

3.3.3 Experiment results

3.3.3.1 Reacted solutions composition

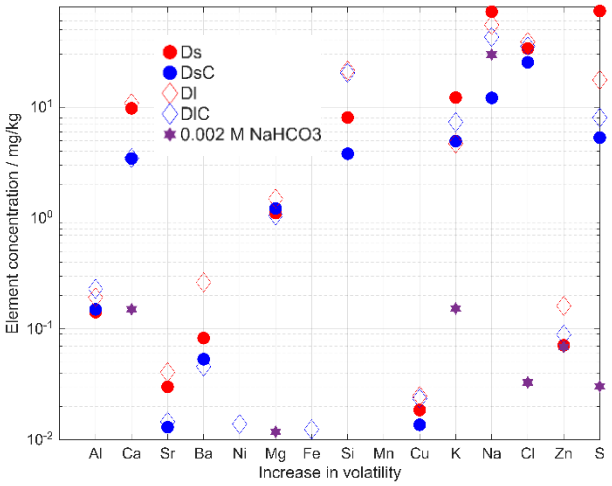

Figure 3.6. Elemental concentrations of experimental reacted solutions (open symbols denoting short and full symbols long experiments) measured by ICP-OES and IC. Elements are arbitrarily ordered by volatility. Samples with concentrations below detection limit or below 0.01 mg/kg are not shown. Analytical errors are smaller than the figure symbols.

The reacted solutions are rich in Na, Cl, S and Si (>10 mg/kg, on average) (blank corrected) with less abundant K, Ca and Mg (>1 mg/kg) and minor Al, Ba, Zn, Sr, Cu, Ni, Fe and Mn (<1 mg/kg) (Tables 3.4 and S3.4, Figure 3.6). Zn, Mn, and Ni were below detection limit in one or more samples and Co, Pb and Cr were not detected in any sample. Concentrations of Ca, Sr, Ba and S are lower in carbonated solution experiments (DsC and DlC) compared to experiments with pure water (Ds and Dl). Longer experiment durations yield similar or only slightly higher concentrations except for Si.

The pH of the reacted solutions were higher than the initial $NaHCO_3$ solution and pure water (pH 8.65 and 8.14, respectively) (Table S3.1). Notably, the pH was lower for the 180 days experiments and oxygen concentrations increased over the timeframe of the experiments. No difference in the weight of the chips was observed except for a slight a slight loss for DlC which broke into >3 fragments during the experiment.

Table 3.4
Blank corrected experimental solution compositions, analysed by ICP-OES and IC (in mg/kg). bdl=below detection limit.

Element/Sample	Ds	DsC	Dl	DlC
Si	8.0784	3.8061	21.389	20.381
Mg	1.1101	1.2209	1.4954	1.0571
Cl	33.838	25.45	38.854	35.42
Sr	0.030005	0.012974	0.04064	0.014564
Na	72.729	12.141	55.212	42.885
Ca	9.7797	3.4489	10.856	3.4789
Zn	0.07115	bdl	0.1611	0.08875
S	73.8	5.32	17.65	8.04
Ba	0.0826	0.05327	0.2628	0.04575
K	12.19	4.942	4.6956	7.3288

Mn	0.001599	0.001088	0.00054	bdl
Cu	0.01854	0.01367	0.0248	0.02351
Al	0.1415	0.1503	0.1926	0.2297
Ni	bdl	bdl	bdl	0.01387
Fe	0.00805	0.0074	0.00479	0.0124

3.3.3.2 Altered chips and thin sections SEM

The goal of the SEM work was to identify potential alteration products and investigate any differences relative to experiment duration and initial solution composition. The reacted chips showed a few sites with notable features of interest; the most prominent ones being elongated crystals in DsC and DlC whose composition, evaluated by point EDS, is a mixture of Ca, C, O and minor Mg, indicative of Ca-carbonate (Figures 3.7b and 3.7d). Chip Ds showed several dark areas as observed in BSE that were rich in carbon, therefore likely insoluble organic matter (Figure 3.7a). Also notable was a ~1.5 mm large lump on chip DlC rich in Fe and O, indicative of a Fe-hydroxide or Fe-oxide (Figure 3.7c). Chip DlC also showed some additional small crystals, 10 µm in size or less with elevated relief; chlorite and other phyllosilicates are possible matches based on EDS point spectra (Figure 3.7d). In contrast to the chip surfaces, polished thin sections made from altered chips DsC, Dl and DlC showed no notable signs of aqueous alteration except for a few carbonate crystals.

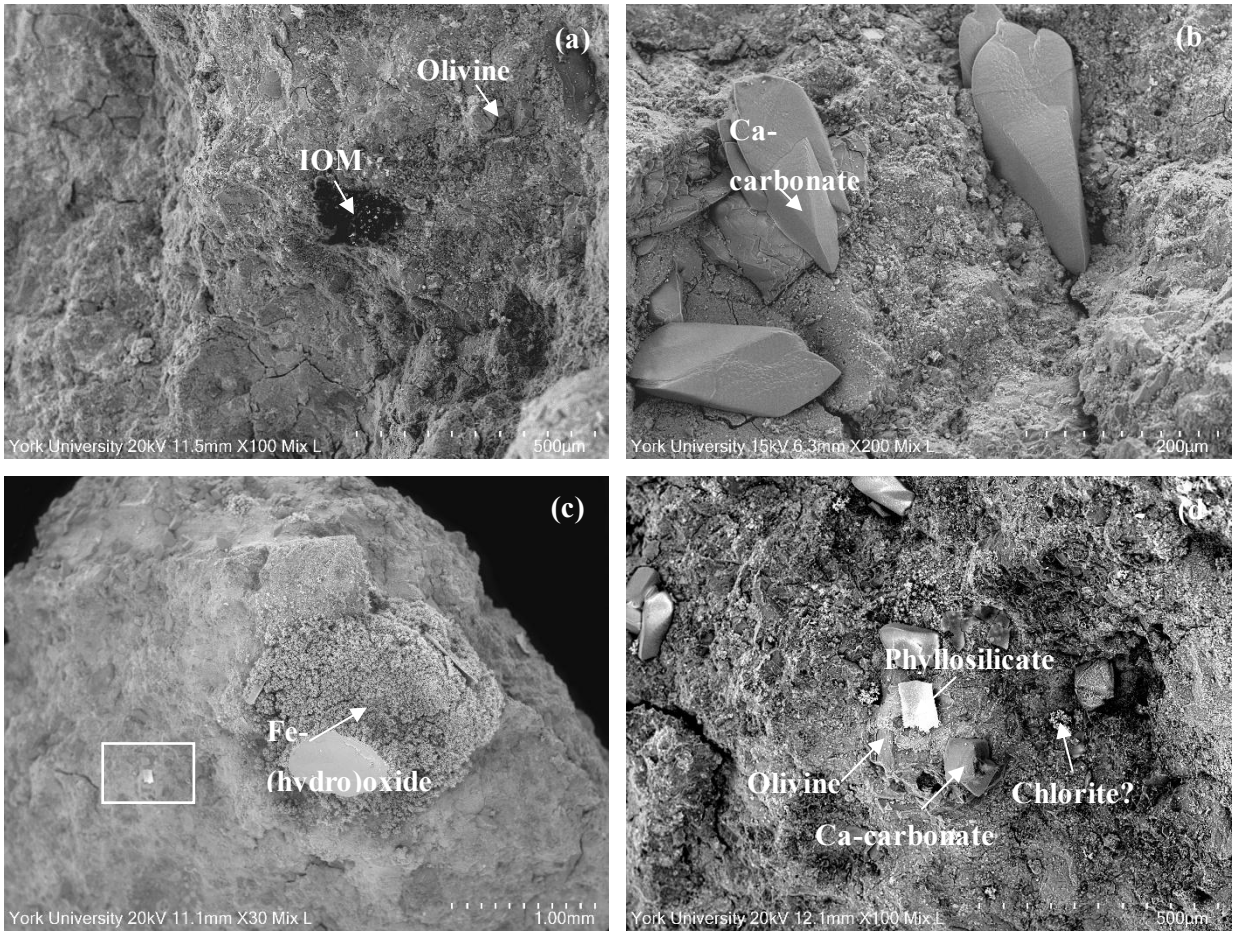

Figure 3.7. Mixed BSE/SE images of altered DOM 08006 chip surfaces with highlighted minerals based on EDS analyses. a) 30 days alteration with deionised water (Ds) with a spot that could be insoluble organic matter (IOM); b) 30 days alteration with carbonated water (DsC) with euhedral Ca-carbonate (Mg-bearing); c) 180 days alteration with carbonated water (DlC) with a large lump of Fe-(hydr)oxide; d) Different site of interest in DlC (inset in c).

3.4 Discussion

3.4.1 Cross-validation and limitations of kinetic models and laboratory experiments

Kinetic models are useful to simulate timespans and conditions that are not readily accessible with laboratory experiments. However, as there are several severe limitations to the models (see further below), their validation is necessary before discussing any modelling results. The laboratory experiments are a good anchor point to compare aqueous solutions with modelled solutions after 30 and 180 days at 50°C; however, the experimental W/R ratios (~150) were much higher (due to the higher amount of water necessary for ICP-OES analyses) than the modelled ones, which makes a direct comparison more challenging. Elements with variable concentrations in both experiments and models are Al, Ca, Fe, Na, Mg, Mn, S, Si. For the comparisons, we calculated concentration ratios (modelled/experimental concentrations) for all modelled W/R ratio values and used the mean, minimum and maximum values for the discussion (Table S3.7). Some of the tabulated elements like Mg or S span a wide range of values, because modelled solutions of low W/R ratio are generally more concentrated and vice versa. Furthermore, mean ratios for 30 days are somewhat different to the values for 180 days,

suggesting that modelled and experimental values are not just offset but there are also some differences in dissolution and/or precipitation mechanisms of minerals. For example, mean S concentration ratios become lower after 180 compared to 30 days, which could be due to too slow modelled dissolution of primary sulphides or the precipitation of sulphides in the experiments is limited due to high W/R ratios. Oxygen concentrations throughout the experiments increased from nearly zero to 100%, which raises also the possibility of enhanced sulphide dissolution due to oxidising conditions paired with limited precipitation of sulphates due to high W/R ratios. Those oxidising conditions would not be representative of parent body alteration. Oxidising conditions in the later stages of the experiments can also be inferred from the large lump of Fe(hydro)oxide seen on chip DlC (Figure 3.7c). Alternatively, measured oxygen concentrations at the end of the experiments could have been skewed to higher values due to swift equilibration with atmospheric oxygen after opening the glass vials, which would also be consistent with the lack of observed sulphates.

The scarcity of secondary minerals seen on chip surfaces, on the other hand, is fairly consistent with modelled mineralogies. Lower concentrations of Ca, Sr, Ba in reacted solutions of DsC and DlC compared to Ds and Dl are further evidence for the precipitation of significant amounts of calcite after 30 days, whereas uncarbonated initial solutions yield little to no calcite. Patches of presumably IOM, as seen on Ds (Figure 3.7a) and Dl surfaces also indicate that precipitation of calcite, at least during early stages of aqueous alteration, requires an external carbon source like accreted CO_2 ice. Calcite is also in the models one of the first minerals to precipitate (Figure 3.1) and some phyllosilicates like chlorite or greenalite (Figure S3.2) typically form in the models after 180 days. Most of the anhydrous minerals, however, only dissolve after 180 days, which matches the low abundance of observed secondary minerals on the meteorite chips well.

Experimental and modelled mineralogies and aqueous solutions can also be compared to other experimental and modelling studies. In their aqueous alteration experiment of CO3.2 Kainsaz samples, Suttle et al. (2022) also observed some calcite although it formed rather late after other primary phases completely dissolved. Some Fe-oxides and -hydroxides also precipitated in addition to secondary fayalite and Fe-sulphides. Experimentally altered Allende samples also yielded some calcite (Jones and Brearley, 2006), in addition to other minerals like interlayered serpentine/saponite and Fe-oxyhydroxides. However, their experiments ran at higher temperatures (100 to 200 °C), which could explain the higher abundances of secondary minerals compared to this study.

The differences between models and experiments, and differences to other studies, could be explained by several factors. The experiments ran at W/R ratios much higher than typically inferred for CM chondrite aqueous alteration (see e.g., Suttle et al., 2021) and even though the experiments started at reducing conditions, air trapped in the headspace of the bottles or diffusion caused increasing oxygen levels during the experiments. Different experimental temperatures and W/R ratios would also be helpful to enable a better comparison to our models and other studies. Regarding the kinetic models, a

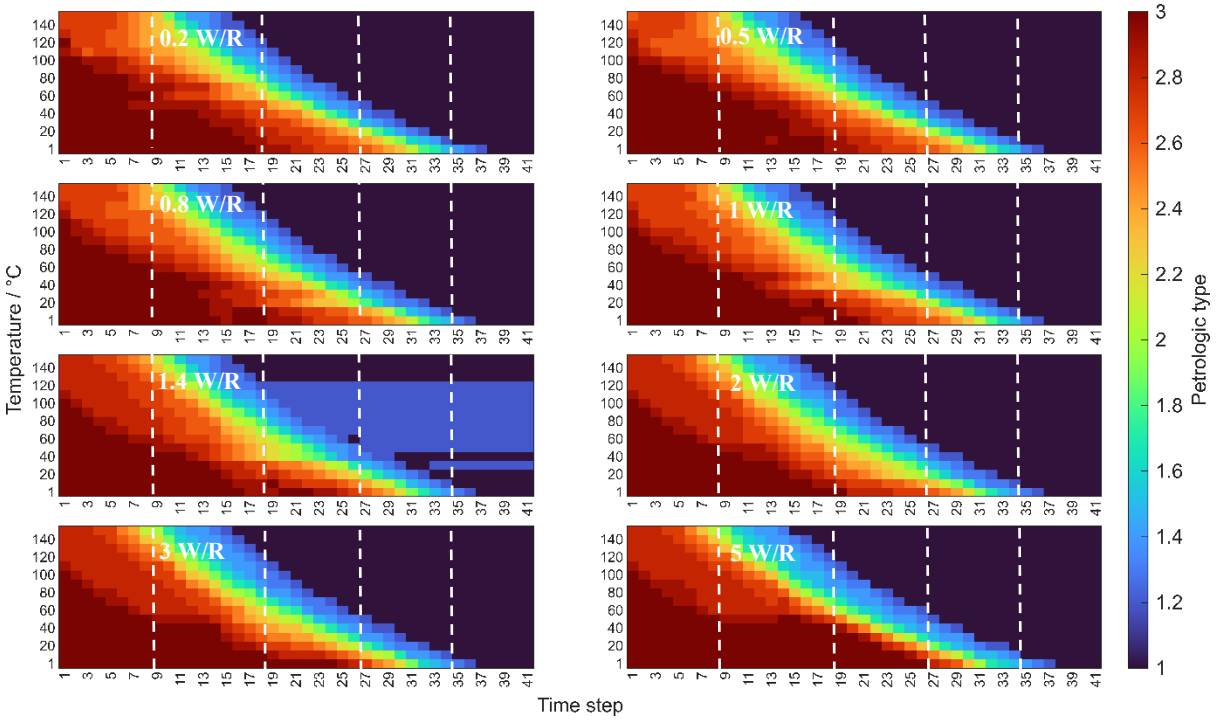

Figure 3.8. Heatmaps of petrologic type, calculated from the phyllosilicate fraction as a function of temperature and time. The different panels denote different values of W/R ratio (by mass). Timesteps are described similarly to Figure 2.The extended petrologic type of 1.2 (blue) seen in the 1.4 W/R ratio panel is caused by a modelling artifact (precipitation of several vol.% of diopside).

severe limitation arises from the lack of modelled solid solutions which were implemented by several other modelling studies (e.g., Zolotov, 2006; Fabre et al., 2024). Another major factor of uncertainty are the modelled surface areas, which are entirely based on approximated grain sizes and geometries. Ideally, surface areas are determined by 2D SEM and 3D XCT imaging that also assesses the connectivity of pores (e.g., Beckingham et al., 2017) or autocorrelation curves that quantify geometric relationships of mineral phases and porosity from 2D or 3D sample images (Anovitz et al., 2023). The evaluated porosity in DOM 08006 thin sections of ~3 area%, however, does not represent the original porosity of a CM3 prior to aqueous alteration because porosities in CM2s are typically around 25% (Macke et al., 2011) and for CM3s, the porosity was potentially as high as 40%, likely similar to ultraporous lithologies found in Acfer 094 (Matsumto et al., 2019). Some minerals that are commonly observed in CM chondrites, most notably tochilinite and pentlandite, are missing in the database used for the models. Tochilinite usually occurs as tochilinite-cronstedtite intergrowths (TCIs) (e.g., Vacher et al., 2019); hence, co-occurring cronstedtite and sulphides like pyrrhotite in the models could be a reasonable proxy for the occurrence of TCIs. Further limiting factors are the limited number of modelled elements, limited minerals with dissolution rates in the thermodynamic database and the occurrence of methane, in contrast to other modelling studies (e.g., Zolotov, 2012). Methane is kinetically inhibited in low temperature and -pressure systems, as experimentally demonstrated by Seewald et al. (2006) and should therefore not form in the kinetic models of this study. Lastly, the modelling results are also influenced by the number and spacing of the timesteps. Naturally, a higher density of timesteps, i.e.,

timesteps per fixed time frame, will result in smoother and more accurate dissolution and precipitation curves, at the cost of higher computational time. As seen in Fig. 3.5, a $\log_{10}$ timestep of 0.25 captures mineral dissolution and precipitation behaviour fairly well, except for the beginning of precipitation and end of dissolution, which would likely benefit from a smaller timestep.

In the database used for these kinetic models (diagenesis_kin.dat), the surface area of a mineral is updated after every timestep according to the following formula: $SA_t = SA_{t-1} * (M/M_0)^{0.67}$, where SA_t is the current surface area, SA_{t-1} the surface area from the previous timestep, M denotes the current amount (moles) of the mineral, whereas M_0 is the initial amount (moles). The additional exponent accounts for a common scenario where the dissolution of a mineral results in smaller grains which have higher surface areas in relation to their volume. In reality, however, dissolution of minerals can result in uneven surfaces or the dissolution is accompanied by precipitation of other secondary minerals; both of those scenarios would result in different surface areas than calculated by the modelling software (PHREEQC). Hence, without further experimental data, the surface area remains a major source of uncertainty for the kinetic models in this study and results should be interpreted with caution.

3.4.2 Discussion of minerals and fluid chemistry from experiments

As described in section 3.3.3.1, solutions in the experiments were rich in Na, Cl, S, Si, K and Ca and less abundant in Mg, Al, Fe and Ni. Only few secondary minerals (notably calcite, Fe-(hydro)oxide and phyllosilicates) were detected by SEM on the altered chip surfaces. Thus, measured ICP-OES concentrations should mainly reflect the extent of dissolution with little influence from precipitation. The high concentration of Na, Cl and K in the leachate relative to their meteoritic abundance (Patzer et al., 2020) suggests that the mineral hosts of these elements are highly susceptible to aqueous alteration. As also discussed in chapter 4, possible sources for those elements are terrestrial weathering products like halite but indigenous minerals like Mg, Na phosphates. High concentrations of sulphur in the leachates indicate considerable alteration of primary sulphides (troilite and pentlandite). Low Ni concentrations relative to Fe as well as other work (see e.g., Singerling and Brearley, 2020) suggest that more S is sourced from troilite than pentlandite, i.e., pentlandite is more resistant to aqueous alteration than troilite. The low Fe and high S concentrations can be explained by precipitation of secondary Fe-minerals; magnetite is a common aqueous alteration product (e.g., Rubin et al., 2007) but Fe-hydroxides like goethite are also possible under more oxidising conditions. Finally, lower elemental concentrations in leachates from experiments with carbonised compared to deionised water arise from either less dissolution of primary minerals or higher abundance of precipitates. Regarding Ca, Ca-carbonates were only detected in carbonised experiments, as Ca-carbonate becomes oversaturated faster in a solution with preexisting Ca and C compared to pure water. For other elements like Si, the reason for the elemental concentration differences is less clear. The main anhydrous silicates in DOM 08006, forsterite and enstatite, dissolve faster in acidic environments (e.g., Palandri and Kharaka, 2004); however, the pH of the carbonised solution was only slightly higher than the deionised water and final pH values

were almost equal (Table S3.1). On the other hand, except for carbonates, the meteorite chips reacting with the carbonised solution did not yield higher abundances of secondary minerals than chips that reacted with pure water. Clearly, more experimental work like XRD and Raman spectroscopy would be needed to characterise and quantify dissolution and precipitation.

3.4.3 Discussion of minerals and fluid chemistry from models

Compared to the experimental results, the kinetic models offer a clearer picture of dissolution and precipitation products and quantification but at the cost of more uncertainty, as previously discussed. The models show that no Cl- and only few Na-bearing minerals become oversaturated over the course of the simulations. Furthermore, albite, the primary Na-mineral, dissolves rapidly; hence, aqueous fluids become rich in Na and Cl (or even brine-like) over time. Nitrogen, if it was initially present on the CM parent body, would also broadly remain in solution as N-bearing minerals require low temperatures to form (e.g., Neveu et al., 2017). High aqueous C concentrations in most solutions are maintained due to limited number of carbonates, as generally, with the exception of rhodochrosite and dolomite, only one carbonate mineral is stable. For example, in systems with stable calcite, most carbon remains in solution due to the limited calcite availability of the system. Decreasing aqueous concentrations over time for elements like Ca or Mg reflect predominant precipitation over dissolution. The main secondary Mg-minerals are Mg-serpentine and Mg-saponite; the latter becomes generally stable over the former at elevated temperatures and pH (see also the discussion in chapter 2). Ca precipitates as calcite when it is stable (cf. Figure 3.1); otherwise, the main Ca-mineral is andradite because the database used for the models has only a limited number of suitable secondary Ca-minerals. In reality, Ca would likely be incorporated as traces in other secondary minerals or it precipitates as hydroandradite which has been recently discovered in CM chondrites (Jenkins et al., 2024). Si, despite being one of the most abundant elements in CM chondrites, is only present in moderate concentrations in the modelled aqueous solutions. This is because the element precipitates as large quantities of phyllosilicates (serpentine, cronstedtite or saponite) and only little Si remains in solution. The average concentration in Table 3.3 stagnates because Si is more resistant to dissolution in primary minerals compared to elements like Mg or Na (e.g., Palandri and Kharaka, 2004). Finally, the concentration of aqueous Fe and S increase slightly over time. As redox conditions are reducing throughout the modelled timespan, Fe exists primarily as Fe^{2+}, although some Fe^{3+} also exists which can combine with Fe^{2+} to form magnetite. Sulphur is also mainly present in reduced form, mainly as HS^-; hence, no secondary sulphates form in the models.

3.4.4 Timescales and conditions of CM chondrite aqueous alteration

As the most abundant secondary mineral in CM chondrites, the precipitation of Mg-serpentine (Figure 3.4) is a good preliminary indicator of the progress of aqueous alteration. However, to also account for other phyllosilicate that are typically present in CM chondrites, a better aqueous alteration metrics is

determining the quantity of phyllosilicates formed relative to anhydrous silicates. Howard et al. (2011, 2015) proposed a petrologic type for CM and CR chondrites, ranging from 3.0 (unaltered) to 1.0 (completely altered) based on the phyllosilicate fraction (PSF); they also proposed a formula to calculate the petrologic type from the commonly used petrologic subtype from Rubin et al. (2007). Based on that formula, CM chondrites span a petrologic type range of 1.7–1.2 (Howard et al., 2015) although the formula did not consider more recently described and less altered CM chondrites like Asuka 12169 (Kimura et al., 2020) and Paris (Hewins et al., 2014). In our models, the petrologic type based on the PSF is dependent on time and temperature but is broadly independent of the W/R ratio (Figure 3.8). A petrologic type of 1.6, representative of a mildly altered CM2 chondrite like Murchison, would be reached between 4 days (150 °C) and 5,000 years (1 °C), whereas an extensively altered CM1 like LAP 02277 requires between 65 days (150 °C) and 50,000 years (1 °C). It is also notable that a petrologic type of 3 is only sustained at <~100 °C for more than a few seconds; at 1 °C and low W/R ratios, a CM3 still only survives for a few months due to precipitation of metastable daphnite (chlorite), whereas with higher W/R ratios, this duration increases to up to 50 years.

To evaluate CM chondrite aqueous alteration conditions in more detail, additional minerals need to be considered to separate the modelled mineralogies from other aqueously altered carbonaceous chondrites like CIs or CRs. Characteristic minerals in CM chondrites are calcite, tochilinite and cronstedtite (as TCIs) but also magnetite and dolomite in more highly aqueously altered samples (e.g., Rubin et al., 2007). In contrast to CI chondrites that have very few remaining anhydrous silicates (e.g., King et al., 2015), even CM1s have at least a few vol.% anhydrous silicates in addition to the aforementioned minerals (King et al., 2017). We created queries to investigate "CM-like" systems with co-occurring anhydrous silicates, calcite, serpentine, Fe-sulphide and optional dolomite, magnetite and cronstedtite. No "CM-like" system has co-occurring dolomite, magnetite and cronstedtite and only two "CM2-like" systems have both cronstedtite and magnetite. Because secondary minerals have not been described by dissolution or precipitation kinetics in the models, it seems likely that either magnetite or cronstedtite are metastable in CM2s. In the models, cronstedtite typically precipitates earlier before being replaced with magnetite but the opposite is also possible and, in some cases, magnetite replaces an earlier generation of cronstedtite before being replaced again by cronstedtite (Figures 3.3 and S3.1). In contrast, "CM1-like" systems with no cronstedtite and optional dolomite occur more often in the models. More commonly, however, dolomite forms early and is replaced later by calcite. Based on clumped isotope thermometry, Clog et al. (2024) suggest that dolomite in CM chondrites precipitated between 75 and 100 °C although in the models, dolomite also occurs as metastable low temperature phase with calcite for W/R ratios of ~3. While the precipitation of dolomite is usually inhibited at low temperatures (see e.g., Arvidson and Mackenzie, 1999), additional factors such as microbial activity in terrestrial environments (Chang et al., 2020) or cycles of over-and undersaturation (Kim et al., 2023) could enable precipitation of dolomite at temperatures <60 °C. "CM1-like" systems of petrologic type 1–1.2 with

magnetite and optional dolomite require temperatures between 100 and 150°C and initial W/R ratios between 2 and 3.5. "CM2-like" systems of petrologic type 1.3–1.7 with cronstedtite and optional dolomite can form for similar initial W/R ratios (0.8–4) but require much lower temperatures (1–100°C, mean of 33°C). Due to the higher temperatures of the "CM1-like" systems, they can form after similar or even shorter timespans compared to "CM2-like" systems.

In short, the key parameter to form CM1 chondrites are elevated temperatures, whereas W/R ratios and alteration duration can be similar for CM2 and CM1 chondrites. If CM1 and CM2 chondrites are from the same parent body, the CM1 chondrites were perhaps altered closer to the centre of parent body where temperature were higher, whereas CM2 chondrites were altered closer to the surface (similar to what is shown in Figure 2.4). A catastrophic event such as disintegration due to gas overpressure (Wilson et al., 1999) could have stopped aqueous alteration and prevented a complete equilibration with the fluid after several months to millennia, depending on the temperature. As all modelled "CM-like" systems require a W/R ratio of 0.8 or higher, it seems unlikely that very low W/R ratios (<0.14) were responsible for the surviving primary phases in CM chondrites.

3.4.5 Multiple generations of calcite and link to CM chondrite samples

One major unresolved question about CM chondrites is whether they sample one or many parent bodies. Even though the kinetic models in this study cannot represent the entire complexity of parent body processes, we aim to explore in this section whether the different mineralogies and petrographic features of CM chondrites could be explained by contrasts in modelled temperature and W/R ratios or whether additional factors are necessary.

Carbonates show a complex precipitation behaviour with dolomite being suggested to precipitate either before calcite (e.g., in C1-ung Flensburg (Bischoff et al., 2021)), contemporaneously with it (e.g., in CM2 Cold Bokkeveld (Farsang et al., 2021)) or after calcite (e.g., in highly altered lithology in CM2 Winchcombe (Suttle et al., 2022) and other CM chondrites (Clog et al., 2024)). Additional complexity arises with different types of calcite that precipitate during alteration. Lee et al. (2014) proposed that type 1a calcite precipitates together with dolomite after an early generation of aragonite, whereas type 2 calcite forms later after the formation of serpentine, tochilinite and sulphides. In low W/R ratio systems (1.4 or lower) calcite of very low abundance can form within days, followed by more abundant calcite later, whereas for higher W/R ratios, the opposite behaviour is seen with more calcite earlier (Figure 3.1). If those calcite generations are interpreted as type 1 (early) and 2 (late) calcite, then CM chondrites like Murray or Cold Bokkeveld with little or no type 2 calcite (Lee et al., 2014) could have been altered at W/R ratios of ~1.5 or higher. Meteorites with higher abundances of calcite would also be expected to form at higher W/R ratios although other factors like time could also have a profound impact on calcite abundances, especially for W/R ratios of 1.4 or lower (Figure 3.1). Co-precipitating calcite and dolomite, which Lee et al. (2014) have described as bimineralic calcite-dolomite in some

CMs like ALH 83100 or MET 01070 require, in most cases, a W/R ratio of 3 in the models. CMs with less dolomite than calcite like MET 01070 could have formed at 120 °C whereas other CMs with roughly equal amount of calcite and dolomite like ALH 83100 are predicted to form at 90 °C. Considering that MET 01070 is classified as a CM1 and ALH 83100 as a CM1/2, we tentatively suggest that higher temperatures could be responsible for the scarcity or absence of dolomite in CM1s. When it is not co-precipitating with calcite, dolomite usually precedes calcite except for a second generation of low-temperature high-W/R ratio dolomite (Figure 3.2). Such conditions could have occurred for CM2 QUE 93005 for which Lee et al. (2012) proposed a second generation of dolomite precipitating after breunnerite.

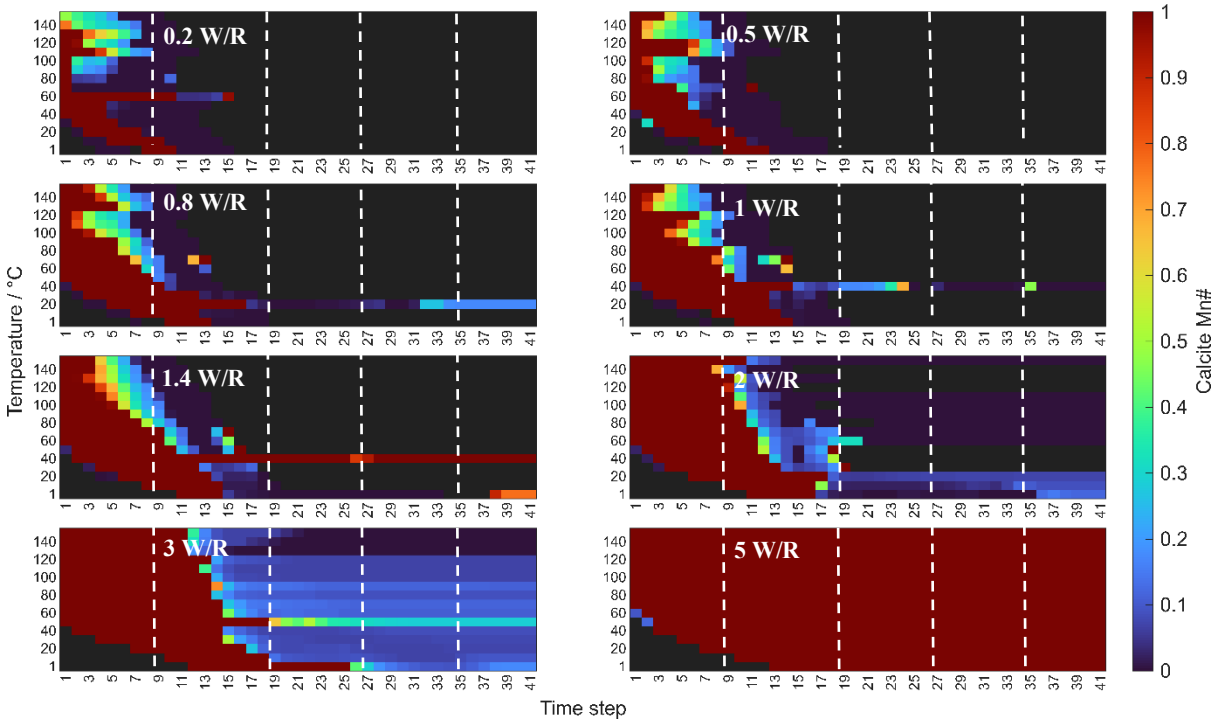

Figure 3.9. Heatmaps of Mn-content of calcite shown as Mn# (values of zero (purple) denote pure calcite, values of one (red) pure rhodochrosite and black areas are without calcite and rhodochrosite) as a function of temperature and time. Timesteps are described similarly to Figure 2.

In addition to calcite, breunnerite and dolomite, some CM chondrites contain siderite (LON 94101 (Lindgren et al., 2013)), Mn-bearing calcite (MET 01070 (Telus et al., 2019)) or aragonite (e.g., Murchison (Lee et al., 2014)). Lindgren et al. (2013) proposed that siderite in LON 94101 precipitates after dolomite and before breunnerite and phyllosilicates. In the models, siderite is metastable and usually forms before dolomite, although in some systems, such as 2 W/R ratio and 70 °C (Figures 3.2 and S3.5), siderite precipitates later. Siderite remains stable for several years at low temperatures and high W/R ratios but dissolves within days in other cases. Because dolomite is usually not stable at lower temperatures, assemblages of siderite and dolomite would not be expected in CM chondrites although LON 94101 might be a candidate for a rare CM chondrite that experienced aqueous alteration at low temperatures (~1–10°C) and high W-R ratios (~5); those conditions could occur at shallow depths on the parent body in which high temperatures are not reached throughout the aqueous alteration history.

For highly altered CMs like MET 01070, Telus et al. (2019) observed Mn-bearing calcite forming after Mn-poor calcite. To calculate the Mn-content of calcite in the models as a "calcite Mn#", rhodochrosite abundances were divided by the sum of rhodochrosite and calcite. Calcite usually precipitates later than rhodochrosite and only in some cases at moderate temperatures, a generation of Mn-bearing calcite would precipitate later (Figure 3.9). However, as Telus et al. (2019) observed Mn-bearing calcite only in highly altered CMs, often together with dolomite for which they estimated a precipitation temperature of 125°C ± 60°C in ALH 83100, it seems more likely that Mn-bearing calcite in CMs either requires a decrease in temperature once a first generation of calcite is formed or the observed petrography reflects conditions not represented by our models, such as an injection of fluid of different composition which has also been proposed by other studies such as Clog et al. (2024) or Rubin et al. (2012). Finally, aragonite which is often observed in mildly altered CMs like LON 94101 (Lee et al., 2014) did not form in any modelled system. However, it seems likely that the absence of aragonite is caused by the more thermodynamically stable calcite because in some preliminary models with kinetically inhibited calcite, aragonite occurred occasionally as metastable phase in low temperature systems. More work with more sophisticated models is needed to investigate precipitation conditions of aragonite for CM chondrites and to further evaluate the CM chondrite aqueous alteration history and conditions.

3.5 Conclusions

The aqueous alteration history of CM chondrites was simulated with kinetic models (temperature, W/R ratio (by mass)) using the CM3 proxy DOM 08006. A typical CM2 chondrite with 1 vol.% calcite could have been altered within ~1,000 years at 50°C, a W/R ratio of 0.8, although alteration timescales can range from months to ~10,000 years depending on temperature. As the more altered CM1 and CM1/2 chondrites typically contain magnetite instead of cronstedtite, the models predict that they required higher temperatures but not necessarily different W/R ratios or duration of aqueous alteration compared to the less altered CM2s. Low temperatures and high W/R ratios could have stabilised nearly unaltered CM3s like A 12169.

Different types of calcite could be represented by various generations in the models and different combinations of W/R ratios and temperature could explain contrasts in mineral assemblages across various CM chondrites. Laboratory experiments of DOM 08006 chips reacting with a carbonated aqueous fluid under reducing conditions yielded considerable quantities of Ca-carbonate after 30 days, whereas no carbonates formed in experiments with deionised water, suggesting that at least early forms of calcite like type 1a calcite require the accretion of C-bearing ice on the CM parent body/bodies. The low abundance of other secondary minerals as well as the overall poor fit of the models with the experiments likely arise from several limitations in the models as well as other factors such as low porosity and some terrestrial weathering observed as Ca-sulphates in DOM 08006 polished thin sections, which could have lowered the reactivity of primary minerals in the experiments. In addition to more sophisticated models with, e.g., solid solutions and precipitation kinetics, a more pristine CM3

proxy is needed that reflects the porous and pristine nature of accreted material on the CM parent body. Overall, the CM parent body could have been thermally stratified with higher temperatures in the centre, producing more altered CM1s, whereas CM2s would have originated closer to the surface where temperatures were lower, similar to the parent body proposed by the equilibrium models (cf. Fig. 2.4).

CRediT authorship contribution statement

Robin Haller: Conceptualization, Methodology, Software, Formal analysis, Investigation, Resources, Data curation, Funding acquisition, Writing – Original Draft Preparation, Writing – Review & Editing. Martin Lee: Conceptualization, Writing – Review & Editing, Supervision, Project administration. Mark Hodson: Conceptualization, Writing – Review & Editing, Supervision, Project administration.

Appendix A. Supplementary Material

Tables S3.1 and S3.2 contain further information on the laboratory experiments, Table S3.3 lists secondary minerals in the models, Table S4 shows errors or ICP-OES and IC analyses, Tables S3.5 and S3.6 summarise SEM point counting results and Table S3.7 compares experimental and modelling results. Figures S3.1–S3.5 show heatmaps of additional modelled minerals of interest.

Acknowledgments

We thank the Antarctic Search for Meteorites (ANSMET) for supplying chips and polished thin sections of DOM 08006 used in these experiments. US Antarctic meteorite samples are recovered by the Antarctic Search for Meteorites (ANSMET) program, which has been funded by NSF and NASA, and characterized and curated by the Department of Mineral Sciences of the Smithsonian Institution and Astromaterials Acquisition and Curation Office at NASA Johnson Space Center. Laboratory work and assistance from Rebecca Sutton (ICP-OES), Matt Pickering (IC) and Gareth Perry (SEM) from the University of York is greatly appreciated. RH acknowledges a research grant from the Meteoritical Society, and MRL funding from the UK Science and Technology Funding Council (STFC) via grants ST/T002328/1, ST/W001128/1 and ST/T506096/1. For the purpose of open access, the author(s) has applied a Creative Commons Attribution (CC BY) licence to any Author Accepted Manuscript version arising from this submission.

3.6 Supplementary Materials

Table S3.1

Initial and dried weight of meteorite chips as well as pH values of leachates after the experiments.

Sample	Initial weight (mg)	Comments	pH	O_2 %	Dried weight (mg)	Comments	Difference (%)
Ds	134	2 fragments	9.4	62	134		0
DsC	147		9.4	54	146		-0.68
Dl	142		8.8	100	143		0.70

DlC	154	2 fragments	9.1	100	157	>3 fragments	1.9

Table S3.2
Detection limits (mg/kg), accuracies (%) and precisions (%) of elements analysed by ICP-OES and IC.

Element	Detection limit	Accuracy	Precision
Si	0.33	88.	0.32
Mg	0.00056	109	0.64
Cl	0.026	113	0.79
Sr	0.000076	130	0.83
Na	0.11	110	0.84
Ca	0.027	100	0.98
Zn	0.0055	100	1.0
S	0.0088	99	1.8
Ba	0.00072	120	1.9
K	0.014	100	1.9
Mn	0.00054	110	2.7
Cu	0.0097	110	4.9
Al	0.0067	160	6.5
Ni	0.014	100	8.9
Fe	0.0045	110	10

Table S3.3
List of secondary minerals appearing in the models, broadly sorted by abundance. Minerals in the second column appear only rarely and/or in low quantities.

Mineral name (adapted from database)	Mineral name (adapted from database)
Mg-serpentine	Rhodochrosite
Greenalite	Fe-Na-saponite
Clinochlore	Fe-beidellite
Mg-saponite	Minnesotaite
Andradite	Pyrophyllite
Magnetite	Amesite
Na-bearing saponite	Epidote
Ankerite	Diaspore
Cronstedtite	Amorphous $Mn(OH)_2$
Daphnite	Vaesite
Fe-bearing saponite	Native Sulphur
NH_4-feldspar	Sodaphlogopite
Fe-saponite	Goethite
Siderite	Hedenbergite
Magnesite	Ca-nontronite
Dolomite	Alabandite
Calcite	Kaolinite
Mg-nontronite	Pyroxmangite
Talc	Mn-chlorite

Pyrrhotite	Mn-chloritoid
Heazlewoodite	Mg-montmorillonite
Polydymite	Nickeloxide
NH_4-muscovite	Tobermorite
Secondary troilite	Mg-Ca-saponite

Table S3.4
Blank corrected experimental solution compositions and analytical error (±), analysed by ICP-OES and IC (in mg/kg). bdl=below detection limit.

Element/Sample	Ds	DsC	Dl	DlC
Si	8.1	3.8	21	20
±	0.026	0.012	0.068	0.065
Mg	1.1	1.2	1.5	1.1
±	0.0071	0.0078	0.0095	0.0067
Cl	34	25	39	35
±	0.27	0.20	0.31	0.28
Sr	0.030	0.013	0.041	0.015
±	0.00025	0.00011	0.00034	0.00012
Na	73	12	55	43
±	0.61	0.10	0.47	0.36
Ca	9.8	3.45	11	3.5
±	0.095	0.034	0.11	0.034
Zn	0.071	bdl	0.16	0.089
±	0.00072	N/A	0.0016	0.00089
S	74	5.3	18	8.0
±	1.3	0.093	0.31	0.14
Ba	0.083	0.053	0.26	0.046
±	0.0016	0.0010	0.0050	0.00088
K	12	4.9	4.7	7.3
±	0.23	0.095	0.090	0.14
Mn	0.0016	0.0011	0.00054	bdl
±	0.000043	0.000029	0.000015	N/A
Cu	0.019	0.014	0.025	0.024
±	0.00091	0.00067	0.0012	0.0011
Al	0.14	0.15	0.19	0.23
±	0.0092	0.0098	0.013	0.015
Ni	bdl	bdl	bdl	0.014
±	N/A	N/A	N/A	0.0012
Fe	0.0081	0.0074	0.0048	0.012
±	0.00084	0.00077	0.00050	0.0013

Table S3.5
Abundance of objects (area %) in unaltered DOM 08006 polished thin sections ,131 and ,135, evaluated by SEM point counting.

Object	,131	,135
CAIs	0.5	0.9
Chondrules	44.5	45
Matrix	44.5	41
Opaques	8	9.7
Porosity	2.5	3.4

Table S3.6
Abundance of minerals as well as porosity (area %) in unaltered DOM 08006 polished thin sections ,131 and ,135, evaluated by SEM point counting. n.d.=not detected.

Mineral	,131	,135
Anorthite	n.d.	0.1
Calcite	n.d.	0.2
Ca-sulphate	1.5	0.4
Diopside	1.5	0.7
Enstatite	17	13.4
En90	7	6.5
En80	2	1.6
En70	0.5	0.3
Fe-sulphide	0.5	2.5
Fe,Ni-sulphide	1	1
Fe,Cr-sulphide	0	0.1
Forsterite	10	9.7
Fo90	1	3.1
Fo80	0.5	1.4
Fo70	n.d.	1.3
Fo60	1.5	1.1
Fo50	n.d.	0.6
Fo40	n.d.	n.d.
Fo30	n.d.	0.1
Magnetite	5.5	4.5
Matrix	43	40.4
Melilite	0.5	0.4
Mesostasis	3.5	5
Metal	1	1.8
Porosity	2.5	3.4
Spinel	n.d.	0.3

Table S3.7
Comparison of experimental and modelled aqueous solution compositions as ratios of modelled over experimental concentrations. Values are averaged across all modelled W/R ratios for a system of 50°C

Element	30 d min ratio	30 d max ratio	30 d mean ratio	180 d min ratio	180 d max ratio	180 d mean ratio
Al	1.90E-06	4.47E+02	4.50E+01	4.18E-04	1.49E+00	2.82E-01
Ca	5.18E-03	7.64E-01	1.24E-01	4.18E-03	1.28E-01	4.20E-02
Fe	8.45E-03	4.18E+03	2.18E+02	2.05E-02	3.54E+03	6.97E+02
Mg	3.63E-07	3.53E+01	2.51E+00	9.44E-06	2.31E+00	2.01E-01
S	9.27E-06	1.13E+01	5.97E-01	1.31E-09	1.84E-01	3.50E-02
Si	4.33E-01	2.21E+02	3.85E+01	1.65E-01	4.04E+00	1.10E+00
Na	1.25E+00	7.51E+02	9.66E+01	2.24E+00	2.88E+02	5.88E+01
Mn	2.20E+00	4.46E+02	6.33E+01	n/a	n/a	n/a

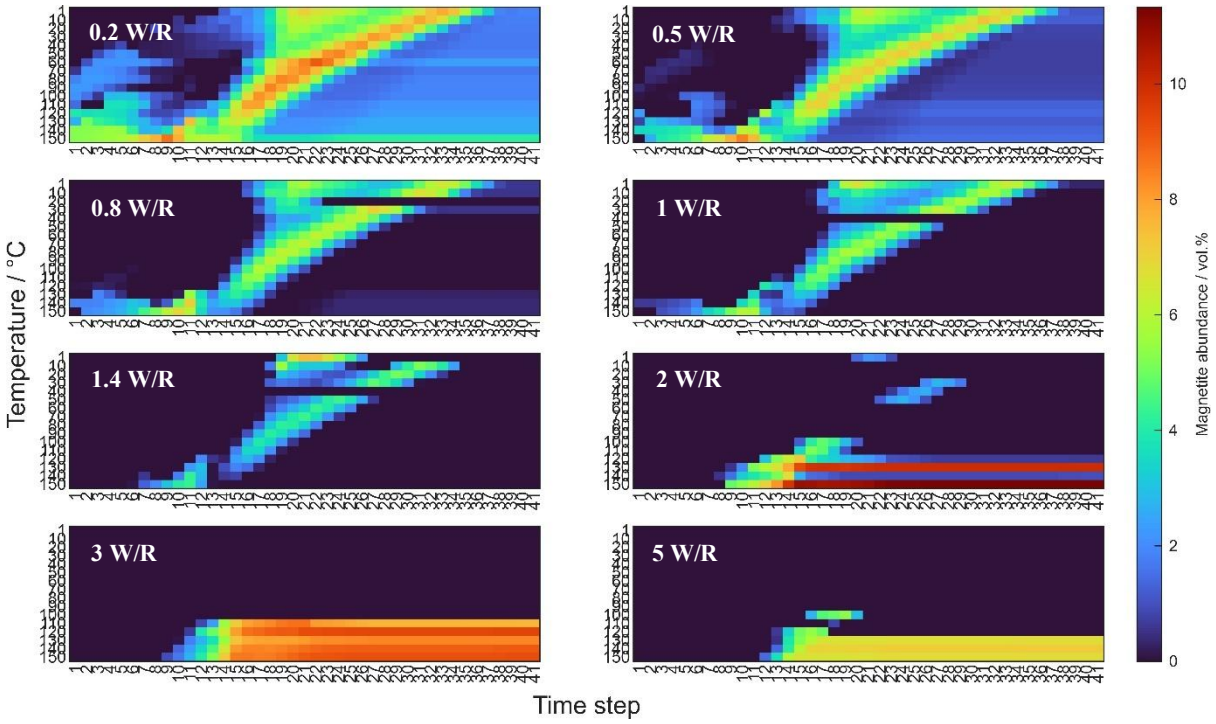

Figure S3.1. Heatmaps of magnetite abundance as a function of temperature and time. The different panels denote different W/R ratio (by mass) values. Timesteps 1–8 represent time of the order of seconds to hours, timesteps 9–18=days to months, timesteps 19–26=years to decades, timesteps 27–34=centuries to millennia, timesteps 35–41=10,000 to 100,000 years.

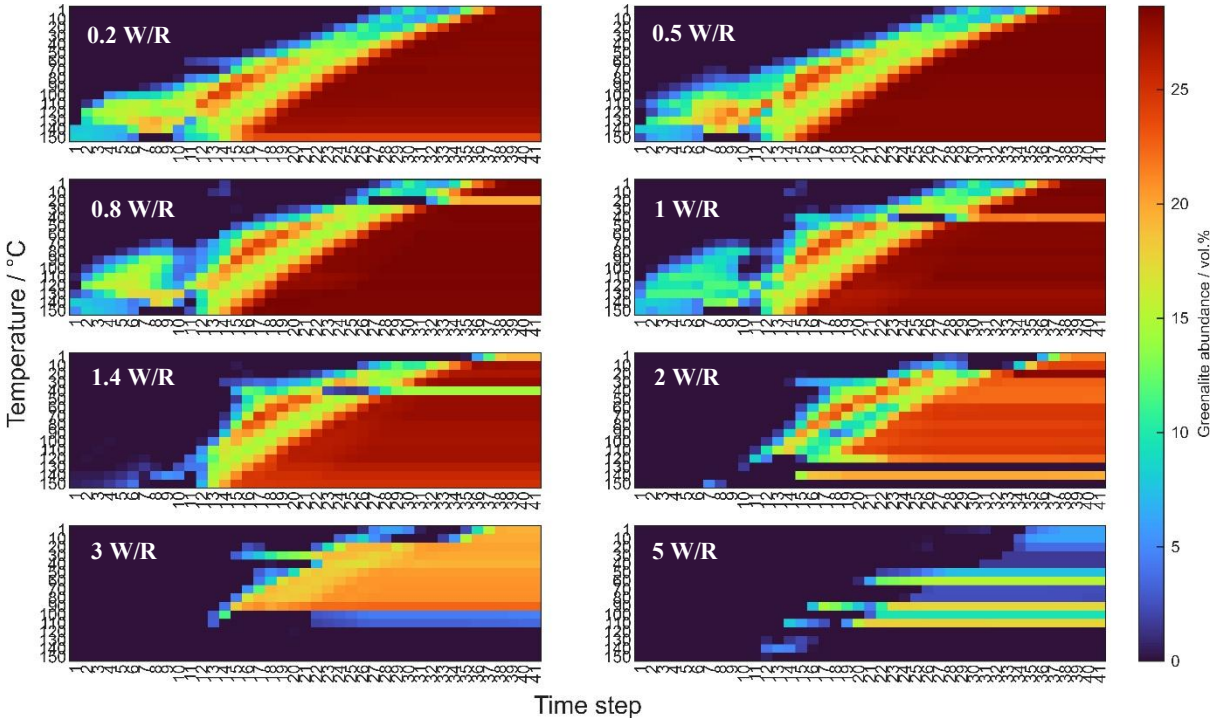

Figure S3.2. Heatmaps of greenalite abundance as a function of temperature and time. The different panels denote different W/R ratio (by mass) values. Timesteps 1–8 represent time of the order of seconds to hours, timesteps 9–18=days to months, timesteps 19–26=years to decades, timesteps 27–34=centuries to millennia, timesteps 35–41=10,000 to 100,000 years.

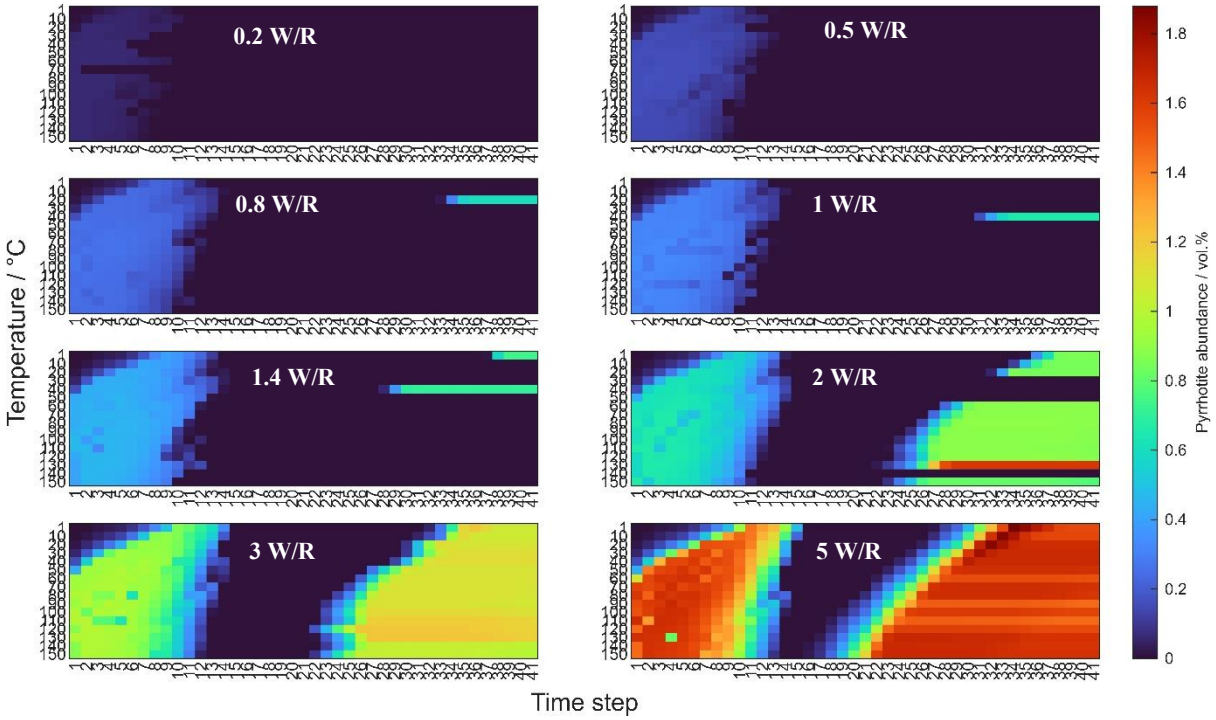

Figure S3.3. Heatmaps of pyrrhotite abundance as a function of temperature and time. The different panels denote different W/R ratio (by mass) values. Timesteps 1–8 represent time of the order of seconds to hours, timesteps 9–18=days to months, timesteps 19–26=years to decades, timesteps 27–34=centuries to millennia, timesteps 35–41=10,000 to 100,000 years.

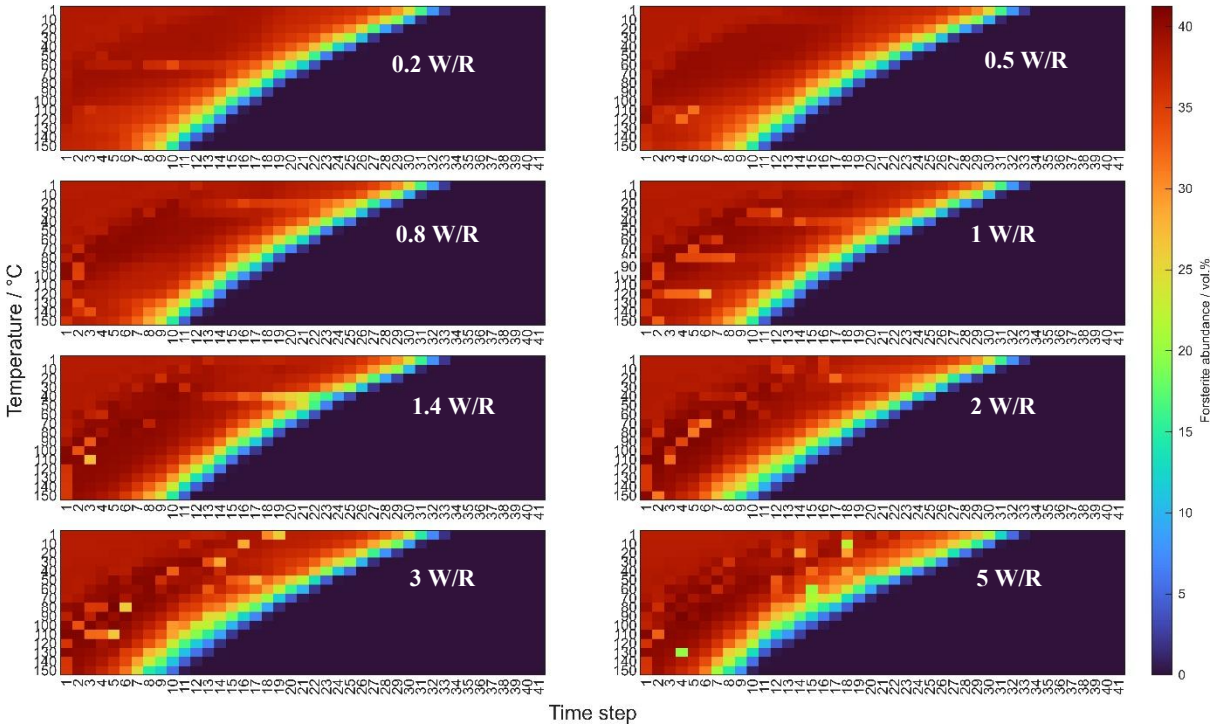

Figure S3.4. Heatmaps of forsterite abundance as a function of temperature and time. The different panels denote different W/R ratio (by mass) values. Timesteps 1–8 represent time of the order of seconds to hours, timesteps 9–18=days to months, timesteps 19–26=years to decades, timesteps 27–34=centuries to millennia, timesteps 35–41=10,000 to 100,000 years.

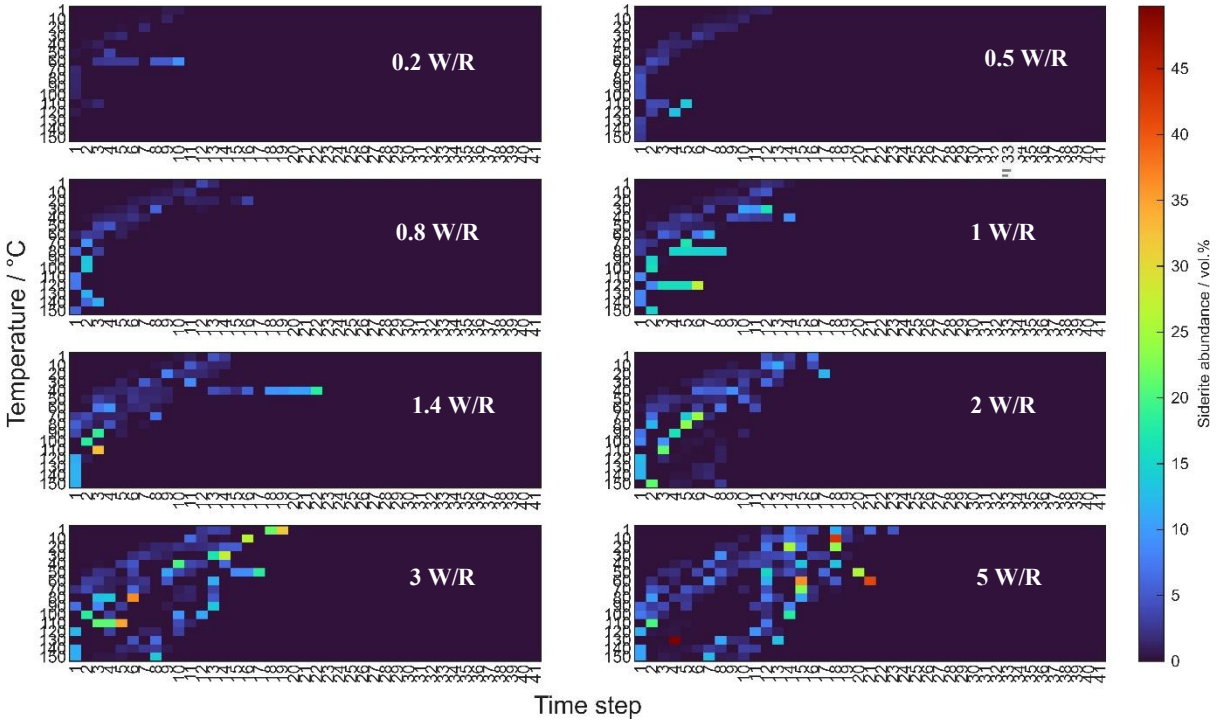

Figure S3.5. Heatmaps of siderite abundance as a function of temperature and time. The different panels denote different W/R ratio (by mass) values. Timesteps 1–8 represent time of the order of seconds to hours, timesteps 9–18=days to months, timesteps 19–26=years to decades, timesteps 27–34=centuries to millennia, timesteps 35–41=10,000 to 100,000 years.

4 The effect of terrestrial weathering on the mineralogy and petrologic (sub)types of CM chondrites explored by kinetic modelling and laboratory experiments

[1]Robin L. Haller*, [1]Martin R. Lee, [2]Mark E. Hodson

[1]*School of Geographical and Earth Sciences, University of Glasgow, Glasgow G12 8QQ, UK*

[2]*Environment Department, University of York, York YO10 5NG, UK*

*Corresponding author: *E-mail address:* robin.haller123@gmail.com

This chapter represents a first manuscript submitted to *Meteoritics & Planetary Science* (under consideration) and differs from the published paper (doi: 10.1111/maps.70145)

4.0 Abstract

Terrestrial weathering alters the chemical and isotopic composition and mineralogy of meteorites; its effects on ordinary chondrites are well studied but relatively little is known about the susceptibility of carbonaceous chondrites. We combined laboratory experiments, whereby Chwichiya 002 (C3-ung find, moderately weathered), Murchison (CM2 fall, unweathered) and Kolang (CM1/2 fall, unweathered) were exposed to artificial rainwater for 30–180 days, with kinetic models to examine the effects of different weathering timespans and environments on mineralogy and petrologic (sub)type. Leachates derived from the Murchison and Kolang experiments were rich in S, Ca, Na, Cl, K and Mg with less abundant Si and Fe, suggesting that calcite and pyrrhotite, together with unknown Na-K-Cl bearing minerals, are particularly susceptible to terrestrial alteration. Chwichiya 002 was less reactive than anticipated, possibly due to earlier hot desert weathering. Models predict that unaltered chondrites with amorphous material, including Chwichiya 002, rapidly oxidise within days when exposed to water, particularly in warm environments (i.e., hot deserts). A terrestrial weathering scale of CM chondrites could be based on the degree of rustiness as well as on calcite and sulphide abundances and anomalies in Ca, S, Na, Cl and K elemental abundances.

4.1 Introduction

Carbonaceous chondrites (CCs) are of high scientific importance due to their high abundance of volatile elements. Several groups of the CCs (Ivuna-like (CI), Mighei-like (CM), Renazzo-like (CR) and ungrouped meteorites) were aqueously altered in a parent body environment very early in solar system history (Brearley et al., 2006). The products of aqueous alteration of these CCs include phyllosilicates, carbonates, oxides, and other minor phases. In CM chondrites, the extent of aqueous alteration has been classified according to various schemes; the ones that are most commonly used involve a combination of texture and mineralogy (from subtype 3.0 (unaltered) to 2.0 (completely altered)) (Rubin et al., 2007; Rubin et al., 2015; Kimura et al., 2020) or the fraction of phyllosilicates to anhydrous silicates (PSF)

(from type 3.0 (unaltered) to 1.0 (completely altered)) (Howard et al., 2015). However, a problem in understanding parent body aqueous alteration is that the CCs are also susceptible to alteration on Earth, potentially producing minerals very similar to those that were generated by parent body processing (e.g., Bland et al., 2006). Terrestrial weathering of chondrites occurs upon entering Earth's atmosphere, during residence in the cold deserts (e.g., Antarctica) and hot deserts where most are collected, and potentially even during their curation in museums or other facilities (Velbel, 1988; Velbel et al., 1991; Bland et al., 2006; Lee et al., 2021). Thus, terrestrial weathering is very important to evaluate for a comprehensive understanding of parent body evolution.

The extent of terrestrial alteration of Antarctic finds is described by weathering categories developed by The Meteorite Working Group. A, B, and C describe the degree of rustiness of a hand specimen, with suffix *e* if they contain evaporites (Velbel, 1988). The oxidation of metal, troilite or mafic silicates as recognised in polished sections is represented on a scale from W1 to W6 (Wlotzka, 1993; Zurfluh et al., 2016), which can also be used for hot desert finds. While these scales are suitable for metal-rich meteorites such as ordinary chondrites, CM chondrites typically contain little to no Fe-Ni metal (Rubin et al., 2007) so that rust is harder to identify. Despite their low abundance of metal, carbonaceous chondrites, especially the CIs and CMs, are susceptible to terrestrial alteration due to their considerable proportion of fine-grained phyllosilicate-rich matrix and enrichment in volatiles and organic matter (Bland et al., 2006; Garvie et al., 2025).

In CM chondrites, the phyllosilicate mineral cronstedtite is ubiquitous and is interpreted as a product of parent body alteration; however, the detection of cronstedtite in heavily altered Antarctic ordinary chondrites (Lee and Bland, 2004) suggests that this mineral could also form in the CMs by terrestrial alteration. When considering the PSF defined by Howard et al. (2015), cronstedtite forms at the expense of anhydrous silicates. The terrestrial production of cronstedtite would lower the petrologic type of CM chondrite finds compared to falls, which could explain why falls, possibly with the exception of a lithology in Winchcombe (Suttle et al., 2023) or Mukundpura (Potin et al., 2020), do not reach the low petrologic types exhibited by some finds such as CM1 LaPaz Icefield 02277 (King et al., 2017). Bland et al. (2006) found a strong positive correlation between the year of fall of CM chondrites and the mineralogic alteration index, a metric for quantifying the meteorite's degree of aqueous alteration (Browning et al., 1996). This finding raises the intriguing possibility of terrestrial weathering lowering the petrologic (sub)type of CM chondrites.

Some of the least aqueously altered CM chondrites, such as Paris or Asuka 12169, are characterised by abundant amorphous silicates (Leroux et al., 2015; Kimura et al., 2020). They are thought to be among the most susceptible phases to aqueous alteration on the CM parent body and are therefore very rare in CM chondrites of low petrologic type. Terrestrial weathering could be an additional factor in the scarcity of amorphous silicates in CM chondrites, i.e., amorphous silicates could have been present in more

meteorites prior to their exposure to the terrestrial environment. Indeed, some samples returned from asteroid 162173 Ryugu contain numerous amorphous silicate objects (Nakamura et al., 2022), which have not so far been detected in any CI1 chondrite falls, possibly due to their terrestrial alteration.

Experimental studies of the terrestrial weathering of CM chondrites are sparse (e.g., Garvie et al., 2024, 2025). However, samples returned from C-complex asteroids Ryugu (Nakamura et al., 2022) and Bennu (Lauretta et al., 2024) have enabled a unique perspective on alteration of the related CI chondrites once in contact with Earth's environment. Imae et al. (2024) compared a Ryugu particle stored for 144 days in a valve-open laboratory desiccator with a pristine sample and noted that gypsum crystals were present only on the terrestrially exposed particle. CI chondrites typically also contain ferrihydrite (Brearley, 2006) in addition to gypsum, but this mineral was not detected on the weathered Ryugu particle, suggesting that ferrihydrite requires more time or different environmental conditions to form compared to gypsum. Garvie et al. (2025) showed experimentally that gypsum can form rapidly on samples of C2-ung Tarda and CM2 Aguas Zarcas (e.g., within 10 min and 24 h, respectively, under conditions of high relative humidity), which suggests that most, if not all, gypsum found in carbonaceous chondrites is terrestrial.

In addition to experiments, geochemical models can help understand the effects of terrestrial weathering, and are potentially powerful tools because they can be used to explore the influence of different parameters such as temperature, pH or water composition, and timescales far beyond those possible in the laboratory. While parent body processes have been the focus of modelling studies (e.g., Zolensky et al., 1989; Zolotov and Shock, 2004; Zolotov, 2007, 2009, 2012, 2014, 2017, 2020; Neveu and Desch, 2015; Shibuya et al., 2024), terrestrial weathering of chondrites so far has been mainly addressed via petrographic and experimental approaches. To our knowledge, only one study to date has modelled the terrestrial weathering of meteorites. Lee et al. (2006) used the software PHREEQC to calculate saturation states of different phases that could form at the end of weathering experiments on an LL6 chondrite. However, little is known about the evolution of mineral abundances and mineral reactivity under different terrestrial conditions, which could be investigated with the help of kinetic modelling to simulate the exposure of a meteorite to water and the terrestrial atmosphere. A caveat with this approach is that natural terrestrial weathering rarely involves constant exposure of the meteorite to water. Nonetheless, a kinetic model could accurately simulate weathering under extreme conditions and could give an upper limit of the susceptibility of different meteoritic minerals to terrestrial exposure.

This study focuses primarily on the effect of terrestrial weathering on the petrologic (sub)type of CM chondrites using a combination of kinetic modelling and laboratory experiments. The kinetic models include a range of different parameters (temperature, water/rock (W/R) ratio (by mass, if not stated otherwise), redox conditions, fluid type and fluid concentration) to simulate terrestrial weathering under different conditions (hot desert vs. Antarctic weathering, amount of water available etc.). The laboratory

experiments give a complementary insight into terrestrial weathering and can also ground-truth the models, albeit with the drawback of a reduced parameter space (limited time, fixed temperature and W/R ratio etc.). Finally, we aim to evaluate the rate and impact of terrestrial weathering on CM chondrites of different petrologic (sub)type to propose a terrestrial weathering scale for the group.

4.2 Materials and Methods

4.2.1 Meteorites

The carbonaceous chondrites selected for this study represent a wide range of petrologic types from nearly unaltered (DOM 08006, CO3.00 and Chwichiya 002, C3.00-ung) to almost completely altered (LAP 02277, CM1) (Table 4.1). Samples of three meteorites were used in the experiments: Murchison, Kolang, and Chwichiya 002. The models utilised four meteorites: DOM 08006, Murchison, Kolang and LAP 02277.

Table 4.1. Meteorite descriptions.

Feature	DOM 08006	Chwichiya 002	Murchison	Kolang	LAP 02277
Type[a]	CO3	C3.00-ung	CM2	CM1/2	CM1
Find/Fall date[a]	Find 2008	Find 2018	Fall 1969	Fall 2020	Find 2002
Weathering grade[a]	A/B	moderate	NA	NA	A
Olivine (vol.%)	51[b]	-	15.2[c]	8.0[d]	5.30[e]
Pyroxene (vol.%)	22[b]	-	8.30[c]	5.0[d]	nd
Sulphides (vol.%)	3.0[b]	-	1.80[c]	1.0[d]	2.20[e]
Glass (vol.%)	15[b]	-	nd	nd	nd
Fe-Ni metal (vol.%)	1.0[b]	-	nd	nd	nd
Mg-Fe serpentine (vol.%)	2.0[b]	-	22.2[c]	50[d]	68.3[e]
Cronstedtite (vol.%)	nd	-	50.3[c]	32[d]	20.6[e]
Magnetite (vol.%)	nd	-	1.10[c]	3.0[d]	1.90[e]
Calcite (vol.%)	nd	-	1.20[c]	1.0[d]	1.70[e]

[a]Meteoritical bulletin
[b]Alexander et al. (2018)
[c]Howard et al. (2011)
[d]King et al. (2021)
[e]King et al. (2017)
nd = not detected

Kimura et al. (2020) proposed the Antarctic find Asuka 12169 to be the first and thus far only CM3.0 recognised; however, information about its bulk mineralogy, which is required for geochemical modelling, is limited and the small mass of the meteorite (2.26 g) makes it unsuitable for destructive laboratory experiments. An alternative to Asuka 12169 is the Saharan desert find Chwichiya 002, which, despite being classified as a C3.00-ung, bears some similarities to CM chondrites like a high matrix/chondrule ratio and abundant tochilinite-cronstedtite intergrowths (TCIs) (Ruggiu et al., 2022). It was therefore selected as a CM3 proxy for the laboratory experiments. However, to our knowledge,

the modal mineralogy of Chwichiya 002 has not yet been determined which is why an alternative CM3 proxy was selected for the models, the Antarctic CO chondrite find DOM 08006. DOM 08006 is one of the most pristine carbonaceous chondrites, as it has experienced very little aqueous and thermal alteration (Davidson et al., 2019); its well-studied mineralogy (Alexander et al., 2018) makes it more suitable for modelling than Asuka 12169 or Chwichiya 002. Astrophysical models (Desch et al., 2018) show that CO and CM chondrites likely accreted on parent bodies in close proximity, and they also have similar properties such as Ca-Al rich inclusions abundance, chondrule chemistry, and chondrule size (e.g., Greenwood et al., 2023; Floyd et al., 2024), meaning that CO chondrites might even represent CM chondrites that have largely escaped parent body aqueous alteration. Regardless of whether CO chondrites are indeed unaltered precursors of CMs, they are a suitable proxy from a modelling perspective and regarding their mineralogy and chemical composition.

Murchison, Kolang and LAP 02277, are all CM chondrites. Murchison and Kolang were observed to fall in 1969 and 2020, respectively, whereas LAP 02277 was found in Antarctica in 2002. Murchison is one of the most studied carbonaceous chondrites (Fendrich and Ebel, 2021) owing to its high mass of 100 kg and rapid recovery after its fall. Among the CM falls, it is the least aqueously altered with a petrologic subtype of 2.5 (Rubin et al., 2007) and 2.7–2.9 (Lentfort et al., 2021). Its mineralogy is also well-studied (Howard et al. 2009, 2015) and consists of mainly serpentine (Mg-Fe serpentine and cronstedtite) with some unaltered olivine and pyroxene and minor sulphides, magnetite and calcite. Additional phases in Murchison that are not measured by X-ray diffraction (XRD) are metal and tochilinite with the latter represented by TCIs (Rubin et al., 2007). Compared with Murchison, Kolang has been more extensively aqueously processed and is the most altered CM fall (King et al., 2021), although other CM falls such as Winchcombe (King et al., 2022) and Mukundpura (Potin et al., 2020) also contain heavily aqueously altered lithologies. In accordance with its classification as CM1/2, Kolang contains more Mg-Fe serpentine than cronstedtite and has a lower abundance of anhydrous silicates compared to CM2s like Murchison. Finally, LAP 02277 is one of the most aqueously altered CM chondrites (Rubin et al., 2007; King et al., 2017) with little surviving olivine and no pyroxene. It was not available for the laboratory experiments but has been included in the kinetic modelling to evaluate whether terrestrial weathering affects CM1 chondrites.

4.2.2 Kinetic Weathering Models

Weathering models to simulate the interaction of meteorites with a terrestrial fluid were built in the geochemical software PHREEQC (Parkhurst, 1995; Parkhurst and Appelo, 1999, 2013). In contrast to equilibrium modelling, the starting mineralogy of each meteorite (DOM 08006, Murchison, Kolang and LAP 02277) was implemented by using the KINETICS keyword (see Parkhurst and Appelo, 2013) to allow for the modelling of systems as a function of time. Within that keyword, each meteorite is specified by the molar abundance of its minerals (Table S4.1) and their surface area and optional scaling

factor. Zhang et al. (2020) created three new databases for PHREEQC with SUPPHREEQC and showed that they perform more accurately compared to older PHREEQC databases. Hence, we selected their database *diagenesis.dat* and combined it with mineralogical information from *core10.dat* (Neveu et al., 2017) into a new database suitable for terrestrial weathering modelling, *diagenesis_terr.dat*. This new database also includes a wider array of kinetic data of minerals, compiled by Zhang et al. (2019). Whereas this database contains abundant thermodynamic information, kinetic data for ferrosilite, troilite, iron metal and $Fe(OH)_2$ (proxy for Fe-rich glass in DOM 08006) are missing. For those minerals, we used proxy rate expressions of minerals with similar chemistry and/or dissolution rates, namely enstatite (for ferrosilite), pyrrhotite (for troilite), magnetite (for iron metal) and goethite (for $Fe(OH)_2$). As magnetite dissolves only slowly (Palandri and Kharaka, 2004) a scaling factor of 10 was used to accelerate the dissolution of iron metal that it represents. Enstatite is expected to dissolve more slowly than forsterite but in meteorites an opposite behaviour is observed with no pyroxene remaining in CM1s like LAP 02277 (King et al., 2017). Frequent fractures observed in pyroxene could explain its higher susceptibility to aqueous alteration (Hanowski and Brearley, 2001) and to reflect this in our models, we implemented a scaling factor of 10 for enstatite and ferrosilite.

In addition to the abundances of minerals, the input file also requires information on their surface areas. Ideally, this value reflects the reactive, sometimes also called 'accessible', surface area of the mineral, which is difficult to determine, as it not only requires knowledge of the mineral surface but also of its contact to connected pore space and its reaction mechanism at a molecular level. Several studies have determined reactive surface area by using 2D- and 3D imaging (e.g., Beckingham et al., 2017; Awolayo et al., 2022) or an autocorrelation approach to quantify mineral-porosity spatial distributions (Anovitz et al., 2023). However, both methodologies require the analysis of an unreacted sample which is not always feasible, especially in meteoritic studies. Hence, reactive surface area is more often approximated from either the geometric surface area of mineral grains, which assumes a regular shape (spheres, cubes etc.) or by applying the Brunauer-Emmett-Teller (BET) theory (Brunauer et al., 1938) to calculate BET surface areas (e.g., Brantley and Mellott, 2000). Brantley and Mellott (2000) showed that the specific surface area (area/mass) of a mineral can be calculated as a function of its grain diameter and empirically derived parameters. The number of minerals analysed by this study, however, was limited. For simplification and due to lack of more specific information about grain sizes in meteorites, we only modelled three variations of specific surface areas (m^2/g): values of 0.2 were assigned to anhydrous silicates that are generally fairly coarse grained with little surface roughness; calcite, metal and sulphides received a value of 10 due to generally smaller grain sizes, and phyllosilicates as well as $Fe(OH)_2$ with even smaller grain sizes and/or higher surface roughness were modelled with values of 20. The rate laws compiled by (Zhang et al., 2019) require surface areas to be expressed in m^2/kg water, for which the specific surface area of each mineral is multiplied by its molar abundance and molar mass.

While those modelled surface areas are only a crude approximation, positive results from preliminary modelling support their choice.

The higher computational costs of the kinetic modelling required some simplifications compared to equilibrium model studies (e.g., Zolotov et al., 2012; Neveu et al., 2017; Shibuya et al., 2024). For example, the elemental composition of the system was simplified to Al, C, Ca, Cl, Fe, H, Mg, Na, O, S and Si, and a less diverse starting mineralogy that only consists of those measured by XRD was chosen from the literature. Seventeen time steps ranging from 10^{-4} to 10^{4} days were selected to investigate both short- and long-term effects of terrestrial weathering; for each time step, the speciation of the dissolved solutes in the water and the primary and secondary mineralogical composition was calculated. Preliminary modelling also showed that using the implicit CVODE method (Cohen et al., 1996) instead of the default Runge-Kutta method to integrate the kinetic rate equations is more beneficial for the models as it led to faster and more stable computations.

Various geographical settings of terrestrial weathering are represented by different modelling parameters (temperature, W/R ratio, redox conditions, fluid type (rainwater and seawater) and fluid concentrations) (Tables 4.2 and S4.2). Differences in temperature aim to model conditions in cold and hot deserts (4°C and 30°C, respectively), a higher W/R ratio (1000 compared to 1) represents a greater influx of water or higher porosity, and an increase in fluid concentration is reached by evaporating 90% of the water, which might be representative of saline water trapped in pore spaces. Meteorites are typically weathered by rainwater; however, the Cl-bearing Fe-hydroxide akageneite has been observed as an alteration product in Antarctic finds (Lee and Bland, 2004), indicating that some meteorites were likely altered by fluids enriched in Cl, probably derived from sea spray. Systems with seawater and/or concentrated fluids could be also applicable to salt lake environments like the Umm as Samim sabkha in Oman (Al-Kathiri et al., 2005).

Table 4.2. Kinetic modelling conditions.

Parameter	Value 1	Value 2
Temperature (°C)	4	30
W/R ratio (by mass)	1	1000
Redox condition	Closed[1] system	Equilibrated with atmosphere
Fluid type	rainwater	seawater
Fluid concentration	1x	1000x

[1]No loss or gain of water or gas

4.2.3 Laboratory Experiments

Samples of Chwichiya 002, Murchison and Kolang, each weighing ~1 g, were crushed to yield six chips per meteorite. The 18 chips were ~100 mg in mass, which is typical of samples used in previous

laboratory weathering experiments (Jones and Brearley, 2006; Lee et al., 2006; Suttle et al., 2022). Artificial rainwater (100x concentrated) was prepared by adding 0.338 g $MgCl_2$, 1.078 g $CaCl_2$, 0.809 g Na_2SO_4 and 1.043 g $NaHCO_3$ salts to 1 L of deionised water, following guidelines of Smith et al. (2002). A dilution factor of 100x was achieved by diluting 10 ml of the 100x concentrated solution to 1 L, from which 20 g was measured to react with the individual meteorite chips in small glass vials to achieve a W/R ratio of ~200. The meteorite chips were reacted with the artificial rainwater in a controlled temperature room (25°C). Three chips of each meteorite were reacted for 30 days (labelled s1, s2 and s3) and three for 180 days (labelled l1, l2 and l3). The reacted chips were carefully extracted from the vials and rinsed with deionised water before being placed in aluminium crucibles and dried overnight (~12 h) in a Thermo Scientific oven at 50°C, after which they were weighed again with a 0.1 mg precision balance. The solutions that reacted with the meteorite chips, hereafter called leachates, were passed through filter paper (Fisherbrand QT210) into 50 ml tubes and stored in a freezer until further analysis by inductively coupled plasma optical emission spectroscopy (ICP-OES) and ion chromatography (IC). The oxygen concentration and pH were measured before and after reaction with the meteorite chips. The pH was measured with a ThermoOrion 420 A+ pH/ISE meter calibrated using three buffer solutions (pH 4.0, 7.0 and 10.0). Oxygen concentrations were measured with an Orion Star A223 dissolved oxygen meter, calibrated using deionised water and a solution of deionised water saturated with nitrogen gas.

4.2.4 Analytical methods

4.2.4.1 ICP-OES and IC

The leachates were measured by ICP-OES for Al, Ba, Ca, Co, Cr, Cu, Fe, K, Mg, Mn, Na, Ni, P, S, Si, Sr and Zn, and by IC for Cl; those elements are fairly abundant in CCs (Lodders, 2021). ICP-OES analyses were carried out at the University of York (UoY) using a Thermo Scientific iCAP PRO. For most elements, a SupelCo ICP multi-element standard solution IV was used to produce calibration standards whereas for Si and S separate single-element Sigma-Aldrich and Specpure standards were used respectively. To ensure that most leachates were within the standard concentrations, they were 10x diluted with deionised water. Ten blank solutions (deionised water) were also analysed for determining detection limits (Walsh, 1997). Detection limits for most elements were ~1 µg/L. The accuracies of measurements were generally around 100%. Duplicate measurements of leachates from three meteorites chips (~10% of all measured samples) allowed for the calculation of the precision (Gill and Ramsey, 1997). Precision values were generally around 1%. Values of detection limits, accuracy and precision are in Table S4.3.

Chlorine was measured by IC (Dionex ICS-2000). The detection limit was 0.026 mg/L, the accuracy was 113% and the precision (median of four leachate duplicates and 5 mg/L standard drift) was 0.79%.

4.2.4.2 SEM of meteorite chips and thin sections

To investigate the extent to which meteorite chips were mineralogically altered by reaction with the artificial rainwater, they were studied by SEM to identify potential secondary phases and alteration textures. From the 18 meteorite chips, eight were selected (at least one per meteorite and experiment duration) for examination. The dried meteorite chips were mounted on a sample stub and placed in a Hitachi TM4000Plus Tabletop low-vacuum, 5-20 kV SEM equipped with an Oxford Instruments EDS and AZtecOne analysis software at the UoY. Due to the low vacuum operation conditions, no sample coating was needed. Mixed SE/BSE images were obtained at 15 kV accelerating voltage for different magnification levels. EDX analyses used 20 kV acceleration voltage and were used to obtain point spectra as well as some line spectra for regions of interest and X-ray maps. Count times were restricted to 60 s.

Polished and carbon coated (~20 nm) thin sections of three meteorite chips (Kolang l3, Murchison l1 and Chwichiya 002 l1) were examined for signs of laboratory alteration products by using a Zeiss Sigma VP Field-Emission SEM at the University of Glasgow.

4.3 Results

4.3.1 Modelling

The chosen parameters (four meteorites, two temperatures, variable W/R ratios, fluid concentrations, fluid compositions and redox states) yielded a total of 128 different simulations, each comprising 17 time steps from 9 seconds to 27 years. Systems with 10x concentrated seawater and 1000 W/R ratios yielded large amounts of precipitates (>10 vol.% evaporites like mirabilite) and were therefore excluded from the results. A list of all primary and secondary minerals appearing in the models is in Table 4.3.

4.3.1.1 Comparison of base model of Murchison with different parameters

As one of the most studied CM chondrites, Murchison was chosen as the base model with which meteorites of higher and lower petrologic type can be compared. Notable quantities (>0.1 vol.%) of alteration products start to appear as early as 0.5 days (Figure 4.1a). The most abundant secondary phases are goethite and talc, which can reach >30 vol.% by the end of the simulation (10,000 days). Amorphous silica also forms early but dissolves later, and gypsum appears only after 50 days. The primary phases most susceptible to alteration are fayalite and magnetite, which completely dissolve within 100 days. Cronstedtite, initially the most abundant mineral, and calcite, dissolve by 1000 days whereas notable changes (>10% differences) in pyrrhotite and forsterite abundance only occur after 1000 days. Mg-serpentine abundance initially follows a similar pattern to cronstedtite but reaches a minimum after 1000 days before increasing again, although its final abundance remains lower than at the start of the model.

Table 4.3. Primary and secondary minerals appearing in the models; the latter are sorted by their overall abundance.

Mineral	Formula	Primary	Secondary
Forsterite	Mg_2SiO_4	x	
Fayalite	Fe_2SiO_4	x	
Enstatite	$MgSiO_3$	x	
Ferrosilite	$FeSiO_3$	x	
Native Iron	Fe	x	x
$Fe(OH)_2$	$Fe(OH)_2$	x	
Troilite	FeS	x	x
Pyrrhotite	$Fe_{0.875}S$	x	
Calcite	$CaCO_3$	x	x
Magnetite	Fe_3O_4	x	x
Mg-serpentine	$Mg_3Si_2O_5(OH)_4$.	x	x
Cronstedtite	$Fe_2Fe_2SiO_5(OH)_4$	x	
Goethite	FeOOH		x
Talc	$Mg_3Si_4O_{10}(OH)_2$		x
Dolomite	$CaMg(CO_3)_2$		x
Sepiolite	$Mg_4Si_6O_{15}(OH)_2(H_2O)_6$		x
Magnesite	$MgCO_3$		x
Greenalite	$Fe_3Si_2O_5(OH)_4$.		x
Pyrite	FeS_2		x
Amorphous silica	SiO_2		x
Brucite	$Mg(OH)_2$		x
Mirabilite	$Na_2SO_4(H_2O)_{10}$		x
Ferropericlase	FeO		x
Ankerite	$CaFe(CO_3)_2$		x
Gypsum	$CaSO_4(H2O)_2$		x
Anhydrite	$CaSO_4$		x
Diopside	$CaMgSi_2O_6$		x
Aragonite	$CaCO_3$		x

Decreasing temperature from 30 to 4 °C results in slower dissolution and later precipitation by around a factor 10 (Fig. 4.1b). Otherwise, the results are identical apart from sepiolite precipitating instead of talc. An increase of W/R ratio to 1000 causes complete dissolution of calcite within hours, whereas other primary phases appear stable or slightly less reactive (Fig. 4.1c). There is no notable difference in the precipitation of goethite, but talc only starts to precipitate after 50 days (instead of 0.5 days) and no amorphous silica and gypsum form. Increasing the concentration of rainwater by a factor of 10 yields no significance difference in results compared to the base model (Fig. 4.1d). Arguably the biggest differences are obtained with seawater (Fig. 4.1e) and reducing conditions (no equilibration with the atmosphere) (Fig. 4.1f). In the seawater system, up to ~0.5 vol.% dolomite forms within hours but dissolves after 5 days. Calcite dissolves rapidly within hours to days, precipitates again after 10 days before completely dissolving after 50 days. Other primary phases are slightly more reactive in this system; for example, pyrrhotite completely dissolves after 5000 days. No amorphous silica forms and both goethite and talc evolve similarly compared to the base model, whereas gypsum forms much faster (as early as 10 days) although with no difference in its maximum abundance (Fig. 4.1e). Finally, no new secondary phases are observed in the reduced system. Instead, abundances of mainly Mg-serpentine and magnetite increase and calcite and olivine decrease. Those changes are only notable after ~100 days of reaction (Fig. 4.1f).

4.3.1.2 Comparison of base model with the other meteorites

Differences in dissolution and precipitation are notable across all four modelled meteorites. Compared to Murchison, primary phases in DOM 08006 dissolve faster, especially the Fe-rich glass (modelled as $Fe(OH)_2$), which dissolves within hours (Fig. 4.2b). Native metal is also fairly reactive, although its complete dissolution occurs slightly later than fayalite and magnetite. Precipitation of goethite starts earlier and reaches ~10 vol.% within hours. Amorphous silica precipitates but also dissolves earlier, and talc is also a metastable phase that disappears after 1000 days. No major dissolution of Mg-serpentine occurs but instead, large quantities of the mineral precipitate after 100 days. Troilite completely dissolves by 5000 days but no sulphates like gypsum precipitate. Magnesite precipitates only after 5000 days in abundances of ~2 vol.%.

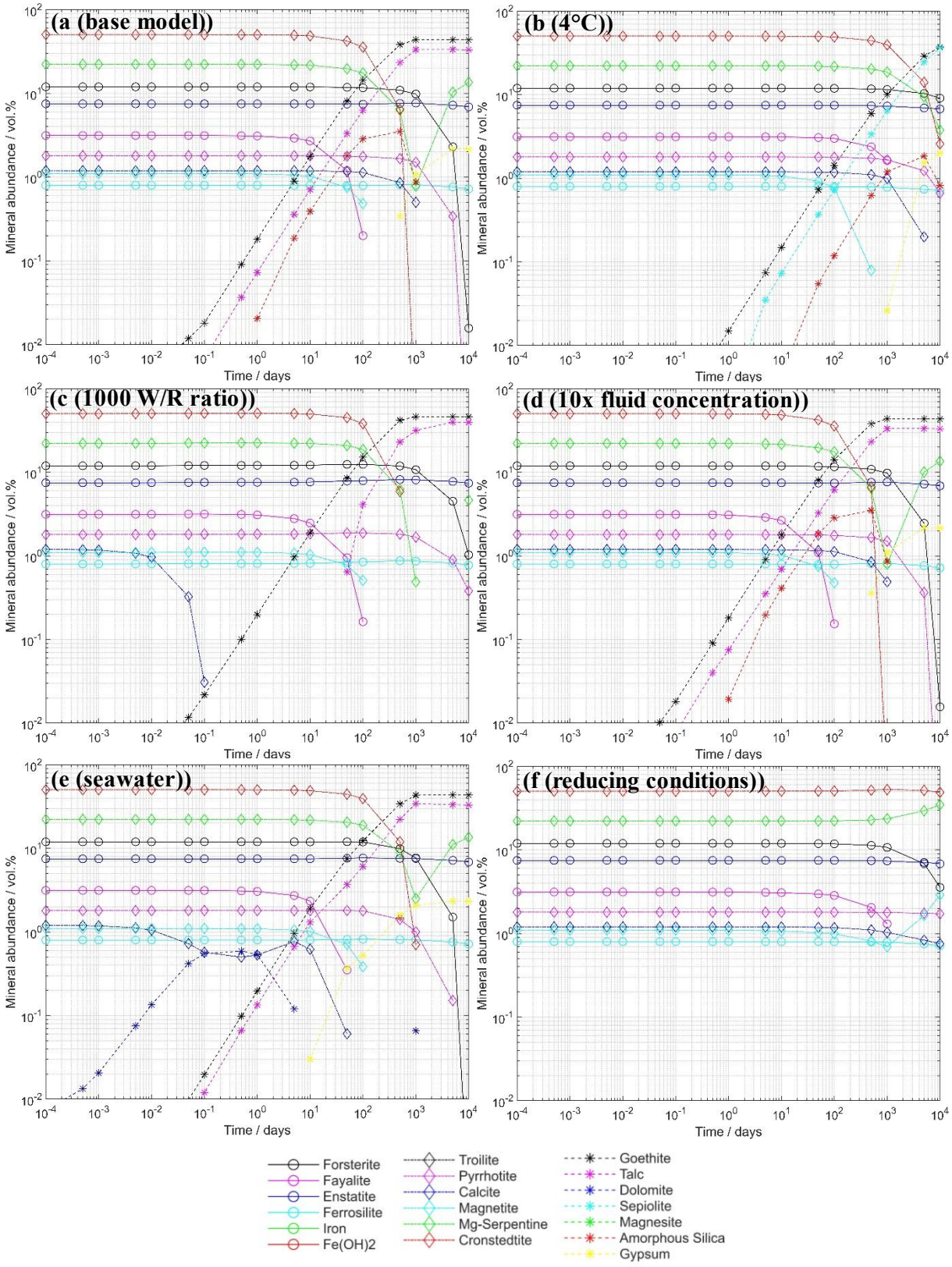

Figure 4.1. Comparison of modelled Murchison weathering (mineral abundances as a function of time) across different parameters: a) base model (30 °C, 1 W/R ratio, 1x fluid concentration, rainwater, oxidised conditions); b) same as a) but with 4°C; c) same as a) but with 1000 W/R ratio; d) same as a) but with 10x fluid concentration; e) same as a) but with seawater; f) same as a) but with reducing conditions (closed system) (no loss or gain of water or gas).

Kolang and LAP 02277 differ from Murchison and DOM 08006 in precipitating dolomite but no amorphous silica. In Kolang, 0.1 vol.% dolomite forms after ~20 days and reaches ~2 vol.% before dissolving again after 1000 days (Fig. 4.2c). Goethite and talc precipitate slightly earlier than dolomite at a similar time than in the base model, whereas gypsum precipitates later. In the LAP 02277 model, goethite, talc and dolomite follow a trend of similar abundances from ~0.1 to ~50 days after which the dolomite abundance, in contrast to goethite and talc, reaches a plateau (Fig. 4.2d). Otherwise, there is little difference between Kolang and LAP 02277.

Some minerals in Table 4.3 require different combinations of parameters and meteorites. Primary phases usually dissolve but the same solid phase can also precipitate in some systems. The latter often requires reducing conditions, especially for native iron and troilite. The secondary minerals ankerite, brucite, diopside, ferropericlase, greenalite and pyrite exclusively form in reduced systems, whereas anhydrite and mirabilite precipitate from the saline solution and not due to meteorite-water interaction. Finally, aragonite is rare (occurs only in seven systems) and is always metastable. Examples of systems in which the aforementioned secondary minerals precipitated are in the supplementary material (Figs. S4.1a–f).

4.3.1.3 Model fluid composition

The mean fluid composition (i.e., leachates) of the models mainly depends on the fluid type; seawater systems (after reacting with the meteorite) are still dominated by Na and Cl, whereas the most abundant elements across all rainwater systems are Mg and S, mainly as Mg^{2+}, $MgSO_4^0$ and SO_4^{2-}. Owing to its high initial salinity, the composition of the fluid in seawater systems is scarcely affected by interaction with the meteorite; therefore, the results in this section focus on rainwater systems which are more influenced by dissolution and precipitation processes. Major differences are seen between oxidised (Figure 4.2e) and reduced (Figure 4.2f) systems. The former show on average an increase of most elements, most notably Mg and S, whereas concentrations of Ca and C increase more moderately. Initially, dissolved Si concentrations increase rapidly but decrease after ~100 days. The average pH value increases from 6.8 to 7.9 and the pe value stays high (>11).

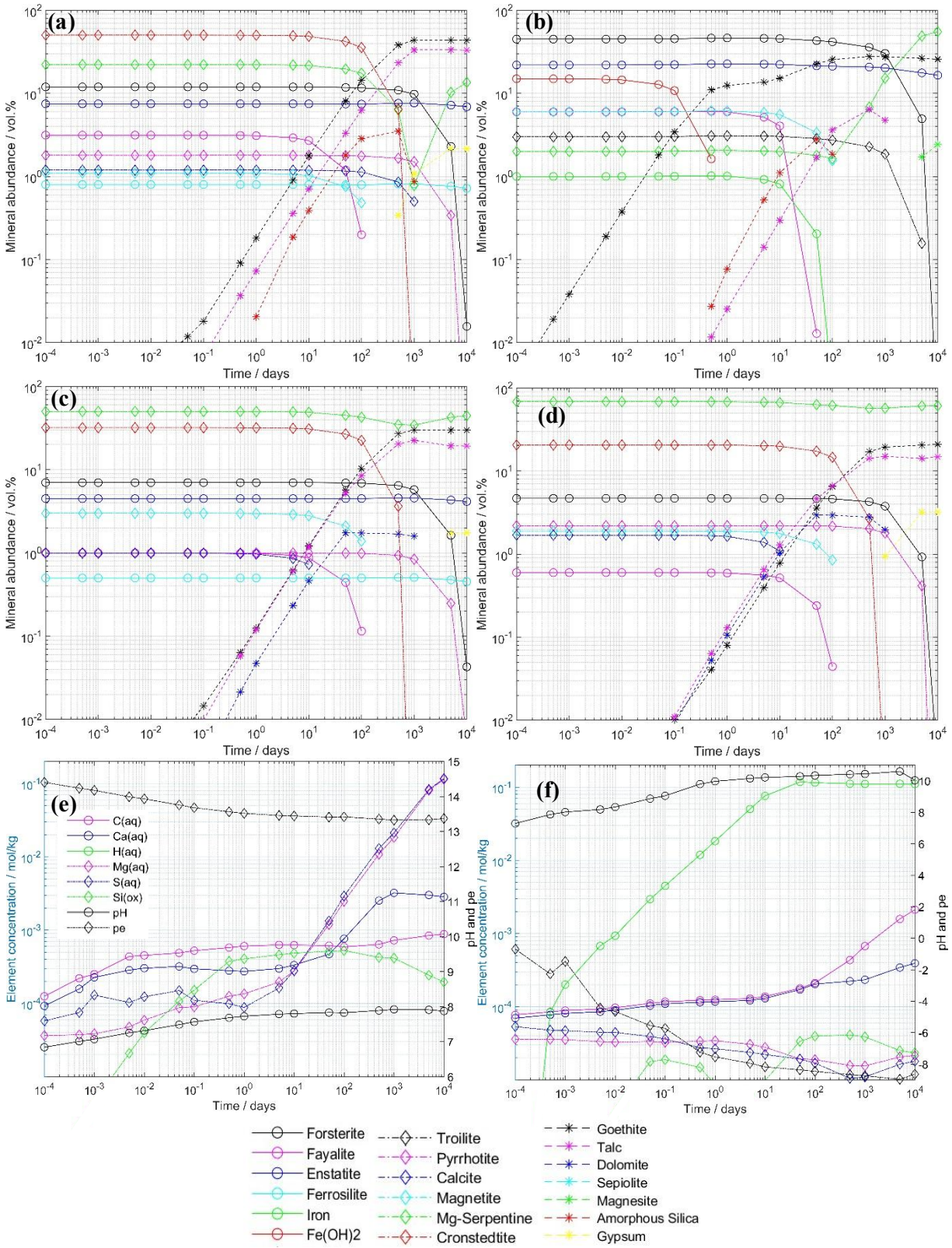

Figure 4.2. (a–d) Comparison of Murchison weathering (mineral abundances as function of time) with different meteorites: a) Murchison (30°C, 1 W/R ratio, 1x fluid concentration, rainwater, oxidised conditions); b) DOM 08006; c) Kolang; d) LAP 02277. (e–f) Mean total element concentration, pH and pe (as function of time) of 1x concentrated rainwater systems (different meteorites, temperature and W/R ratios) separated as: e) oxidised systems f) reduced systems. (closed system) (no loss or gain of water or gas).

In reduced rainwater systems, pH and pe values change more strongly with the former rising to ~10 and the latter dropping to ~-9. The speciation of most elements is similar to oxidised systems except for C, which occurs mainly as CH_4 instead of HCO_3^-. Apart from H, C is the only element with higher abundance in reduced systems whereas other elements, especially S, Mg and Si are much less concentrated than in oxidised systems, which is overall reflected by a lower mean ionic strength (0.0014 mol/kg) compared to oxidised systems (0.31 mol/kg). Ca still shows a moderate increase in concentrations but final concentrations of Mg and S are lower than they were initially, and Si concentrations remain low. Elemental concentrations of Al and Fe are not shown in Figures 4.2e–f because they were low throughout all simulations (<10^{-5} mol/kg). Cl, Na and O were also excluded as they show no variation in concentration.

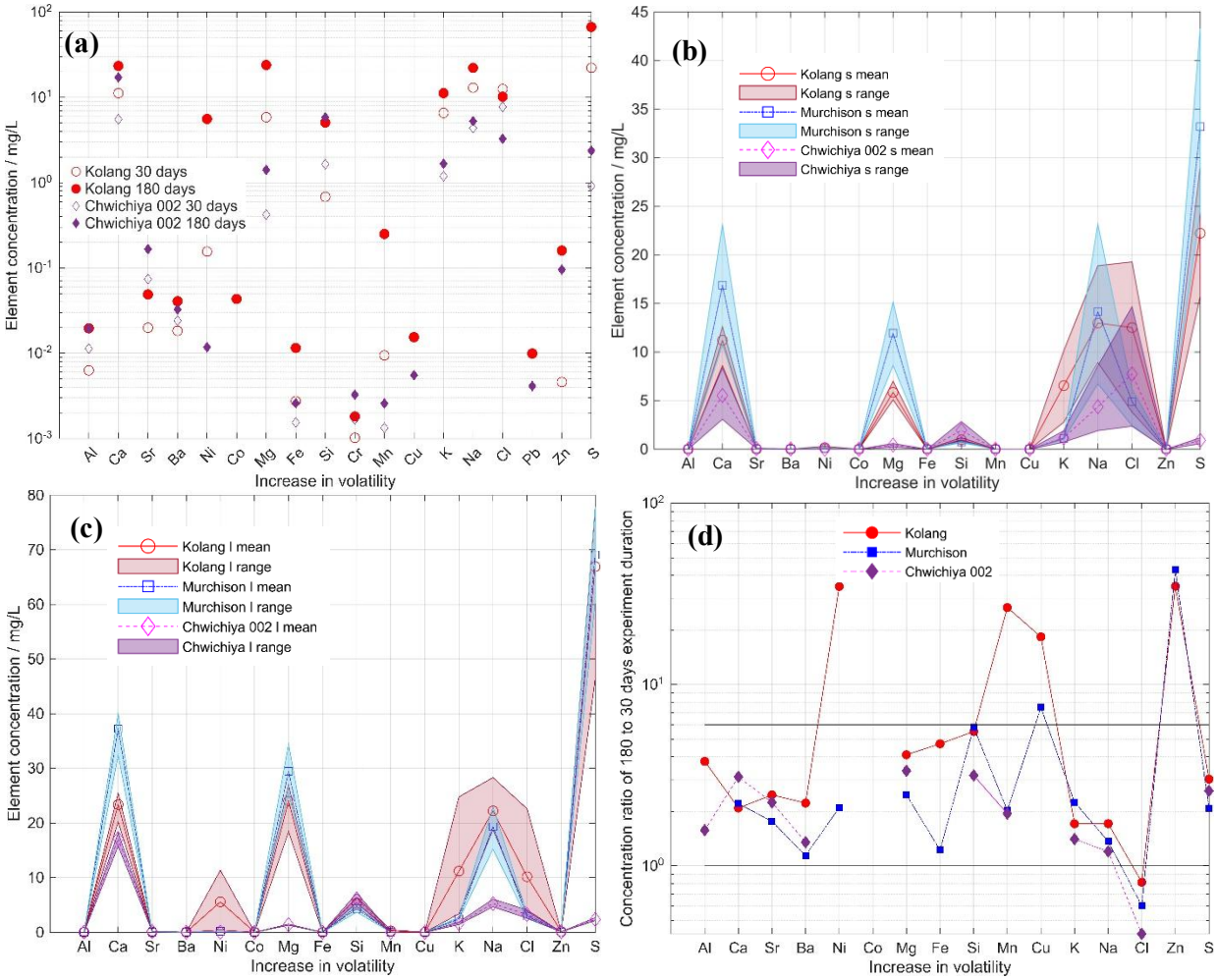

Figure 4.3. a) Mean element abundance for experimental Kolang and Chwichiya 002 leachates (blank corrected) (ordered by volatility) by ICP-OES and IC; some data points not plotted due to values below detection limit. b) Mean (line) and range (shaded area) of leachate concentrations after 30 days and c) after 190 days. Note the difference in the y-axis limit. d) Concentration ratio of 180 to 30 days. Values of 6 (thick black line) denote constant dissolution speed, whereas values of 1 (thin black line) signify constant concentration. Some element abundances were below detection limit in 30- and or 180-day experiment leachates, leading to missing data points.

4.3.2 Experiments

4.3.2.1 Leachate compositions and meteorite chips weight

Elemental concentrations in leachates collected after the experiments were determined by ICP-OES (see Table 4.4, Table S4.4 and Figure 4.3). Figure 4.3a shows blank corrected concentrations averaged across the three triplicates of Kolang and Chwichiya 002 for different experiment durations as well as the initial rainwater for reference. The full data is shown in the supplementary material (Figure S4.2). On average, S, Ca, Na and Mg are the most abundant elements in the leachates (>10 ppm), followed by Cl, K, Si and Ni with average concentrations of >1 ppm. Of lower concentration but present in all samples above the detection limits are Sr, Zn, Ba and Mn, whereas Cu, Al, Fe, Co and Ni are below detection limit for one or more meteorite chips. Pb and Cr were not detected in any samples and were therefore not considered in Figure 4.3. Some elements like S or Ni show substantial differences between meteorites and/or experiment durations, whereas elements like Si or Cl have more consistent concentrations.

Figures 4.3b (30 days experiments) and 3c (180 days experiments) show differences across meteorites and experiment triplicates in more detail. The shaded envelope shows the range of concentration defined by the maximum and minimum concentration measured across the triplicates of each meteorite. Overall, Murchison and Kolang have similar concentrations of total elements but with some differences: Murchison leachates are more enriched in Mg, Ca and S whereas Kolang has higher levels of K and Cl. High concentration elements show a wider range of concentration than the lower concentration elements, i.e., relative variabilities are fairly constant, although volatile elements like K, Na, Cl and S show greater variations, especially for Kolang. Chwichiya 002, on the other hand, shows generally much lower concentrations and variabilities of elements, apart from Ca, Si and Cl for which means and ranges of concentrations are only slightly lower compared to the other meteorites. In addition to higher concentrations, longer experiment duration (Figure 4.3c) results in lower relative triplicate variability, except for volatile elements in Kolang samples. Nickel, which otherwise occurs at low concentrations, was strongly enriched in two Kolang leachate samples compared to the third. Figure 4.3d shows a better illustration of the influence of experiment duration on the concentration of different elements by dividing average concentrations in Figure 4.3c with concentrations in Figure 4.3b. Data points are missing for some samples with no detectable Al, Ni, Fe, Cu, and Zn, especially for the short duration experiments. Cobalt was not detected in any short duration experiment sample and is therefore not plotted in Figure 4.3d. Most elements in Figure 4.3d have concentration ratios between 1 and 6, i.e., the reaction speed decreased after 30 days. For major elements, concentration ratios appear to be correlated with ion charge, with Si ratios being close to a ratio of six (i.e., constant net dissolution), elements with divalent ions (Ca, Mg and S) are around 3, and K and Na are closer to 1. Some elements show a concentration ratio of >6; however, as those elements are generally of low concentration, absolute

concentration differences (apart from Ni) are small. On the other hand, concentration ratios of Cl are <1 and are particularly low for Chwichiya 002 which in general shows lower concentration ratios than Murchison and Kolang. Murchison and Kolang both show a total element concentration increase of a factor ~2 (slightly higher for Kolang) from 30 to 180 days of reaction time, with larger increases in Mg, Na and S and slower decrease in Cl for Kolang, compared to Murchison, whereas the opposite can be seen for Ca, Si and K.

Meteorite chips initially weighed between 92 and 182 mg, whereas the weight of dried chips at the end of the experiments was on average ~5% lower, with a range of 0.5% (Chwichiya 002 s1) to 20% (Murchison l3) (see Table S4.5). However, especially during the longer experiments, some Kolang samples disintegrated and some of the resulting powder was likely lost. Murchison and Chwichiya 002 samples remained intact but Murchison l3 initially consisted of >25 tiny fragments of which some might have been lost before drying. In contrast to the other meteorites, Chwichiya 002 chips preserved their original number of fragments and lost only a few percent of weight. There are some differences between different triplicates which seem to be negatively correlated with initial weight (i.e., lighter triplicates experienced a larger relative decrease in weight), although this is not observed for Murchison l and Kolang samples, where material from one or more triplicates was likely lost. Chwichiya 002 samples that reacted for 30 days have pH values of ~8.3; otherwise, values are ~7.7 regardless of meteorite and experiment duration, which is slightly higher than the initial slightly acidic artificial rainwater (pH 6.6).

Table 4.4. Blank corrected elemental composition of leachates analysed by ICP-OES and IC (in ppm). bdl=below detection limit

Sample	Si	Mg	Cl	Sr	Na	Ca	Zn	S	Ba	K	Mn	Cu	Al	Ni	Fe	Co
Kolang l1	4.7	27	23	0.062	28	25	0.18	77	0.038	25	0.29	0.019	0.035	5.0	0.016	0.038
Kolang l2	5.0	27	4.1	0.055	20	24	0.20	77	0.044	5.4	0.44	0.017	0.014	11	0.011	0.096
Kolang l3	6.4	18	3.8	0.031	19	20	0.10	46	0.040	3.4	0.014	0.010	0.019	0.43	0.0084	bdl
Murchison l1	3.7	25	3.0	0.039	15	32	0.10	60	0.029	2.4	0.024	0.011	0.014	0.20	0.0049	bdl
Murchison l2	5.3	34	3.4	0.045	20	39	0.091	78	0.021	2.8	0.027	0.0086	0.021	0.20	bdl	bdl
Murchison l3	4.0	29	2.5	0.052	23	40	0.10	69	0.052	2.3	0.025	0.016	0.023	0.15	0.010	bdl
Chwichiya 002 l1	5.4	1.5	3.1	0.15	4.7	16	0.10	2.2	0.035	1.6	0.0028	0.0026	0.014	0.017	bdl	bdl
Chwichiya 002 l2	5.8	1.4	4.1	0.18	6.1	17	0.093	2.7	0.031	1.9	0.0025	0.0090	0.033	0.019	bdl	bdl
Chwichiya 002 l3	7.2	1.3	2.6	0.17	5.0	18	0.092	2.3	0.032	1.4	0.0024	0.0049	0.020	0.015	bdl	bdl
Kolang s1	1.2	5.5	19	0.025	19	8.6	0.0059	16	0.026	10	0.0025	0.0025	0.018	0.11	0.0074	bdl
Kolang s2	0.85	5.1	14	0.013	8.9	13	0.0035	22	0.021	6.7	0.0072	bdl	bdl	0.073	bdl	bdl
Kolang s3	0.87	7.0	3.8	0.022	11	12	0.0043	29	0.0084	2.8	0.018	bdl	bdl	0.30	bdl	bdl
Murchison s1	0.67	8.6	2.4	0.017	6.7	11	bdl	24	0.025	1.2	0.0099	bdl	bdl	0.071	bdl	bdl
Murchison s2	0.77	12	6.1	0.03	23	17	0.0072	32	0.055	1.1	0.012	0.0047	bdl	0.066	0.012	bdl
Murchison s3	0.79	15	6.2	0.029	13	23	0.00059	43	0.0097	1.1	0.016	bdl	bdl	0.13	bdl	bdl
Chwichiya 002 s1	2.0	0.60	15	0.067	8.6	5.2	bdl	1.2	0.013	1.9	0.0015	bdl	0.012	bdl	bdl	bdl
Chwichiya 002 s2	0.92	0.23	6.2	0.052	1.9	3.1	bdl	0.57	0.025	0.73	0.00086	bdl	0.0099	bdl	bdl	bdl
Chwichiya 002 s3	2.8	0.43	2.4	0.10	2.6	8.4	bdl	0.99	0.034	0.87	0.0017	bdl	0.021	bdl	bdl	bdl

4.3.2.2 SEM

The SEM work focused on identifying alteration textures and potential secondary phases. Whereas the surfaces of some chips, especially those that reacted for 180 days, showed some etch features and broken surfaces, it was unclear whether they were caused by dissolution or by the sample preparation (crushing of meteorite chips). Sites of interest (one or two per sample) were chosen based on morphologies or particularly dark or bright areas as observed in BSE. Bright areas were often rich in Fe, S and Ni and were therefore likely pentlandite, whereas other bright areas were likely magnetite (Fe but no S and Ni); notably, no EDS analysis could be associated with pyrrhotite (i.e., no areas of just Fe and S were observed). Very dark areas found in Kolang and Murchison samples were rich in C but had little to no other elements and were therefore likely carbonaceous material like insoluble organic matter (IOM). Larger medium-dark crystals, mainly found in Chwichiya 002 but also in the other meteorites were likely olivine and in some cases pyroxene based on elemental composition. Analyses of smaller crystals or the groundmass/matrix were often consistent with serpentine, based on the Mg:Si ratio of the quantitative EDS analysis.

Overall, meteorite chips that had reacted for 30 days showed no notable secondary mineral or texture. For the longer experiment duration, however, one Murchison sample showed crystals (likely olivine based on elemental composition) overgrown by submicron sized bright Fe-rich crystals, which are likely magnetite or another iron oxide or –hydroxide. One Chwichiya 002 sample had micrometre sized bright spots composed of Fe, S and also some Mg and Si, which could be indicative of tochilinite-cronstedtite intergrowths. Representative SEM images of the different meteorites and experiment durations are in Figure S4.3. Thin sections made from three long duration experiment chips revealed no notable secondary phases or texture changes.

4.4 Discussion

4.4.1 Validity of models and comparison to laboratory experiments

The kinetic models offer a prediction of mineralogical changes occurring in CM chondrites undergoing terrestrial weathering. However, as several limiting factors needed to be considered (see Section 2.2), it is crucial to first discuss the validity of the models before considering their value for understanding terrestrial weathering. Experimental leachates offer a comparison to the model fluid concentrations, although with some caveats, such as differences in W/R ratio (200 in the experiment vs. 1 or 1000 in the models), time steps (two in the experiments vs. 17 in the models), and potentially also in terms of starting composition, as CM chondrites are often brecciated which could cause differences between the composition of the chips used in the experiments and the literature values used for the models.

Calcium, Mg, Si and S, as shown in Figures 4.4a–c, are the only elements suitable for a comparison between models and experiments, as the models do not have any primary Na-, K- or Cl-bearing

minerals. The experiments can be compared with the modelled rainwater systems (30 °C, 1x concentration, oxidised) for 1 and 1000 modelled W/R ratios (Figures 4.4a–c).

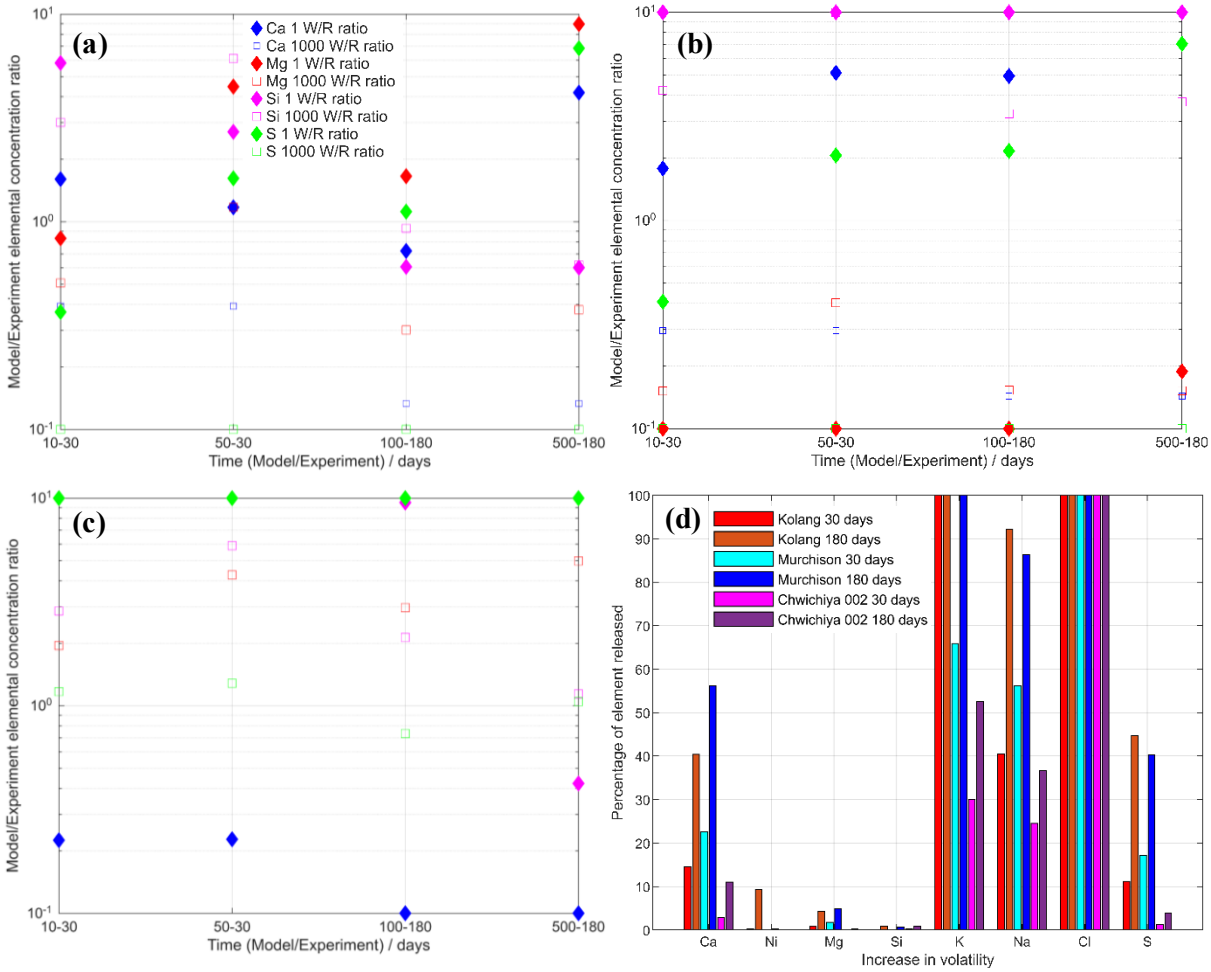

Figure 4.4. Elemental concentration ratios of experiments and models (30°C, 1x fluid concentration, rainwater, oxidised conditions; a) Kolang(experiment)/Kolang(model); b) Murchison(experiment)/Murchison(model); c) Chwichiya 002(experiment)/DOM 08006(model)) and mass balance (percentage of element dissolved) between experiments and meteorites (d). As the experiments ran with different timesteps and W/R ratios (by mass) than the models, the next-closest timesteps (10, 50, 100 and 500 days) and W/R ratios (1 and 1000) need to be used for a comparison with the models. DOM 08006 had no initial Ca (no calcite) and modelled Ca concentrations therefore remained constant. Plotted concentration ratios were capped at 0.1 and 10 for better readability. In Fig 4d, the y-axis was capped at 100% for better readability of lower percentages (see Table S4.4 for a complete view of the data).

Overall, experimental and modelled concentrations are fairly similar although with differences among elements and meteorites. Kolang (Fig. 4.4a) shows a good fit between experiments and models for Ca, Mg and S, and modelled Si concentrations are only too high compared to the 30 days experiments. For Murchison (Figure 4.4b), modelled Mg concentrations are too low and Si too high, but concentrations are in reasonable agreement for Ca and S. Regarding Chwichiya 002 (Figure 4.4c), modelled concentrations (based on DOM 08006) are too high, especially for Mg and Si. Also notable is that a

modelled W/R ratio of 1 is generally a better fit for Kolang and Murchison while experimental Chwichiya 002 concentrations are more similar to a W/R ratio of 1000 for DOM 08006 systems.

The overall fairly good fit implies that modelled and experimental mineral dissolution rates are similar; however, elemental concentrations can also be lowered in the experiments by precipitation of secondary phases, which could explain some of the differences between experiments and models. Whereas the models predict the formation of precipitates like goethite and talc within days, examination of meteorite chips and thin sections did not reveal significant quantities of secondary minerals, although goethite might be present as thin layers that are hard to identify by SEM. This lack of precipitation of minerals during the experiments could explain the rather high concentrations of Ca, Mg and S in Kolang and Murchison leachates. The low concentrations of Si in the experimental leachates, on the other hand, could be caused by incongruent dissolution of anhydrous silicates whereby mono- and divalent cations are removed preferably over Si (e.g., Brantley, 2008). The rather poor fit between the experimental and modelled C3s (Figure 4.3c) could be caused by chemical differences between Chwichiya 002 and its proxy, DOM 08006, although it seems more likely that Chwichiya 002 is less reactive than expected from its mineralogy, being mainly a mixture of olivine, pyroxene and glass. Amorphous silicates are expected to react very rapidly (within days or even hours) (e.g., Le Guillou et al., 2015; Igami et al., 2021) and at least some anhydrous silicates are expected to alter to phyllosilicates based on experiments on carbonaceous chondrites such as Allende (Jones and Brearley, 2006) and Kainsaz (Suttle et al., 2022). Whereas model simplifications could explain some differences, it seems likely that additional factors are responsible for the slow reactivity of Chwichiya 002 chips; for example a larger average grain size, a lower porosity, or passivation of surfaces by natural terrestrial weathering. The first option seems unlikely, as parent body alteration preferably targets smaller grains, resulting in larger remaining olivine and pyroxene grains in Murchison and Kolang compared to the unaltered Chwichiya 002. Hence, it is more likely that the moderate hot desert weathering of Chwichiya 002 is responsible for its lower reactivity than expected from DOM 08006 models. The Chwichiya 002 chips were also more robust and compact than the ones from Murchison and Kolang, which could hint at a lower porosity. SEM images and EDS analysis did not reveal any evidence for terrestrial weathering of Chwichiya 002; however, alteration products could be present as thin films on mineral grains that are difficult to detect by SEM. In addition, Chwichiya 002 leachate Sr concentrations were higher than for Kolang and Murchison, which is also suggestive of addition of Sr by hot desert weathering (e.g., Bland et al., 2006; Zurfluh et al., 2013).

In most models, cronstedtite is unstable and reacts to goethite and talc. The latter has not been observed in any studied CM chondrite; hence, it is perhaps more likely that Fe is leached from cronstedtite to form goethite and Fe-deficient cronstedtite, i.e., Mg-serpentine remains, instead of talc. Other Fe-hydroxides such as akaganeite or evaporites such as nesquehonite are also common terrestrial weathering products (e.g., Velbel, 1988; Buchwald and Clarke, 1989) but were not present in the

thermodynamic database used. Instead, magnesite and especially dolomite appear frequently in the models, which could be considered proxies for Antarctic evaporites (Velbel, 1988). Another carbonate that is often regarded as a product of terrestrial weathering is calcite (e.g., Al-Kathiri et al., 2015) but in most modelled cases, primary calcite dissolves and sometimes dolomite grows instead (e.g., Figure 4.2c). In the models, dissolution but also precipitation of minerals used in the starting mineralogy was governed by additional kinetic factors whereas secondary minerals that are not initially present in the meteorites can form instantaneously when supersaturated. Implementing kinetic descriptions for all possible secondary minerals could prevent the formation of dolomite and perhaps also talc but in practice, this was not feasible as calculations became rapidly too computationally expensive, especially for more complex systems with seawater, and thermodynamic databases also only have a limited number of minerals with kinetic descriptions.

Further limitations of the models arise from the limited number of elements in the systems and simplified starting mineralogy, which prevents modelling of minerals like celestite or barite that are occasionally found in hot desert finds (e.g., Zurfluh et al., 2013). The models used the extended Debye-Hückel equation for activity calculations which is only reliable for ionic strengths lower than 0.1 mol/kg (Parkhurst and Appelo, 2013); however, many systems with seawater and some rainwater systems with extensive dissolution have ionic strengths >0.1 or even >1, meaning that results of such systems should be only regarded qualitatively. There are some thermodynamic databases compatible with PHREEQC that allow for modelling of higher ionic strength like *sit.dat* or *pitzer.dat*; however, those databases have a limited number of phases and species, making them unsuitable for modelling terrestrial weathering of CM chondrites. The models also do not consider solid solutions which were implemented by some other studies (e.g., Zolotov, 2006; Fabre et al., 2024). As olivine in CM chondrites is often Mg-rich with some Fe (e.g., Howard et al., 2011), terrestrial weathering of olivine can be expected to be slower and slightly faster than the modelled fayalite and forsterite, respectively.

4.4.2 Discussion of minerals and fluid chemistry from experiments

The leachate composition measured by ICP-OES reflects the sum of dissolution and precipitation. Due to the high water/rock ratio (~200) (by mass) of the experiments, it can be expected that the elemental concentration is primarily driven by dissolution, as saturation indices are generally low. An exception are minerals with ferric iron like goethite or ferrihydrite, which precipitate due to the insolubility of Fe^{3+} that is more abundant than Fe^{2+} at the oxidising conditions of the experiments. Si is also present in lower concentrations than other major elements in the meteorites, particularly for experiments of short duration (30 days). It is known that in silicates like anorthite or pyroxenes, Si^{4+} is more resistant to dissolution compared to mono- or divalent cations (e.g., Palandri and Kharaka, 2004); hence, the low concentration of Si in the leachates is likely caused by incongruent dissolution. On the other hand, in the longer experiments, the higher Si concentrations in the leachates probably suggest more complete

dissolution. Similarly to Fe, Al is also of very low concentration or even below detection limit in the leachates, even though it is present as a major element in the meteorite. This is likely because Al^{3+} is both difficult to leach from the mineral surface and is fairly insoluble, meaning that any dissolved Al precipitates as secondary minerals like Al-bearing phyllosilicates. Regarding other measured elements by ICP-OES of low concentration (Sr, Zn, Ba, Mn, Cu, Co), they are only minor elements in carbonaceous chondrites and their low abundance or absence in the leachates is therefore unsurprising. The other elements measured by ICP-OES like Ca or Na will be discussed in section 4.4.5.

4.4.3 Discussion of minerals and fluid chemistry from models

As stated in the methods, the kinetic weathering models included a much broader range of weathering conditions compared to the models. Significant differences exist between oxidising and reducing conditions as well as models with seawater or with rainwater. As mentioned earlier, the combination of oxidising conditions (equilibration with the atmosphere), rainwater and elevated temperature (~25°C) can be compared with experimental results and can be taken as an approximation of hot desert weathering. The primary sulphides are unstable when exposed to the oxidising alteration conditions; however, due to relatively slow dissolution rates, significant amounts of sulphide are only dissolved after ~100 to 1000 years, which is reflected by a late increase of dissolved sulphur. The dissolution of anhydrous silicates releases mainly Mg and Si caused by the lower Mg:Si ratio of the dominant secondary phyllosilicate, talc, compared to primary Mg-Si minerals. As a result, Mg and S concentrations are rising throughout the models because no Mg-sulphate in the database becomes supersaturated. Instead, sulphates only precipitate when enough Ca is available from the dissolution of calcite to form Ca-sulphates (mainly gypsum). has a lower Mg:Si ratio than high aqueous Mg and S concentrations shown in the results can be explained by the high solubility of Mg-sulphates. Other elements like Fe remain at low concentration or show only a moderate increase over time because they are incorporated in secondary minerals like goethite. Elements like Na or K are not present in the models but it can be predicted that their concentration rise throughout the modelled time due to the lack of Na-K-bearing precipitates.

4.4.4 Comparison with laboratory experiments in the literature

Our experiments can be compared with previous laboratory studies, even if they differ in scope and/or materials. Bland et al. (1997) artificially weathered Allegan (H5), simulating both cold and hot desert conditions. The hot desert experiment, where a 4 g meteorite experienced wetting and drying cycles for 25 days at room temperature, revealed that metal is oxidised much more rapidly than troilite, which oxidises at a comparable rate to olivine and pyroxene. Terrestrial weathering of another ordinary chondrite, Bensour (LL6) was studied by Lee et al. (2006); in one of their experiments, they reacted three 1.2–1.4 g subsamples with 50 ml water at room temperature for 68 days. Leachates were concentrated in Si, Mg and Na with more minor Al, whereas S, Cl and Fe were not detected in one or

more subsamples. Another experiment at elevated temperature released higher quantities of Cl, S and Fe and yielded considerably more weathering products compared to the other experiment at room temperature. Based on mass balance calculations, Lee et al. (2006) suggest that chlorapatite and feldspar dissolve rapidly, whereas the apparently slower dissolution of anhydrous silicates and low concentration of Al could reflect precipitation of secondary minerals. Leachate compositions were also examined in studies by Zurfluh et al. (2013) and Izawa et al. (2010). Zurfluh et al. (2013) conducted leaching experiments on 15 Omani desert finds (all OCs) and on the H5 Tamdakht for 48 days; leachates of most finds were rich in SO_4^{2-}, Cl^-, Mg, Ca and Fe, whereas the Tamdakht leachate yielded lower abundances of most elements/compounds except HCO_3^-. Total leachate concentrations were in the range of 596 to 8817 µg/g, which is much higher than the 224 µg/g yielded for one of the Kolang triplicates.

To our knowledge, there are no data available on experimental leachates from CM chondrites although there is information on the C2-ung Tagish Lake examined by Izawa et al. (2010). Their leaching experiments (reaction of ~10 mg meteorite aliquots with deionised water for up to 30 min) were too short for a direct comparison with the present study, but solutions were dominated by SO_4^{2-}, Mg and Ca with less abundant Cl^-, K and Na.

4.4.5 Mineral reactivity and rate of terrestrial alteration in CM falls and finds

The measured concentrations of leached elements enable mass balance calculations of removed elements from the meteorite. As we did not measure the chemical compositions of the meteorites studied, literature data was used: Fuchs et al. (1973) for Murchison, Ruggiu et al. (2022) for Chwichiya 002, and Bates et al. (2024) for Kolang (using Winchcombe as a proxy). As Cl was not measured in those studies, Cl data from Lodders (2021) (CM chondrites) was taken instead for all three meteorites in the experiment. Major elements like Mg and Fe have multiple potential primary mineral sources; for example, in chondrites, Fe could be sourced from iron metal, sulphides, magnetite, olivine, pyroxene or weathering products like akaganeite, and Lee et al. (2006) suggested that precipitation of secondary minerals can lower the concentration of Mg, Fe and Al in solution. Some S could be sourced from terrestrial sulphates like gypsum, as even falls like Winchcombe that have been rapidly collected can still form sulphate weathering products (Jenkins et al., 2024). However, as S is about twice as abundant as Ca in the leachates (by mass), even if all Ca was sourced from the dissolution of gypsum, the other half of the S in solution needs to be sourced from the dissolution of sulphides (pyrrhotite/troilite and/or pentlandite). Pentlandite is known to be more resilient than pyrrhotite to aqueous alteration (e.g., Singerling and Brearley, 2020), which explains the generally low abundance of Ni in the leachate and suggests that the S abundance reflects dissolution of pyrrhotite/pentlandite, although the low Ni concentrations could also denote precipitation of some Ni-serpentine like pecoraite (Al-Kathiri et al., 2005). The high Ni concentration measured in two Kolang samples (Figure 4.3c) could be caused by a nugget effect with those samples having more and/or larger Ni-sulphides.

The volatile elements Na, K and Cl are fairly abundant in the leachates, especially Kolang (Figures 4.3a–c). The source of those elements in CM chondrites is poorly understood; Piralla et al. (2021) found apatite in the CM2 Boriskino but its Cl-poor composition would still require an additional primary Cl-bearing mineral to explain the abundance of Cl in the leachate. In their OC leaching experiments Zurfluh et al. (2013) proposed that Cl and Na are sourced from halite and K from sylvite; however, as primary halides so far have not been found in CM chondrites, it is likely that Cl, Na and K in the leachates reflect dissolution of terrestrially sourced halides. If this was the case, however, then higher abundances of those elements would be expected from more intensely terrestrially altered meteorites (particularly hot desert finds) but leachates from Kolang show the highest and Chwichiya 002 the lowest abundances. Perhaps the higher water abundances in meteorites of lower petrologic type (Alexander et al., 2013) facilitates the formation of secondary halides even on recent and rapidly recovered falls, as seen in the Winchcombe meteorite (Jenkins et al., 2024), whereas C3s like Chwichiya 002 are more resilient. McCoy et al. (2025) found halite as well as other Na-K-Cl-SO_4 phases in Bennu samples that are highly susceptible to terrestrial weathering. Those phases could have also been present in CM chondrites and terrestrial weathering could lead to redistribution or leaching of Na, K and Cl, depending on the weathering conditions. More experiments with different meteorites are needed to investigate those hypotheses.

Figure 4.4d provides an overview of the amount of each element dissolved for each meteorite and experiment duration based on elemental abundances in Table S4.6. The amount of leached Cl and K in some experiments exceeds 100% and can be as high as 700% for Cl and 550% for K, showing that the abundance of those elements in the meteorites was higher than the values taken from the literature, particularly in the case of Cl, although it is unclear whether those higher concentrations can be attributed to intrinsic chemical differences between the samples (e.g., due to brecciation) or whether the samples in the experiments already had more terrestrial weathering products than reported in the literature. Furthermore, with the exception of some Chwichiya 002 experiments (Figure 4.3b), the amount of Cl in the leachate does not balance the concentration of Na and K, i.e., Na and/or K must be sourced from an additional primary mineral; one possibility is Mg-Na phosphates which have been found in samples returned from asteroid Ryugu (e.g., Nakamura et al., 2022), Bennu (McCoy et al., 2025) and CM2 Bold Bokkeveld (Lee et al., 2025). Carbonates like calcite should not occur in C3s (Kimura et al., 2020); however, Ruggiu et al. (2022) detected 1-3% carbonates in Chwichiya 002 and considering that leaching of Chwichiya 002 yielded little S (Figure 4.3a–c), the majority of Ca in the examined meteorites is likely sourced from calcite as it is the main Ca-phase in CM chondrites. Some Ca could also be sourced from apatite and/or plagioclase feldspar, as proposed by Lee et al. (2006) in their experiment. As a simplification, if all S in the leachate is sourced from pyrrhotite and all Ca from calcite, and both minerals were present initially at ~1 vol.% in CM chondrites, the experiments suggest that after 30 days of weathering, the abundance of those minerals are decreased to ~0.8–0.9 vol.% and after 180 days,

only about half of the original quantity remains. In other words, in addition to the development of rust caused by oxidation of metal and sulphides, a terrestrially weathered CM chondrite should have an unusually low abundance of carbonates (calcite) and pyrrhotite and a low pyrrhotite/pentlandite ratio, as the latter appears more resistant to terrestrial weathering. However, carbonates are a product of aqueous alteration on the parent body; hence, the abundance of carbonate in CM chondrites prior to their exposure to terrestrial alteration is likely dependent on the extent and the conditions of aqueous alteration that it experienced on the parent body. Sulphides, while they were initially formed in the solar nebula, are also modified by parent body aqueous alteration (Singerling and Brearley, 2020), which affects the abundance and composition of sulphides as a function of petrologic type. Hence, unless the initial carbonate and sulphide abundance is known, a better metric to determine the extent of CM chondrite weathering is rustiness (i.e., abundance of Fe-oxides and -hydroxides) as well as anomalies in Na, K and Cl abundances. In environments similar to the experiments with high W/R (e.g., a body of standing water or an environment with abundant rainfall), abundances of those elements should be lower than expected whereas in drier environments abundances could also be higher due to precipitation of halides like halite.

4.4.6 Predicted alteration rates for different environments and possible metrices for a CM weathering scale

The results of the kinetic models can be used to evaluate terrestrial weathering for a wider range of timespans and environments than the experiments (temperature, W/R, fluid concentration, fluid type and redox conditions). The different modelled meteorites (DOM 08006, Murchison, Kolang and LAP 02277) produce contrasting secondary mineral types, abundances and formation times. This is especially the case for DOM 08006 (Fig. 4.2b) whereby goethite forms much faster due to abundant metal and amorphous material (modelled as $Fe(OH)_2$). Due to those differences across different environments and meteorites, there is a need for a common metric to assess the progress of terrestrial weathering. Bland et al. (2006) found that the degree of weathering in ordinary chondrites can be measured with the abundance of ferric iron, represented as oxidation percentage. In the modelled meteorites, a similar measure for rustiness (oxidation %) could be defined by dividing the volume fraction of goethite (the only ferric mineral in the models) by the sum of Fe-minerals (primary and secondary). The results of those calculations are in Figure 4.5 for the different modelled meteorites and variations in temperature, fluid type (rainwater vs. seawater) and redox conditions — W/R ratio and fluid concentration were omitted, as they did not result in notable differences in goethite precipitation (see Figures 4.1c and d). Figure 4.5 shows that the main difference in oxidation speed for $t<500$ d is caused by differences in temperature and the presence of amorphous material in C3s like DOM 08006, whereas Murchison, even though it has some iron metal (1 vol.%) alters at a similar rate to the other two CMs of lower petrologic (sub)type. From Figure 4.5, it is also evident that oxidation does not occur under reduced conditions (e.g., no equilibration with the atmosphere) as they do not yield any ferric

minerals. As Figure 4.5 shows time on a logarithmic scale, the linear increase of oxidation denotes a power law, similar to that described for OC finds by Bland et al. (2006), at least for the first 1000 days. Compared to Bland et al. (2006), the modelled meteorites oxidise much faster with DOM 08006 reaching ~50% oxidation after only ~50 days, whereas hot desert finds studied by Bland et al. (2006) required 10,000s years for similar levels of oxidation. An obvious explanation for this difference is the modelled constant exposure to water although even with that caveat in mind, the experimental alteration of Chwichiya 002 should have shown a much higher level of "rustiness". This highlights again that Chwichiya 002 is likely less reactive due to "preexisting terrestrial weathering" (see Section 4.1).

Based on their extensive survey, Losiak and Velbel (2011) suggested that the formation of evaporites on Antarctic finds is not correlated with the degree of rustiness or proximity to the Antarctic Ocean. They also found that a higher proportion of CM chondrites have evaporites compared to the population of Antarctic finds but they did not discuss differences across different CM chondrite petrologic types. As discussed previously, nesquehonite, was not present in the models but the appearance of other carbonates (magnesite or also ankerite, calcite and aragonite) could be taken as a proxy for Antarctic evaporites. Across the systems of interest (i.e., systems with rainwater at 4 °C), the only evaporite-like mineral that forms within reasonable time (<500 days) is dolomite with typical abundances of 0.1 vol.% after ~50 days and 1 vol.% after ~100 days. Notably, dolomite mostly forms in Kolang and LAP 02277 but is absent in all Murchison systems. As dolomite in the models forms at the expense of calcite, DOM 08006 with no primary calcite rarely has secondary dolomite, whereas calcite in Murchison systems dissolves much slower than in Kolang and LAP 02277. Dolomite forms at a similar rate or slower than goethite, i.e., based on the models, CM chondrites with evaporites should also have a notable degree of rustiness which was not the case in all meteorites studied by Losiak and Velbel (2011). The differences are likely caused by the absence of nesquehonite in the model database but there could also be additional primary Ca-Mg minerals whose alteration could facilitate an earlier formation of evaporites. Despite the model's limitations, it would be interesting to examine whether evaporites are more readily formed on more altered CM chondrites compared to less altered ones like Murchison with more experimental and modelling work.

Information derived from the kinetic models and weathering experiments can be combined to propose a weathering scale for CM chondrites. For ordinary chondrites, Wlotzka (1993) and Zurfluh et al. (2016) proposed a weathering scale from W1 to W6 based on the oxidation of iron metal and troilite. However, as most CMs have little to no iron metal, a different weathering scale is required with different metrics. Lower calcite and sulphide abundances, formation of Fe-hydroxides, a higher Ni/Fe ratio in sulphides could all be possible indicators for weathering and with abundant water, weathered samples should be particularly poor in Cl, K, Na, S and Ca whereas in more water-poor environments, sulphates should form rapidly as documented in other studies (e.g., Jenkins et al., 2024; Garvie et al., 2025). Chemical compositions of CM finds compared to falls analysed by Braukmüller et al. (2018) do not show any

clear differences, indicating that the effect of terrestrial weathering on the chemical composition is more complex and perhaps specific to collection sites and weathering conditions. More experimental work is needed, especially regarding weathering products and differences across CMs of different petrologic

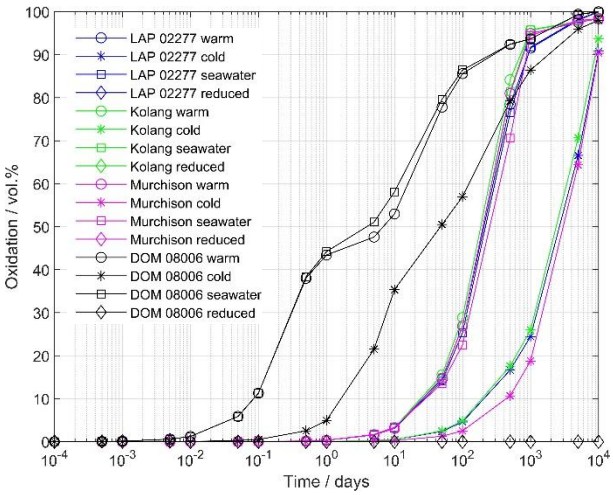

Figure 4.5. Progressive oxidation, defined as goethite volume fraction (goethite/∑Fe-phases), of different meteorites and variations in parameters (temperature, fluid type and redox conditions). The base model (labelled as warm) is the same as in Figure 4.1a. Reduced conditions do not yield any oxidation for any meteorite.

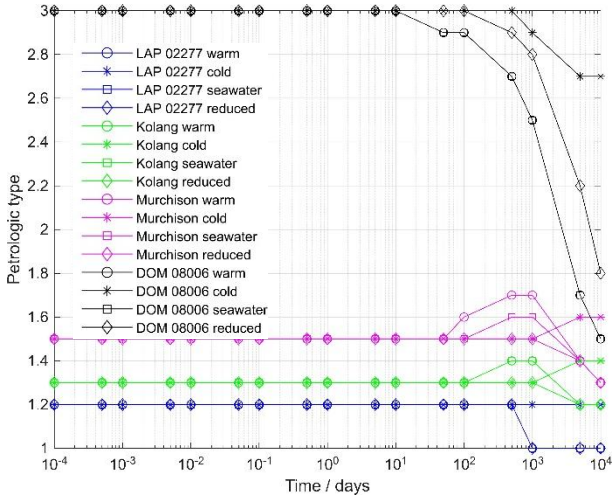

Figure 4.6. Evolution of the petrologic type calculated from the phyllosilicate fraction (PSF, Howard et al., 2015) for different meteorites and variations in parameters (temperature, fluid type and redox conditions). The base model (labelled as warm) is the same as in Figure 4.1a.

type to establish a sophisticated weathering scale that is ideally valid for all CM chondrites or even carbonaceous chondrites.

4.4.7 Can terrestrial alteration lower the petrologic (sub)type of a CM chondrite?

To date, no CM chondrite fall has been classified as a CM1, and minimally altered CM chondrites like Asuka 12169 are very rare. As there are more CM finds than falls in the database (Meteoritical Bulletin), the lack of a CM1 fall could be statistically expected but there is also the possibility that extensive terrestrial weathering could lower the petrologic type of a CM chondrite find. In oxidised environments, terrestrial weathering of CM chondrites is accompanied by formation of goethite (or other Fe-hydroxides); however, in models with reduced conditions, no or little goethite forms even though primary minerals like anhydrous silicates react to secondary minerals like serpentine. In other words, terrestrial weathering in environments with limited oxygen or additional microbial activity could result in alteration conditions that resemble aqueous alteration on the CM parent body/bodies (see e.g., Figure 4.1f). Figure 4.6 shows the evolution of petrologic type calculated after Howard et al. (2015) for the same meteorites and environmental conditions as in Figure 4.5. Very little change occurs for CM2s and CM1s and in cold environments, the petrologic type can even increase due to slow dissolution of anhydrous silicates and reaction of cronstedtite to goethite, suggesting that most if not all CM1 finds

have been of petrologic type 1 before the onset of terrestrial weathering. DOM 08006, despite rapid oxidation within days (Figure 4.5), requires at least 50 days of aqueous alteration with liquid water for a decrease in petrologic type to 2.9 and a comparable subtype to Murchison can only be reached after 5000 days, suggesting that even a heavily terrestrially altered CM chondrite has never developed from a CM3. However, even though the timeframes required for changes in petrologic types in Figure 4.6 will rarely be reached in hot and cold desert weathering, it highlights that the degree of terrestrial weathering in a CM chondrite needs to be assessed not only by its rustiness but also through other means like chemical composition, integrity of organic matter etc., as also suggested by other publications (e.g., Bland et al., 2006; Lee et al., 2021; Jenkins et al., 2024).

4.5. Conclusions

In this study, the terrestrial weathering of CM and related carbonaceous chondrites was examined by a combination of laboratory experiments and kinetic models. In the experiments, chips of Chwichiya 002, Murchison and Kolang were reacted at room temperature with artificial rainwater for 30–180 days. Kinetic models simulated the reaction of Dominion Range 08006, Murchison, Kolang, and LaPaz Icefield 02277 across a timespan from 9 seconds to 27 years for different environmental conditions (temperature, W/R ratio (by mass), fluid type, fluid concentration and redox conditions). The following main points come from the models and experiments:

1. Leachates from the Kolang and Murchison experiments are rich in S, Ca, Na, Cl, K and Mg with less abundant Si and Fe. These results suggest that the most susceptible phases to terrestrial weathering in those meteorites are Fe-sulphides, calcite and unknown Na-K-Cl minerals.
2. Chwichiya 002 leachates yielded generally low elemental concentrations, likely due to pre-existing terrestrial weathering reducing pore space or passivating mineral surfaces.
3. The kinetic models predict rapid oxidation, especially for unaltered meteorites with amorphous material and in warm environments, whereas reducing conditions result in mineralogies akin to those produced in meteorite parent body environments.
4. The models also predict that extensive terrestrial weathering of CM chondrites of high petrologic (sub)type cannot produce CM1 chondrites. However, terrestrial weathering could partially explain the scarcity of CM3 chondrite finds.
5. Dolomite forms in some Kolang and LAP 02277 models with rainwater; however, its abundance is correlated with the formation of goethite (i.e., rustiness).
6. Whereas rustiness/abundance of ferric iron can be a good weathering metric for CM chondrites with abundant metal and sulphides, a more general CM chondrite weathering scale should be established from additional factors such as lower calcite and sulphide abundances and anomalies in Ca, S, Na, Cl and K elemental abundances.

7. The models could be improved by involving more kinetic descriptions of minerals such as talc and dolomite as well as better dissolution rates for metal and sulphides and lower W/R ratios. Lower W/R ratios in the experiments could also promote the formation of more secondary minerals and knowledge of the initial composition and mineralogy of the meteorites as well as more regular sampling of leachates could help to establish more sophisticated mass balance calculations and dissolution rates. Finally, more experiments with more CM chondrites of different petrologic type and terrestrial history are needed to confirm and expand on the findings of this study.

Table 4.5. Comparison of features produced by parent body alteration (several millennia of alteration) versus moderate terrestrial weathering (exposure of several months to liquid water).

Feature	Terrestrial weathering	Parent body alteration
Typical alteration conditions	Variable W/R ratios, variable temperatures, episodic alteration, oxidising	Long, likely continuous alteration duration with relatively little variability in W/R ratio and temperature, reducing
Most vulnerable primary minerals	Metal, Fe-sulphides, Na-K-Cl minerals	Metal, olivine, pyroxene
Typical secondary minerals	Goethite, talc, sulphates	Serpentine, tochilinite, magnetite
Chemistry	Depletion in Ca, Cl, Na, K and S	Isochemical
Rustiness	Rustiness of metal and some sulphides	No rustiness
Sample cohesion	Potential disintegration, especially meteorites of lower petrologic type	No disintegration but more vulnerable to additional stress such as terrestrial weathering with increasing alteration

Acknowledgments – We thank Mendy Ouzillou (SkyFall Meteorites) for supplying the samples used in these experiments. Laboratory work and assistance from Rebecca Sutton (ICP-OES), Matt Pickering (IC) and Gareth Perry (SEM) from the University of York is greatly appreciated. RH acknowledges a research grant from the Meteoritical Society, and MRL grains from the UK Science and Technology Facilities Council (ST/T002328/1, ST/W001128/1, ST/T506096/1).

Data availability statement – The data and code used to create these findings are available upon reasonable request from the corresponding author.

4.6 Supplementary Material

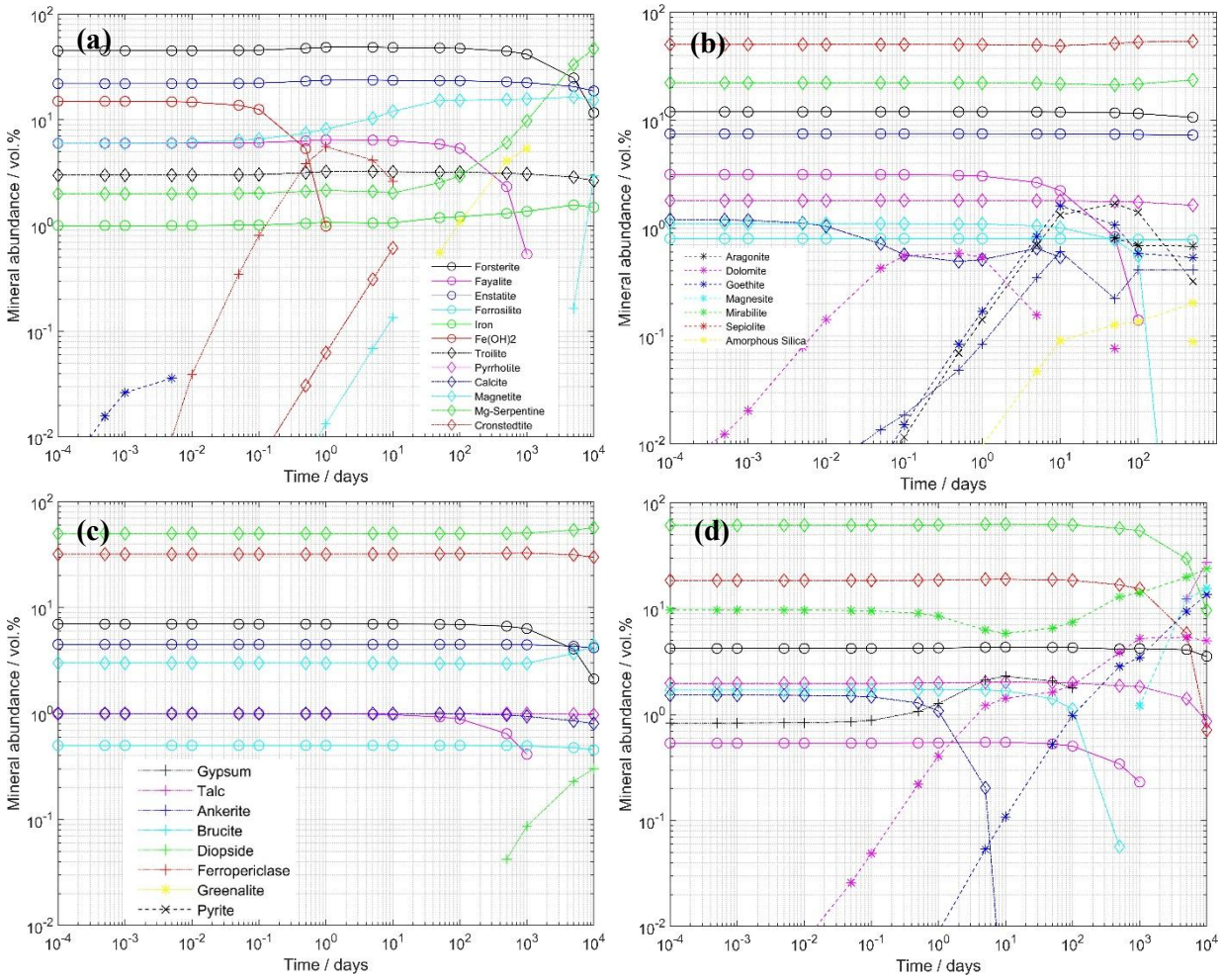

Figure S4.1. Examples of additional minerals described in Table 4.3: a) reducing conditions resulting in secondary metal and troilite as well as brucite, cronstedtite, greenalite and ferropericlase (DOM 08006, 30°C, 1 W/R, 1x fluid concentration, rainwater, reduced); b) Aragonite, ankerite, pyrite (Murchison, 30°C, 1 W/R, 1x fluid concentration, seawater, reduced); c) Diopside (Kolang, 30°C, 1 W/R, 1x fluid concentration, rainwater, reduced); d) Mirabilite and gypsum from concentrated seawater (LAP 02277, 4°C, 1 W/R, oxidised).

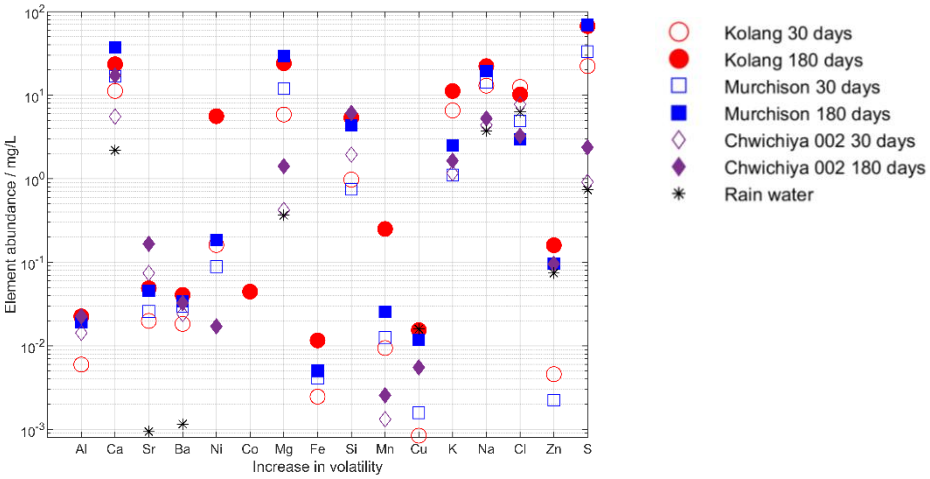

Figure S4.2. Mean element abundance for experimental meteorite leachates (blank corrected) (ordered by volatility) and rainwater by ICP-OES and IC; some data points were not plotted due to values below detection limit.

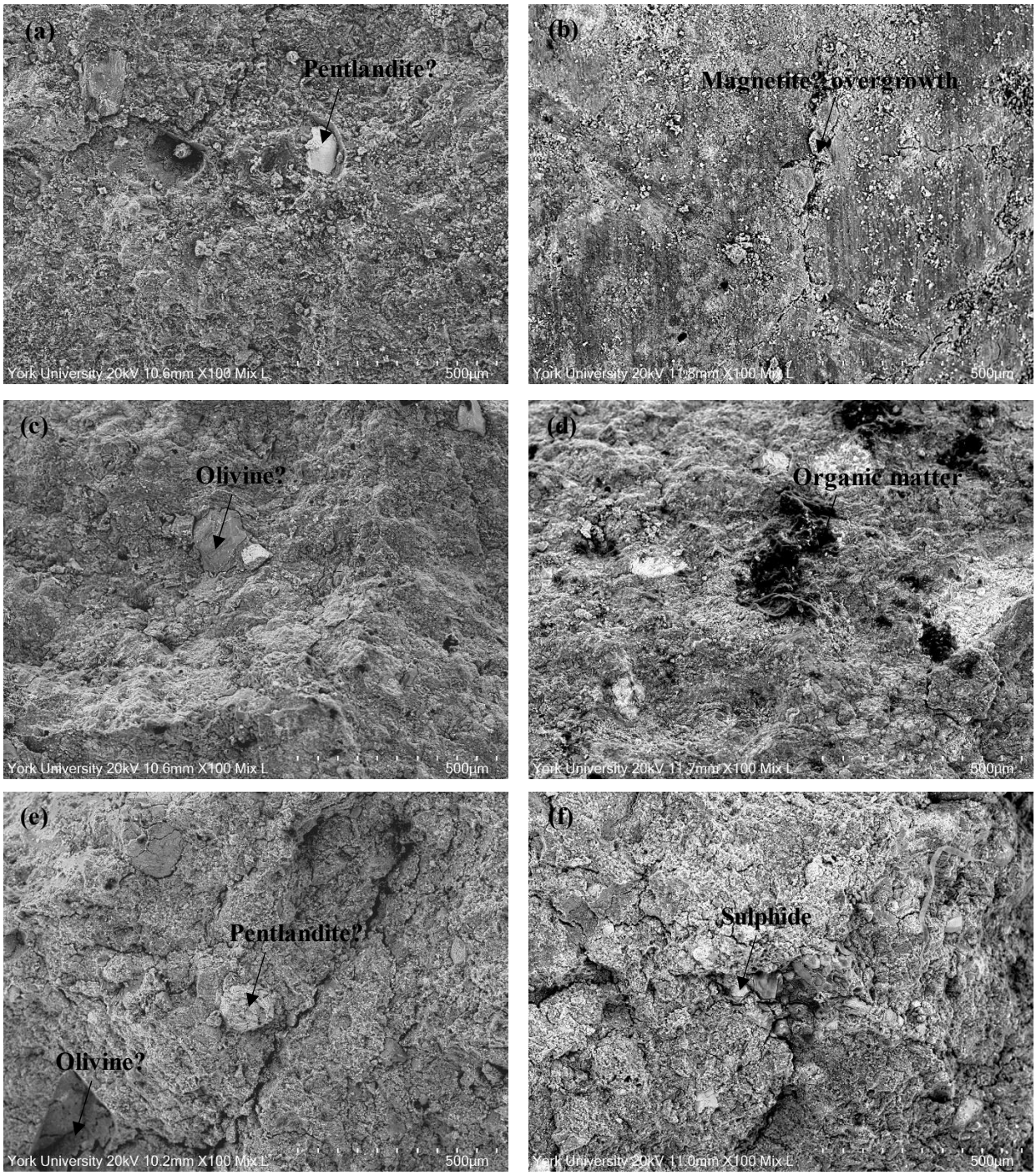

Figure S4.3. Examples of mixed SE/BSE images of altered meteorite chip surfaces: a) Kolang 30 days; b) Kolang 180 days; c) Murchison 30 days; d) Murchison 180 days; e) Chwichiya 002 30 days; f) Chwichiya 002 180 days.

Table S4.1. Solid phases used for kinetic modelling. Molar abundances were calculated from XRD abundances (vol.%) (see Table 4.1), whereas surface areas (SA) were based on estimates of grain sizes and surface roughness.

	DOM 08006		Murchison		Kolang		LAP 02277	
Mineral	Abundance (mol)	SA (m^2/kg water)	Abundance (mol)	SA (m^2/kg water)	Abundance (mol)	SA (m^2/kg water)	Abundance (mol)	SA (m^2/kg water)
Forsterite	2.93	82.33	0.816	22.96	0.516	14.51	0.367	10.34
Fayalite	0.368	15.01	0.202	8.241	0.0695	2.833	0.0443	1.805
Enstatite	2.00	40.17	0.716	14.37	0.464	9.306	0	0
Ferrosilite	0	0	0.0725	1.913	0.0489	1.291	0	0
Iron metal	0.401	224.2	0	0	0	0	0	0
$Fe(OH)_2$	1.62	2904	0	0	0	0	0	0
Troilite	0	0	0.309	246.1	0.186	147.6	0.433	344.7
Pyrrhotite	0.467	412.8	0	0	0	0	0	0
Calcite	0	0	0.0972	85.59	0.0874	77.00	0.158	139.0
Magnetite	0.384	888.5	0.0738	170.9	0.217	503.1	0.146	338.3
Mg-serpentine	0.0530	293.7	0.617	3421	1.50	8316	2.176	12060
Cronstedtite	0	0	1.36	10826	0.931	7435	0.636	5081

Table S4.2. Composition of rainwater (after Herut et al., 2000) and seawater (after Nordstrom et al., 1979) used for kinetic modelling.

Feature	Rainwater	Seawater
pH	6.46	8.22
pe	7.44	8.45
density (kg/dm^3)	1.00000	1.02336
Na (mol/kg)	1.81×10^{-4}	0.49
Ca (mol/kg)	9.3×10^{-5}	0.011
Mg (mol/kg)	3.6×10^{-5}	0.054
S (as SO_4^{2-}) (mol/kg)	5.7×10^{-5}	0.029
Cl (mol/kg)	2.13×10^{-4}	0.559
Fe (mol/kg)	N/A	3.7×10^{-8}
Si (mol/kg)	N/A	7.3×10^{-5}
Al (mol/kg)	N/A	7.6×10^{-8}
C (as HCO_3^-) (mol/kg)	6.0×10^{-5}	0.002

Table S4.3. Detection limits (mg/kg), accuracies (%) and precisions (%) of elements analysed by ICP-OES and IC.

Element	Si	Mg	Cl	Sr	Na	Ca	Zn	S	Ba	K	Mn	Cu	Al	Ni	Fe	Co
Detection	0.32508	0.00055	0.025783	0.0000760	0.11341	0.0269	0.0055	0.0087	0.00071	0.013	0.00053	0.0097	0.0067	0.013	0.004	0.007
limits		676		68		85	39	80	82	67	72	49	20	56	53	61
Accuracy	88.084	109.39	112.93	130.80	107.29	102.70	102.61	99.46	118.0	100.9	108.7	110.5	156.3	103.6	106	105
Precision						0.9749	1.0047			1.920						
	0.31919	0.63786	0.79365	0.83383	0.84220	5	1	1.7541	1.9122	3	2.689	4.883	6.513	8.879	10.4	48.3

Table S4.4. Elemental composition and analytical errors in leachates analysed by ICP-OES and IC (in ppm).

Sample	Si	±	Mg	±	Cl	±	Sr	±	Na	±	Ca	±	Zn	±	S	±	Ba	±	K	±	Mn	±	Cu	±	Al	±	Ni	±	Fe	±	Co	±
							0.0	0.0																								
	4.6	0.0	26.		22	0.	61	00	28	0.	25	0.			77		0.0	0.0	24				0.0	0.0	0.0	0.0			0.0	0.0	0.	4.6
Kl	86	15	93	0.1	.6	17	52	51	.3	23	.4	24	0.1	0.0	.2	1.	38	00	.7	0.	0.2	0.0	18	00	34	02	4.9	0.4	15	01	03	86
1	1	0	1	72	05	9	0	3	18	8	96	9	796	018	2	35	32	73	8	48	926	079	91	92	60	25	92	43	7	6	81	1
							0.0	0.0																								
	5.0	0.0	26.		4.	0.	54	00	19	0.	24	0.			77		0.0	0.0	5.	0.			0.0	0.0	0.0	0.0			0.0	0.0	0.	5.0
Kl	22	16	69	0.1	12	03	69	45	.5	16	.4	23	0.1	0.0	.1	1.	44	00	39	10	0.4	0.0	17	00	13	00	11.	1.0	10	01	09	22
2	4	0	7	70	41	27	0	6	64	5	67	9	990	020	2	35	24	85	8	4	445	120	09	83	95	91	35	1	7	1	55	4
							0.0	0.0																								
	6.3	0.0	18.		3.	0.	30	00	18	0.	20	0.			46		0.0	0.0	3.	0.	0.0	0.0	0.0	0.0	0.0	0.0	0.4	0.0	0.0	0.0		6.3
Kl	94	20	40	0.1	81	03	51	25	.7	15	.2	19	0.1	0.0	.3	0.	39	00	39	06	135	003	10	00	19	01	28	38	08	00	bd	94
3	5	4	7	17	41	03	6	4	70	8	26	7	008	010	2	81	58	76	0	5	8	7	32	50	05	24	5	0	48	88	1	5
							0.0	0.0																								
	3.7	0.0	25.		2.	0.	38	00	15	0.	32	0.	0.0	0.0	60		0.0	0.0	2.	0.	0.0	0.0	0.0	0.0	0.0	0.0	0.2	0.0	0.0	0.0		3.7
Ml	07	11	40	0.1	96	02	89	32	.2	12	.4	31	970	009	.2	1.	28	00	38	04	242	006	11	00	14	00	03	18	04	00	bd	07
1	7	8	0	62	59	35	4	4	42	8	11	6	9	8	7	06	68	55	3	6	9	5	20	55	16	92	9	1	91	51	1	7
							0.0	0.0															0.0	0.0								
	5.2	0.0	34.		3.	0.	45	00	19	0.	39	0.	0.0	0.0	77		0.0	0.0	2.	0.	0.0	0.0	08	00	0.0	0.0	0.2	0.0				5.2
Ml	95	16	42	0.2	37	02	23	37	.8	16	.3	38	916	009	.8	1.	21	00	80	05	274	007	58	41	20	01	01	17	bd	N/	bd	95
2	3	9	1	20	28	68	5	7	15	7	06	3	3	2	8	37	48	41	3	4	0	4	5	9	64	34	5	9	1	A	1	3
							0.0	0.0																								
	3.9	0.0	28.		2.	0.	52	00	23	0.	40	0.			69		0.0	0.0	2.	0.	0.0	0.0	0.0	0.0	0.0	0.0	0.1	0.0	0.0	0.0		3.9
Ml	75	12	62	0.1	51	02	22	43	.0	19	.0	39	0.1	0.0	.0	1.	51	00	29	04	246	006	15	00	23	01	51	13	10	01	bd	75
3	9	7	3	83	60	00	5	5	04	4	45	0	003	010	6	21	89	99	2	4	1	6	70	77	12	51	6	5	1	1	1	9

																							0.0	0.0								
	5.4	0.0	1.5	0.0	3.	0.	0.1	0.0	4.	0.	15	0.			2.	0.	0.0	0.0	1.	0.	0.0	0.0	02	00	0.0	0.0	0.0	0.0				5.4
Cl	28	17	16	09	08	02	49	01	67	03	.7	15	0.1	0.0	15	03	34	00	59	03	027	000	62	12	14	00	17	01	bd	N/	bd	28
1	7	3	9	7	16	45	21	24	09	93	90	4	013	010	0	8	99	67	1	1	53	74	3	8	49	94	23	53	l	A	l	7
																							0.0	0.0								
	5.7	0.0	1.4	0.0	4.	0.	0.1	0.0	6.	0.	17	0.	0.0	0.0	2.	0.	0.0	0.0	1.	0.	0.0	0.0	09	00	0.0	0.0	0.0	0.0				5.7
Cl	57	18	24	09	10	03	82	01	07	05	.3	16	935	009	67	04	30	00	90	03	025	000	02	44	32	02	18	01	bd	N/	bd	57
2	9	4	6	1	38	26	92	53	71	12	81	9	3	4	9	7	75	59	2	7	25	68	8	1	59	12	61	65	l	A	l	9
																							0.0	0.0								
	7.1	0.0	1.2	0.0	2.	0.	0.1	0.0	5.	0.	18	0.	0.0	0.0	2.	0.	0.0	0.0	1.	0.	0.0	0.0	04	00	0.0	0.0	0.0	0.0				7.1
Cl	75	22	90	08	60	02	65	01	00	04	.2	17	916	009	27	04	31	00	41	02	024	000	94	24	20	01	15	01	bd	N/	bd	75
3	8	9	5	2	35	07	56	38	92	22	47	8	0	2	9	0	83	61	8	7	23	65	3	1	32	32	44	37	l	A	l	8
							0.0	0.0															0.0	0.0								
	1.2	0.0	5.4	0.0	19	0.	24	00	18	0.	8.	0.	0.0	0.0	15		0.0	0.0	10		0.0	0.0	02	00	0.0	0.0	0.1	0.0	0.0	0.0		1.2
Ks	03	03	91	35	.2	15	72	20	.8	15	60	08	059	000	.7	0.	26	00	.1	0.	025	000	52	12	17	01	06	09	07	00	bd	03
1	2	8	1	0	82	3	0	6	79	9	58	39	17	59	4	28	31	50	4	19	28	68	8	3	91	17	4	4	40	77	l	2
							0.0	0.0																								
	0.8	0.0	5.0	0.0	14	0.	13	00	8.	0.	12	0.	0.0	0.0	21		0.0	0.0	6.	0.	0.0	0.0					0.0	0.0				0.8
Ks	49	02	90	32	.4	11	10	10	92	07	.6	12	035	000	.8	0.	20	00	74	12	072	001		N/		N/	73	06	bd	N/	bd	49
2	73	71	0	5	52	5	4	9	28	51	17	3	32	35	7	38	26	39	1	9	17	94	bdl	A	bdl	A	28	51	l	A	l	73
																							-	-								
							0.0	0.0									0.0	0.0					0.0	0.0								
	0.8	0.0	6.9	0.0	3.	0.	21	00	11	0.	12	0.	0.0	0.0	29		08	00	2.	0.	0.0	0.0	04	00			0.3	0.0				0.8
Ks	71	02	90	44	81	03	79	18	.1	09	.4	12	043	000	.0	0.	38	16	77	05	184	005	07	19		N/	03	26	bd	N/	bd	71
3	11	78	3	6	50	03	2	2	48	4	19	1	00	43	6	51	5	0	4	3	9	0	3	9	bdl	A	1	9	l	A	l	11
							0.0	0.0					-	-																		
	0.6	0.0	8.6	0.0	2.	0.	16	00	6.	0.	10	0.	0.0	0.0	24		0.0	0.0	1.	0.	0.0	0.0					0.0	0.0				0.6
M	71	02	18	55	42	01	54	13	73	05	.7	10	010	000	.4	0.	25	00	16	02	099	002		N/		N/	71	06	bd	N/	bd	71
s1	45	14	5	0	39	92	5	8	39	67	45	5	38	10	1	43	06	48	1	2	01	66	bdl	A	bdl	A	23	32	l	A	l	45
	0.7	0.0	12.		6.	0.			23	0.	16	0.	0.0	0.0	31		0.0	0.0	1.	0.	0.0	0.0					0.0	0.0	0.0	0.0		0.7
M	68	02	07	0.0	09	04	0.0	0.0	.1	19	.7	16	071	000	.8	0.	54	01	05	02	115	003	0.0	0.0		N/	66	05	12	01	bd	68
s2	74	45	0	77	60	84	32	00	74	5	76	4	52	72	6	56	63	04	6	0	6	1	04	00	bdl	A	07	87	3	3	l	74

							15	26															74	23								
							2	8															0	1								
																							-	-								
							0.0	0.0									0.0	0.0					0.0	0.0								
	0.7	0.0	15.		6.	0.	28	00	12	0.	23	0.	0.0	0.0	43		09	00	1.	0.	0.0	0.0	02	00			0.1	0.0				0.7
M	92	02	15	0.0	17	04	79	24	.6	10	.1	22	005	000	.3	0.	65	18	11	02	162	004	91	14		N/	28	11	bd	N/	bd	92
s3	33	53	4	97	82	90	0	0	12	6	23	5	930	060	1	76	0	5	2	1	8	4	7	2	bdl	A	6	4	l	A	l	33
																							-	-								
							0.0	0.0					-	-									0.0	0.0								
	2.0	0.0	0.5	0.0	14	0.	67	00	8.	0.	5.	0.	0.0	0.0	1.	0.	0.0	0.0	1.	0.	0.0	0.0	04	00	0.0	0.0						2.0
Cs	47	06	98	03	.6	11	48	56	58	07	15	05	043	000	18	02	13	00	89	03	014	000	70	23	11	00	bd	N/	bd	N/	bd	47
1	9	5	83	82	71	6	6	3	04	23	29	02	01	43	7	1	39	26	8	6	50	39	8	0	64	76	l	A	l	A	l	9
																							-	-								
							0.0	0.0					-	-									0.0	0.0	0.0	0.0						
	0.9	0.0	0.2	0.0	6.	0.	52	00	1.	0.	3.	0.	0.0	0.0	0.	0.	0.0	0.0	0.	0.	0.0	0.0	04	00	09	00						0.9
Cs	23	02	35	01	19	04	15	43	91	01	07	03	022	000	57	01	24	00	73	01	008	000	13	20	92	64	bd	N/	bd	N/	bd	23
2	43	95	48	50	03	91	3	5	22	61	81	00	85	23	00	00	62	47	14	40	644	233	6	2	8	7	l	A	l	A	l	43
																							-	-								
													-	-									0.0	0.0								
	2.8	0.0	0.4	0.0	2.	0.	0.1	0.0	2.	0.	8.	0.	0.0	0.0	0.	0.	0.0	0.0	0.	0.	0.0	0.0	04	00	0.0	0.0						2.8
Cs	48	09	30	02	36	01	02	00	62	02	36	08	033	000	98	01	34	00	86	01	016	000	36	21	21	01	bd	N/	bd	N/	bd	48
3	8	1	82	75	59	88	39	85	05	21	57	16	70	34	52	73	23	65	69	66	51	44	7	3	24	38	l	A	l	A	l	8

Table S4.5. Initial and dried weight of meteorite chips as well as pH values of leachates after the experiments.

Sample	Initial weight (mg)	Comments	pH	Dried weight (mg)	Comments	Difference (%)
Ks1	105		7.73	100		-4.76
Ks2	152		7.61	143	3 fragments	-5.92
Ks3	149		7.57	134	disintegrated	-10.1
Ms1	102	2 fragments	7.87	96		-5.88
Ms2	133		7.79	129		-3.01
Ms3	138	3 fragments	7.68	133	tiny fragment lost	-3.62
Cs1	182		8.49	181		-0.55
Cs2	109		8.43	108		-0.92
Cs3	114	7 fragments	8.25	112		-1.75
Kl1	104		7.69	87	powdered	-16.4
Kl2	106	2 fragments	7.70	93	disintegrated	-12.3
Kl3	116	8 fragments	7.70	104	partially powdered	-10.3
Ml1	102		7.47	96		-5.88
Ml2	114		7.47	108		-5.26
Ml3	143	> 25 fragments	7.54	114	lots of material lost	-20.3
Cl1	92		7.70	87		-5.43
Cl2	148		7.78	146		-1.35
Cl3	93	2 fragments	7.83	89		-4.30

Table S4.6. Average elemental concentrations (mg) in meteorite chips (calculated from elemental concentrations) and leachates for mass balance calculations. (a=Bates et al., 2024 (Winchcombe proxy), b=Fuchs et al., 1973, c=Ruggiu et al., 2022, d=Lodders, 2021).

Sample	**Si**	**Mg**	**Cl**[d]	**Na**	**Ca**	**S**	**K**	**Ni**
Kolang s chips[a]	16.2	14.6	0.0377	0.641	1.54	3.97	0.0534	1.59
Kolang s leachates	0.0195	0.117	0.250	0.260	0.224	0.444	0.131	0.00322
Kolang l chips[a]	12.2	11.0	0.0284	0.483	1.16	2.99	0.0402	1.20
Kolang l leachates	0.107	0.480	0.204	0.444	0.468	1.34	0.224	0.112
Murchison s chips[b]	15.4	13.6	0.0358	0.505	1.49	3.87	0.0337	1.62
Murchison s leachates	0.0149	0.239	0.0980	0.283	0.338	0.664	0.0222	0.00177
Murchison l chips[b]	13.7	12.1	0.0318	0.448	1.33	3.43	0.0299	1.44
Murchison l leachates	0.0865	0.590	0.0590	0.387	0.745	1.38	0.0499	0.00371
Chwichiya 002 chips[c]	18.2	15.4	0.0401	0.357	3.88	1.51	0.0777	2.07
Chwichiya 002 s leachates	0.039	0.00843	0.155	0.0874	0.111	0.0183	0.0233	bdl
Chwichiya 002 l chips[c]	14.7	12.4	0.0322	0.287	3.11	1.21	0.0624	1.66
Chwichiya 002 l leachates	0.122	0.0282	0.0653	0.105	0.343	0.0474	0.0327	0.000342

5 Conclusions and future work

This thesis aimed to improve the understanding of the aqueous alteration of CM chondrite on their parent body (chapters 2 and 3) and their alteration in a terrestrial environment (chapter 4). Especially the aqueous alteration conditions (notably temperature, water/rock (W/R) ratio and time) are difficult to determine from petrological studies of meteorites alone and benefit from additional geochemical modelling and laboratory experiments, which were the main scope of this thesis. The equilibrium models (chapter 2) focused on a wide parameter space (temperature, W/R ratio and aqueous CO_2 concentration) and different scenarios to constrain aqueous alteration conditions of CM chondrites. CM-like mineralogies were obtained for a wide range of temperature (1–140°C), initial W/R ratio (by mass) (0.3–5), solute concentration (0.2–2 m CO_2), pH (8.5–12.6) and pe. Furthermore, CM1s with magnetite and no cronstedtite likely form at elevated temperatures (>75°C) compared to CM2s, which could be explained by a thermally stratified CM parent body where CM1s would have formed close to its core. The kinetic models (chapter 3) studied possible timescales required for the aqueous alteration with the trade-off of a narrower parameter space. A typical CM2 chondrite could have formed within ~1000 years from a CM3. Laboratory experiments on CO3.00 DOM 08006, a CM3 proxy, show that calcite in CMs forms within months and when exposed to a carbonated solution. Kinetic models and laboratory experiments were also used to examine the effects of terrestrial weathering on CMs and CM-like meteorites. Amorphous material, Fe-sulphides, calcite and unknown Na-K-Cl phases are the most susceptible phases to weathering. A more specific CM weathering scale could be established based on their abundance as well as on the rustiness of the meteorite.

It is important to note that no definitive answers to the thesis aims in section 1.5 could be given due to the limitations of the experiments and the models. The models would benefit most from the availability of thermodynamic data of more minerals (notably tochilinite and pentlandite) and from more detailed knowledge of the starting composition of the solid material (particularly minor phases that are usually not detected by XRD) and of the aqueous fluid (which could be derived from fluid inclusions in CM chondrites). For the experiments, more experimental conditions such as shorter and longer durations, different temperatures, W/R ratios and fluid compositions are required to mimic different alteration conditions and to better validate modelling results. A broader range of different meteorites regarding petrologic type and weathering grade is also beneficial to further evaluate their effect on parent body and terrestrial alteration. For both the models and experiments, the starting material should ideally be more akin to more porous material that did not experience any form of alteration. Such material would very likely be too fragile to survive the transport to Earth but could still be present on the surface of primitive, volatile-rich asteroids, such as D- or P-type asteroids that are the target of the ongoing Lucy mission (e.g., Levison et al., 2021). The improved equilibrium and kinetic models could be further incorporated into reactive transport models to provide a better insight into the evolution of the CM parent body/bodies.

6 References

Alexander, C.M.O.D., Bowden, R., Fogel M.L., Howard K.T., 2015. Carbonate abundances and isotopic compositions in chondrites. *Meteorit. Planet. Sci.* **50**, 810–833.

Alexander, C.M.O.D., Greenwood, R.C., Bowden, R., Gibson, J.M., Howard, K.T., Franchi, I.A., 2018. A multi-technique search for the most primitive CO chondrites *Geochimica et Cosmochimica Acta* **221**, 406–420.

Alexander, C.M.O.D., Howard, K.T., Bowden, R., Fogel, M. L., 2013. The classification of CM and CR chondrites using bulk H, C and N abundances and isotopic compositions. *Geochim. Cosmochim. Acta* **123**, 244–260.

Alexander, C.M.O.D., 2019. Quantitative models for the elemental and isotopic fractionations in chondrites: The carbonaceous chondrites. *Geochimica et Cosmochimica Acta* **254**, 277–309.

Al-Kathiri, A., Hofmann, B.A., Jull, A.J.T., Gnos, E., 2005. Weathering of meteorites from Oman: Correlation of chemical and mineralogical weathering proxies with 14C terrestrial ages and the influence of soil chemistry. *Meteoritics & Planetary Science* 40: 1215–1239.

Anovitz, L.M., Beckingham, L.E., Sheets, J,M., Cole, D.R., 2022. A quantitative approach to the analysis of reactive mineralogy and surface area. *ACS Earth and Space Chemistry* **6**, 272–287.

Appelo, C.A.J., 2015. Principles, caveats and improvements in databases for calculating hydrogeochemical reactions in saline waters from 0 to 200°C and 1 to 1000atm. *Applied Geochemistry* **55**, 62–71.

Arvidson, R.S., Mackenzie, F.T., 1999. The dolomite problem; control of precipitation kinetics by temperature and saturation state. *American Journal of Science* **299**, 257–288.

Awolayo, A.N., Laureijs, C.T., Byng, J., Luhmann, A.J., Lauer, R., Tutolo, B.M., 2022. Mineral surface area accessibility and sensitivity constraints on carbon mineralization in basaltic aquifers. *Geochimica et Cosmochimica Acta* **334**, 293–315.

Bates, H.C., King, A.J., Shirley, K.S., Bonsall, E., Schroeder, C., Wombacher, F. et al., 2024. The bulk mineralogy, elemental composition, and water content of the Winchcombe CM chondrite fall. *Meteoritics & Planetary Science* 59: 1006–1028.

Beckingham, L.E., Steefel, C.I., Swift, A.M., Voltolini, M., Yang, L., Anovitz, L.M., et al., 2017. Evaluation of accessible mineral surface areas for improved prediction of mineral reaction rates in porous media. *Geochimica et Cosmochimica Acta* **205**, 31–49.

Bischoff, A., Alexander, C.M.O.D., Barrat, J.A., Burkhardt, C., Busemann, H., et al., 2021. The old, unique C1 chondrite Flensburg–insight into the first processes of aqueous alteration, brecciation, and the diversity of water-bearing parent bodies and lithologies. *Geochimica et Cosmochimica Acta* **293**, 142–186.

Bland, P.A., Jackson, M.D., Coker, R.F., Cohen, B.A., Webber, J.B.W., Lee, M.R., Duffy, C.M., Chater, R.J., Ardakani, M.G., McPhail, D.S., McComb, D.W., Benedix, G.K., 2009. Why aqueous alteration in asteroids was isochemical: High porosity ≠ high permeability. *Earth and Planetary Science Letters* **287**, 559–568.

Bland, P.A., Travis, B.J., 2017. Giant convecting mud balls of the early solar system. *Science Advances* **3**, e1602514.

Brantley, S.L., Mellott, N.P., 2000. Surface area and porosity of primary silicate minerals. *American Mineralogist* **85**, 1767–1783.

Brantley, S.L., 2008. "Kinetics of mineral dissolution." In *Kinetics of water-rock interaction*, edited by S.L. Brantley, J.D. Kubicki, A.F. White, 151–210. New York,+ NY: Springer New York.

Braukmüller, N., Wombacher, F., Hezel, D.C., Escoube, R., Münker, C., 2018. The chemical composition of carbonaceous chondrites: Implications for volatile element depletion, complementarity and alteration. *Geochimica et Cosmochimica Acta*, 239: 17–48.

Brearley, A.J., 2006. The action of water. In: Lauretta, D.S., McSween Jr, H.Y. (Eds), *Meteorites and the Early Solar System II*. The University of Arizona Press, Tucson, 584–624.

Brearley, A.J., Krot, A.N., 2012. Metasomatism in the early solar system: The record from chondritic meteorites. In *Metasomatism and the chemical transformation of rock: The role of fluids in terrestrial and extraterrestrial processes*,. Berlin, Heidelberg: Springer Berlin Heidelberg, 659–789.

Browning, L.B., McSween Jr, H.Y., Zolensky, M.E., 1996. Correlated alteration effects in CM carbonaceous chondrites. *Geochim. Cosmochim. Acta* **60**, 2621–2633.

Brunauer, S., Emmett, P.H., Teller, E., 1938. Adsorption of gases in multimolecular layers. *Journal of the American chemical society* 60: 309–319.

Buchwald, V.F., Clarke, R.S., 1989. Corrosion of Fe-Ni Alloys by Cl-Containing Akaganeite β-FeOOH); the Antarctic Meteorite Case. *American mineralogist*: 74: 656–667.

Burbine, T. H. (2017). Asteroids (Vol. 17). Cambridge University Press.

Carrozzo, F.G., De Sanctis, M.C., Raponi, A., et al., 2018. Nature, formation, and distribution of carbonates on Ceres. Science advances, **4**, e1701645.

Castillo-Rogez, J., Daswani, M.M., Glein, C.R., Vance, S.D., Cochrane, C.J., 2022. Contribution of non-water ices to salinity and electrical conductivity in ocean worlds. *Geophysical Research Letters* **49**, e2021GL097256.

Castillo-Rogez, J., Neveu, M., McSween Jr, H.Y., Fu, R.R., Toplis, M.J., Prettyman, T., 2018. Insights into Ceres's evolution from surface composition. *Meteoritics & Planetary Science* **53**, 1820–1843.

Chang, B., Li, C., Liu, D., Foster, I., Tripati, A., Lloyd, M. K., et al., 2020. Massive formation of early diagenetic dolomite in the Ediacaran ocean: Constraints on the "dolomite problem". *Proceedings of the national academy of sciences* **117**, 14005–14014.

Che, S., Domanik, K.J., Zega, T.J., 2023. In-situ formation of halite in the Sidi El Habib 001 (H5) ordinary chondrite: Implications for hydrothermal alteration in ordinary chondrite parent bodies. *Geochimica et Cosmochimica Acta*, **348**, 85–106.

Clog, M., Lindgren, P., Modestou, S., McDonald, A., Tait, A., Donnelly, T., Darren, M., Lee, M., 2024. Clumped isotope and Δ17O measurements of carbonates in CM carbonaceous chondrites: new insights into parent body thermal and fluid evolution. *Geochimica et Cosmochimica Acta* **369**, 1–16.

Cohen, S.D., Hindmarsh, A.C., Dubois, P.F., 1996. CVODE, a stiff/nonstiff ODE solver in C. *Computers in physics* **10**, 138–143.

Davidson, J., Alexander, C.M.O.D., Stroud, R.M., Busemann, H., Nittler, L.R., 2019. Mineralogy and petrology of Dominion Range 08006: A very primitive CO3 carbonaceous chondrite. *Geochimica et Cosmochimica Acta* **265**, 259–278.

DeMeo, F.E., Burt, B.J., Marsset, M., Polishook, D., Burbine, T. H., Carry B., Binzel, R.P., Vernazza, P., Reddy, V., Tang, M., Thomas, C.A., Rivkin, A.S., Moskovitz, N.A., Slivan S.M., Bus, S.J., 2022. Connecting asteroids and meteorites with visible and near-infrared spectroscopy. *Icarus* **380**, 114971.

De Sanctis, M.C., Mitri, G., Castillo-Rogez, J., House, C.H., Marchi, S., Raymond, C.A., Sekine, Y., 2020. Relict ocean worlds: Ceres. *Space Science Reviews*, **216**, 60.

De Sanctis, M. C., Raponi, A., Ammannito, E., Ciarniello, M., Toplis, M. J., McSween, H. Y., et al., 2016. Bright carbonate deposits as evidence of aqueous alteration on (1) Ceres. *Nature*, **536**, 54–57.

Desch, S.J., Kalyaan, A., Alexander, C.M.O.D., 2018. The Effect of Jupiter's Formation on the Distribution of Refractory Elements and Inclusions in Meteorites. *Astrophys. J. Suppl. Ser.* **238**, 11.

Dobrică, E., Ohtaki, K.K., Engrand, C., 2022. Dolomites in hydrated fine-grained Antarctic micrometeorites: Effective tools for analyzing secondary processes. *Geochimica et Cosmochimica Acta*, **317**, 286–305.

Fabre, S., Bêche, E., Esvan, J., Thébault, Y., Munsch, P., Quitté, G., 2024. Iron and Sulfur Secondary Phases as Proxies of Aqueous Alteration on Chondrite Parent Bodies. *ACS Earth and Space Chemistry* **8**, 174–193.

Farsang, S., Franchi, I.A., Zhao, X., Raub, T.D., Redfern, S.A., Grady, M.M., 2021. Carbonate assemblages in Cold Bokkeveld CM chondrite reveal complex parent body evolution. *Meteoritics & Planetary Science* **56**, 723–741.

Fatah, A., Mahmud, H.B., Bennour, Z., Gholami, R., Hossain, M., 2022. Geochemical modelling of CO2 interactions with shale: Kinetics of mineral dissolution and precipitation on geological time scales. *Chemical Geology* **592**, 120742.

Fedoseev, G., Ioppolo, S., Zhao, D., Lamberts, T., Linnartz, H., 2015. Low-temperature surface formation of NH3 and HNCO: hydrogenation of nitrogen atoms in CO-rich interstellar ice analogues. *Monthly Notices of the Royal Astronomical Society* **446**, 439–448.

Fendrich, K.V., Ebel, D.S. 2021. Comparison of the Murchison CM2 and Allende CV3 chondrites. *Meteoritics & Planetary Science* 56: 77–95.

Floyd, C.J., Benito, S., Martin, P.E., Jenkins, L.E., Dunham, E., Daly, L., Lee, M.R., 2024. Chondrule sizes within the CM carbonaceous chondrites and measurement methodologies. *Meteoritics & Planetary Science* **59**, 2769–2788.

Fuchs, L.H., Olsen, E., Jensen, K.J., 1973. Mineralogy, mineral-chemistry, and composition of the Murchison (C2) meteorite. *Smithsonian contributions to the earth sciences*.

Fuhr, M., Geilert, S., Schmidt, M., Liebetrau, V., Vogt, C., Ledwig, B., Wallmann, K., 2022. Kinetics of olivine weathering in seawater: an experimental study. *Frontiers in Climate* **4**, 831587.

Fujiya, W., Hoppe, P., Ushikubo, T., Fukuda, K., Lindgren, P., Lee, M.R., et al., 2019. Migration of D-type asteroids from the outer Solar System inferred from carbonate in meteorites. *Nature Astronomy*, **3**, 910–915.

Fujiya, W., Sugiura, N., Hotta, H., Ichimura, K., Sano, Y., 2012. Evidence for the late formation of hydrous asteroids from young meteoritic carbonates. *Nature communications* **3**, 627.

Garvie, L.A., Trif, L., Cotto-Figueroa, D., Asphaug, E., Hoover, C.G., 2024. High surface area and interconnected nanoporosity of clay-rich astromaterials. *Scientific reports* **14**, 10358.

Garvie, L.A., Trif, L., Hoover, C.G., 2025. The breathing of clay-rich astromaterials on Earth: Insights from the Tarda (C2-ung) and Aguas Zarcas (CM2) meteorites. *Meteoritics & Planetary Science*.

Gill, R., Ramsey, M.H., 1997. "What a geochemical analysis means." In *Modern Analytical Geochemistry: An Introduction to Quantitative Chemical Analysis Techniques for Earth, Environment and Materials Scientists* edited by R. Gill, 1–11. Longman Geochemistry Series.

Gladman, B., & Volk, K. (2021). Transneptunian space. *Annual Review of Astronomy and Astrophysics*, *59*(1), 203-246.

Greenwood, R.C., Burbine, T.H., Franchi, I.A., 2020. Linking asteroids and meteorites to the primordial planetesimal population. *Geochimica et Cosmochimica Acta*, **277**, 377–406.

Greenwood, R.C., Findlay, R., Martins, R., Steele, R.C.J., Shaw, K.M.M., Morton, E., Savage, P.S., Murphy, M.E., Rehkämper, M., Franchi, I.A., et. al., 2023. The formation and aqueous alteration of CM2 chondrites and their relationship to CO3 chondrites: A fresh isotopic (O, Cd, Cr, Si, Te, Ti, and Zn) perspective from the Winchcombe CM2 fall. *Meteoritics & Planetary Science* **24**, 1–24.

Greshake, A., 1997. The primitive matrix components of the unique carbonaceous chondrite Acfer 094: A TEM study. *Geochimica et Cosmochimica Acta*, **61**, 437–452.

Grimm, R.E., McSween Jr, H.Y., 1989. Water and the thermal evolution of carbonaceous chondrite parent bodies. *Icarus* **82**, 244–280.

Guo, W., Eiler, J.M, 2007. Temperatures of aqueous alteration and evidence for methane generation on the parent bodies of the CM chondrites. *Geochim. Cosmochim. Acta* **71**, 5565–5575.

Hanowski, N.P., Brearley, A.J., 2001. Aqueous alteration of chondrules in the CM carbonaceous chondrite, Allan Hills 81002: Implications for parent body alteration. *Geochimica et Cosmochimica Acta* 65: 495–518.

Herut, B., Starinsky, A., Katz, A. and Rosenfeld, D., 2000. Relationship between the acidity and chemical composition of rainwater and climatological conditions along a transition zone between large deserts and Mediterranean climate, Israel. *Atmospheric Environment* 34: 1281–1292.

Hewins, R.H., Bourot-Denise, M., Zanda, B., Leroux, H., Barrat, J.A., Humayun, M., et al., 2014. The Paris meteorite, the least altered CM chondrite so far. *Geochimica et Cosmochimica Acta* **124**, 190–222.

Holt, M.C., Herd, C.D., 2022. Fe-Ni sulfides in Tagish Lake: Implications for nebular and parent body conditions of formation. *Meteoritics & Planetary Science*, **57**, 1267–1287.

Hopp, T., Vollmer, C., 2018. Chemical composition and iron oxidation state of amorphous matrix silicates in the carbonaceous chondrite Acfer 094. *Meteoritics & Planetary Science*, **53**, 153–166.

Howard, K.T., Alexander, C.M.O.D., Schrader, D.L., Dyl, K.A., 2015. Classification of hydrous meteorites (CR, CM and C2 ungrouped) by phyllosilicate fraction: PSD-XRD modal mineralogy and planetesimal environments. *Geochimica et Cosmochimica Acta* **149**, 206–222.

Howard, K.T., Benedix, G.K., Bland, P.A., Cressey, G., 2011. Modal mineralogy of CM chondrites by X-ray diffraction (PSD-XRD): Part 2. Degree, nature and settings of aqueous alteration. *Geochimica et Cosmochimica Acta* **75**, 2735–2751.

Hu, Y., Moynier, F., Dai, W., Paquet, M., Yokoyama, T., Abe, Y., et al., 2024. Pervasive aqueous alteration in the early Solar System revealed by potassium isotopic variations in Ryugu samples and carbonaceous chondrites. *Icarus*, **409**, 115884.

Igami, Y., Tsuchiyama, A., Yamazaki, T., Matsumoto, M., Kimura, Y., 2021. In-situ water-immersion experiments on amorphous silicates in the MgO–SiO2 system: implications for the onset of aqueous alteration in primitive meteorites. *Geochimica et Cosmochimica Acta* **293**, 86–102.

Jiang, Y., Koefoed, P., Pravdivtseva, O., Chen, H., Li, C.H., Huang, F., et al., 2021. Early solar system aqueous activity: K isotope evidence from Allende. *Meteoritics & Planetary Science*, **56**, 61–76.

Jenkins, L.E., Lee, M.R., Daly, L., King, A.J., Chung, P., Griffin, S., Li, S., 2024. Identification of Hydroandradite in CM Carbonaceous Chondrites: A Product of Calc-Silicate Alteration on C-Complex Asteroids. *American Mineralogist* (in press).

Jenniskens, P., 2018. Review of asteroid-family and meteorite-type links. *Proceedings of the International Astronomical Union*, **14**, 9–12.

Jones, C.L., Brearley, A.J., 2006. Experimental aqueous alteration of the Allende meteorite under oxidizing conditions: constraints on asteroidal alteration. *Geochimica et Cosmochimica Acta* **70**, 1040–1058.

Kaplan, H.H., Lauretta, D.S., Simon, A.A., Hamilton, V.E., DellaGiustina, D.N., et al., 2020. Bright carbonate veins on asteroid (101955) Bennu: Implications for aqueous alteration history. *Science* **370**, eabc3557.

Kasting, J.F. ,1991. CO2 condensation and the climate of early Mars. *Icarus **94***, 1-13.

Kim, J., Kimura, Y., Puchala, B., Yamazaki, T., Becker, U., Sun, W., 2023. Dissolution enables dolomite crystal growth near ambient conditions. *Science* **28**, 915–920.

Kimura, M., Greenwood, R.C., Komatsu, M., Imae, N., Yamaguchi, A., Sato, R., 2022. Petrology and classification of A-9003, A 09535, and Y-82094: A new type of carbonaceous chondrite. *Meteoritics & Planetary Science*, **57**, 302–316.

Kimura, M., Imae, N., Komatsu, M., Barrat, J.A., Greenwood, R.C., Yamaguchi, A., Noguchi, T., 2020. The most primitive CM chondrites, Asuka 12085, 12169, and 12236, of subtypes 3.0–2.8: Their characteristic features and classification. *Polar Science* **26**, 100565.

Kimura, M., Weisberg, M.K., Yamaguchi, A., 2024. Subtype 3.0 chondrites: Petrologic classification criteria. *Meteoritics & Planetary Science*, **59**, 858–877.

King, A.J., Bates, H.C., Krietsch, D., Busemann, H., Clay, P.L., Schofield, P.F., Russell, S.S., 2019. The Yamato-type (CY) carbonaceous chondrite group: Analogues for the surface of asteroid Ryugu?. *Geochemistry*, **79**, 125531.

King, A.J., Bates, H.C., Schofield, P.F., Russell, S.S. 2021. The bulk mineralogy and water contents of the carbonaceous chondrite falls Kolang and Tarda. (Abstract #1909). 52nd Lunar and Planetary Science Conference. CD-ROM.

King, A.J., Daly, L., Rowe, J., et al., 2022. The Winchcombe meteorite, a unique and pristine witness from the outer solar system. *Sci. Adv.* **8**, 1–18.

King, A.J., Schofield, P.F., Howard, K.T., Russell, S.S., 2015. Modal mineralogy of CI and CI-like chondrites by X-ray diffraction. *Geochimica et Cosmochimica Acta* **165**, 148–160.

King, A.J., Schofield, P.F., Russell, S.S., 2017. Type 1 aqueous alteration in CM carbonaceous chondrites: Implications for the evolution of water-rich asteroids. *Meteoritics & Planetary Science* **52**, 1197–1215.

Kopp, R. E., Humayun, M., 2003. Kinetic model of carbonate dissolution in Martian meteorite ALH84001. *Geochimica et Cosmochimica Acta* **67**, 3247–3256.

Krot, A.N., Dunn, T.L., Petaev, M.I., Ma, C., Nagashima, K., Zipfel, J., 2024. Metasomatic alteration of coarse-grained igneous calcium-aluminum-rich inclusions from CK3 carbonaceous chondrites. *Meteoritics & Planetary Science*, **59**, 809–835.

Kurokawa, H., Shibuya, T., Sekine, Y., Ehlmann, B.Y., Usui, F., Kikuchi, S., Yoda, M., 2021. Distant Formation and Differentiation of Outer Main Belt Asteroids and Carbonaceous Chondrite Parent Bodies. *AGU Advances* **3**, 1–23.

Lauretta, D.S., Connolly Jr, H.C., Aebersold, J.E., Alexander, C.M.O.D., et al., 2024. Asteroid (101955) Bennu in the laboratory: Properties of the sample collected by OSIRIS-REx. *Meteorit. Planet. Sci.* **59**, 2453–2486.

Leal, A.M., Kulik, D.A., Smith, W.R., Saar, M.O., 2017. An overview of computational methods for chemical equilibrium and kinetic calculations for geochemical and reactive transport modeling. *Pure and Applied Chemistry* **89**, 597–643.

Lee, M.R., Alexander, C.M.O.D., Bischoff, A., Brearley, A.J., Dobrică, E., Fujiya, W., et al., 2025. Low-temperature aqueous alteration of chondrites. *Space Science Reviews*, **221**, 11.

Lee, M.R., Bland, P.A., 2004. Mechanisms of weathering of meteorites recovered from hot and cold deserts and the formation of phyllosilicates. *Geochimica et Cosmochimica Acta* 68: 893–916.

Lee, M.R., Cohen, B.E., King, A.J., Greenwood, R.C., 2019a. The diversity of CM carbonaceous chondrite parent bodies explored using Lewis Cliff 85311. *Geochimica et Cosmochimica Acta*, **264**, 224–244.

Lee, M.R., Cohen, B.E., King, A.J. 2019b. Alkali-halogen metasomatism of the CM carbonaceous chondrites. *Meteoritics & Planetary Science*, **54**, 3052–3063.

Lee, M.R., Daly, L., Floyd, C., Martin, P.E., 2021. CM carbonaceous chondrite falls and their terrestrial alteration. *Meteoritics & Planetary Science* 56: 34–48.

Lee, M.R., Lindgren, P., Sofe, M.R., Alexander, C.M.O.D., Wang, J., 2012. Extended chronologies of aqueous alteration in the CM2 carbonaceous chondrites: Evidence from carbonates in Queen Alexandra Range 93005. *Geochimica et Cosmochimica Acta*, **92**, 148–169.

Lee, M.R., Lindgren, P., Sofe, M.R., 2014. Aragonite, breunnerite, calcite and dolomite in the CM carbonaceous chondrites: High fidelity recorders of progressive parent body aqueous alteration. *Geochimica et Cosmochimica Acta* **144**, 126–156.

Lee, M.R., Salge, T., Maclaren, I., 2025. Magnesium phosphate in the Cold Bokkeveld (CM2) carbonaceous chondrite. *Meteoritics & Planetary Science* 60: 2017–2032.

Lee, M.R., Sofe, M.R., Lindgren, P., Starkey, N.A., Franchi, I.A., 2013. The oxygen isotope evolution of parent body aqueous solutions as recorded by multiple carbonate generations in the Lonewolf Nunataks 94101 CM2 carbonaceous chondrite. *Geochimica et Cosmochimica Acta* **121**, 452–466.

Lee, M.R., Smith, C.L., Gordon, S.H., Hodson, M.E., 2006. Laboratory simulation of terrestrial meteorite weathering using the Bensour (LL6) ordinary chondrite. *Meteoritics & Planetary Science* **41**, 1123–1138.

Le Guillou, C., Dohmen, R., Rogalla, D., Müller, T., Vollmer, C., Becker, H.W., 2015. New experimental approach to study aqueous alteration of amorphous silicates at low reaction rates. *Chemical Geology* **412**, 179–192.

Lauretta, D.S., Balram-Knutson, S.S., Beshore, E., Boynton, W.V., et al., 2017. OSIRIS-REx: sample return from asteroid (101955) Bennu. *Space Science Reviews*, **212**, 925–984.

Lauretta, D.S., Connolly Jr, H.C., Aebersold, J.E., Alexander, C.M.O.D., Ballouz, R.L., Barnes, J.J., et al., 2024. Asteroid (101955) Bennu in the laboratory: Properties of the sample collected by OSIRIS-REx. *Meteoritics & Planetary Science*, **59**, 2453–2486.

Lauretta, D. S., & McSween, H. Y. (Eds.). (2006). *Meteorites and the early solar system II*. University of Arizona Press.

Lentfort, S., Bischoff, A., Ebert, S., Patzek, M., 2021. Classification of CM chondrite breccias — Implications for the evaluation of samples from the OSIRIS-REx and Hayabusa 2 missions. *Meteorit. Planet. Sci.* **56**, 127–147.

Leroux, H., Cuvillier, P., Zanda, B., Hewins, R.H., 2015. GEMS-like material in the matrix of the Paris meteorite and the early stages of alteration of CM chondrites. *Geochimica et Cosmochimica Acta* **170**, 247–265.

Levison, H.F., Olkin, C.B., Noll, K.S., Marchi, S., Bell III, J.F., Bierhaus, E., et al., 2021. Lucy mission to the Trojan asteroids: science goals. *The Planetary Science Journal*, **2**, 171.

Lindgren, P., Lee, M.R., Sofe, M.R., Zolensky, M.E., 2013. Clasts in the CM 2 carbonaceous chondrite Lonewolf Nunataks 94101: Evidence for aqueous alteration prior to complex mixing. *Meteoritics & Planetary Science* **48**, 1074–1090.

Lodders, K., 2021. Relative atomic solar system abundances, mass fractions, and atomic masses of the elements and their isotopes, composition of the solar photosphere, and compositions of the major chondritic meteorite groups. *Space Science Reviews* **217**, 44.

Losiak, A. and Velbel, M.A., 2011. Evaporite formation during weathering of Antarctic meteorites—A weathering census analysis based on the ANSMET database. *Meteoritics & Planetary Science* 46: 443–458.

Lugmair, G.W., Shukolyukov, A., 1998. Early solar system timescales according to 53Mn-53Cr systematics. *Geochimica et Cosmochimica Acta* **62**, 2863–2886.

Macke, R.J., Consolmagno, G.J., Britt, D.T., 2011. Density, porosity, and magnetic susceptibility of carbonaceous chondrites. *Meteoritics & Planetary Science* **46**, 1842–1862.

Marieni, C., Matter, J.M., Teagle, D.A.H., 2020. Experimental study on mafic rock dissolution rates within CO2-seawater-rock systems. *Geochim. Cosmochim. Acta* **272**, 259–275.

Marrocchi, Y., Bekaert, D.V., Piani, L., 2018. Origin and abundance of water in carbonaceous asteroids. *Earth and Planetary Science Letters* **482**, 23–32.

Marrocchi, Y., Rigaudier, T., Piralla, M., Piani, L., 2023. Hydrogen isotopic evidence for nebular pre-hydration and the limited role of parent-body processes in CM chondrites. *Earth and Planetary Science Letters* **611**, 118151.

Martin, B., Fyfe, W.S., 1970. Some experimental and theoretical observations on the kinetics of hydration reactions with particular reference to serpentinization. *Chemical Geology*, **6**, 185–202.

Matsumoto, M., Tsuchiyama, A., Miyake, A., Ito, M., Matsuno, J., Uesugi, K., et al., 2022. Three-dimensional microstructure and mineralogy of a cosmic symplectite in the Acfer 094 carbonaceous chondrite: Implication for its origin. *Geochimica et Cosmochimica Acta*, **323**, 220–241.

Matsumoto, M., Tsuchiyama, A., Nakato, A., Matsuno, J., Miyake, A., Kataoka, A., et al., 2019. Discovery of fossil asteroidal ice in primitive meteorite Acfer 094. *Science Advances*, **5**, eaax5078.

McCollom, T.M., Klein, F., Moskowitz, B., Solheid, P., 2022. Experimental serpentinization of iron-rich olivine (hortonolite): Implications for hydrogen generation and secondary mineralization on Mars and icy moons. *Geochimica et Cosmochimica Acta* **335**, 98–110.

McCord, T.B., Combe, J.P., Castillo-Rogez, J.C., McSween, H.Y., Prettyman, T.H., 2022. Ceres, a wet planet: The view after Dawn. *Geochemistry*, **82**, 125745.

McCoy, T.J., et al., 2025. An evaporite sequence from ancient brine recorded in Bennu samples. *Nature* 637: 1072–1077.

McSween Jr, H.Y., 1979. Alteration in CM carbonaceous chondrites inferred from modal and chemical variations in matrix. *Geochim. Cosmochim. Acta* **43**, 1761–1770.

McSween Jr, H.Y., Emery, J.P., Rivkin, A.S., Toplis, M.J., Castillo-Rogez, J., Prettyman, T.H., et al., 2018. Carbonaceous chondrites as analogs for the composition and alteration of Ceres. *Meteoritics & Planetary Science*, **53**, 1793–1804.

McSween, Jr, H.Y., Moersch, J.E., Burr, D.M., Dunne, W.M., Emery, J.P., Kah, L.C., McCanta, M.C., 2019. Planetary Geoscience. In *Cambridge University Press*.

Metzler, K., Hezel, D.C., Barosch, J., Wölfer, E., Schneider, J.M., Hellmann, J.L., et al., 2021. The Loongana (CL) group of carbonaceous chondrites. *Geochimica et Cosmochimica Acta*, **304**, 1–31.

Morbidelli, A., Chambers, J., Lunine, J.I., Petit, J.M., Robert, F., Valsecchi, G.B., Cyr, K.E., 2000. Source regions and timescales for the delivery of water to the Earth. *Meteoritics & Planetary Science*, **35**, 1309–1320.

Mumma, M.J., Charnley, S.B., 2011. The chemical composition of comets—emerging taxonomies and natal heritage. *Annual Review of Astronomy and Astrophysics* **49**, 471–524.

Nakamura, T., Matsumoto, M., Amano, K. et al., 2022. Formation and evolution of carbonaceous asteroid Ryugu: Direct evidence from returned samples. *Science* **379**, 8671.

Neumann, W., Grott, M., Trieloff, M., Jaumann, R., Biele, J., Hamm, M., Kührt, E., 2021. Microporosity and parent body of the rubble-pile NEA (162173) Ryugu. *Icarus* **358**, 114166.

Neveu, M., Desch, S.J., 2015. Geochemistry, thermal evolution, and cryovolcanism on Ceres with a muddy ice mantle. *Geophys. Res. Lett.* **42**, 10197–10206.

Neveu, M., Desch, S.J., Castillo-Rogez, J.C., 2017. Aqueous geochemistry in icy world interiors: Equilibrium fluid, rock, and gas compositions, and fate of antifreezes and radionuclides. *Geochimica et Cosmochimica Acta* **212**, 324–371.

Newton, J., Bischoff, A., Arden, J.W., Franchi, I.A., Geiger, T., Greshake, A., Pillinger, C.T., 1995. Acfer 094, a uniquely primitive carbonaceous chondrite from the Sahara. *Meteoritics*, **30**, 47–56.

Noguchi, T., Nakashima, D., Ushikubo, T., Fujiya, W., Ohashi, N., Bradley, J.P., et al., 2024. Chondrule-like objects and a Ca-Al-rich inclusion from comets or comet-like icy bodies. *Geochimica et Cosmochimica Acta*, **381**, 131–155.

Noguchi, T., Yasutake, M., Tsuchiyama, A., Miyake, A., Kimura, M., Yamaguchi, A., et al., 2021. Mineralogy of fine-grained matrix, fine-grained rim, chondrule rim, and altered mesostasis of a chondrule in Asuka 12169, one of the least altered CM chondrites. *Polar Science*, **29**, 100727.

Nordstrom, D.K, Plummer, L.N., Wigley, T.M.L., Wolery, T.J., Ball, T.W., Jenne, E.A., et al., 1979. A Comparison of Computerized Chemical Models for Equilibrium Calculations in Aqueous Systems. *Chemical Modeling in Aqueous Systems* 38: 857–892.

Nuth III, J. A., McCoy, T., Johnson, N., & Abreu, N. M. (2018). Exploring the possible continuum between comets and asteroids. In *Primitive Meteorites and Asteroids* (pp. 409-438). Elsevier.

Palandri, J.L., Kharaka, Y.K., 2004. A compilation of rate parameters of water-mineral interaction kinetics for application to geochemical modeling. *U.S. Geological Survey*.

Palguta, J., Schubert, G., Travis, B.J., 2010. Fluid flow and chemical alteration in carbonaceous chondrite parent bodies. *Earth and Planetary Science Letters* **296**, 235–243.

Palme, H., Mezger, K., 2024. Nucleosynthetic isotope variations in chondritic meteorites and their relationship to bulk chemistry. *Meteoritics & Planetary Science*, **59**, 382–394.

Palmer, E.E., Lauretta, D.S., 2011. Aqueous alteration of kamacite in CM chondrites. *Meteorit. Planet. Sci.* **46**, 1587–1607.

Parkhurst, D.L., 1995. User's Guide to PHREEQC-A Computer Program for Speciation, Reaction-Path, Advective Transport, and Inverse Geochemical Calculations. *US Department of the Interior, US Geological Survey*.

Parkhurst, D.L., Appelo, C.A.J., 1999. User's guide to PHREEQC (Version 2): A computer program for speciation, batch-reaction, one-dimensional transport, and inverse geochemical calculations. *US Geological Survey*.

Parkhurst, D.L., Appelo, C.A.J., 2013. Description of input and examples for PHREEQC version 3—a computer program for speciation, batch-reaction, one-dimensional transport, and inverse geochemical calculations. *US geological survey techniques and methods* **6**, 497.

Patzek, M., Hoppe, P., Bischoff, A., Visser, R., John, T, 2020. Hydrogen isotopic composition of CI-and CM-like clasts from meteorite breccias–sampling unknown sources of carbonaceous chondrite materials. *Geochimica et Cosmochimica Acta*, **272**, 177–197.

Patzer, A., Bullock, E.S., Alexander, C.M.O.D., 2021. Testing models for the compositions of chondrites and their components: I. CO chondrites. *Geochimica et Cosmochimica Acta* **304**, 119–140.

Patzer, A., Bullock, E.S., Alexander, C.M.O.D., 2023. Testing models for the compositions of chondrites and their components: III. CM chondrites. *Geochim. Cosmochim. Acta* **359**, 30–45.

Piralla, M., Tartese, R., Marrocchi, Y., Joy, K.H., 2021. Apatite halogen and hydrogen isotope constraints on the conditions of hydrothermal alteration in carbonaceous chondrites. *Meteoritics & Planetary Science*, **56**, 809–828.

Potin, S., Beck, P., Bonal, L., Schmitt, B., Garenne, A., Moynier, F., Agranier, A., Schmitt-Kopplin, P., Malik, A.K., Quirico, E., 2020. Mineralogy, chemistry, and composition of organic compounds in the fresh carbonaceous chondrite Mukundpura: CM1 or CM2? *Meteorit. Planet. Sci.* **55**, 1681–1696.

Pravdivtseva, O., Krot, A.N., Hohenberg, C.M., 2018. I-Xe dating of aqueous alteration in the CI chondrite Orgueil: I. Magnetite and ferromagnetic separates. *Geochimica et Cosmochimica Acta*, **227**, 38–47.

Riciputi, L.R., McSween Jr, H.Y., Johnson, C.A., Prinz, M., 1994. Minor and trace element concentrations in carbonates of carbonaceous chondrites, and implications for the compositions of coexisting fluids. *Geochim. Cosmochim. Acta* **58**, 1343–1351.

Rosenberg, N.D., Browning, L., Bourcier, W.L., 2001. Modeling aqueous alteration of CM carbonaceous chondrites. *Meteoritics & Planetary Science* **36**, 239–244.

Rubin, A.E., Trigo-Rodríguez, J.M., Huber, H., Wasson, J.T., 2007. Progressive aqueous alteration of CM carbonaceous chondrites. *Geochim. Cosmochim. Acta* **71**, 2361–2382.

Rubin, A.E., 2012. Collisional facilitation of aqueous alteration of CM and CV carbonaceous chondrites. *Geochimica et Cosmochimica Acta* **90**, 181–194.

Rubin, A.E., 2015. An American on Paris: Extent of aqueous alteration of a CM chondrite and the petrography of its refractory and amoeboid olivine inclusions. *Meteoritics & Planetary Science* 50: 1595–1612.

Ruggiu, L.K., Devouard, B., Gattacceca, J., Bonal, L., Leroux, H., Eschrig, J., Borschneck, D., King, A.J., Beck, P., Marrocchi, Y., Debaille, V., 2022. Detection of incipient aqueous alteration in carbonaceous chondrites. *Geochimica et Cosmochimica Acta* 336: 308–331.

Russell, C.T., Raymond, C.A., 2011. The dawn mission to Vesta and Ceres. *Space Science Reviews*, **163**, 3–23.

Sandford, S.A., Allamandola, L.J. ,1988. The condensation and vaporization behavior of H2O: CO ices and implications for interstellar grains and cometary activity. *Icarus* **76**, 201–224.

Sandford, S.A., Allamandola, L.J., 1993. The condensation and vaporization behavior of ices containing SO2, H2S, and CO2: Implications for Io. *Icarus* **106**, 478–488.

Schmitt-Kopplin, P., Gabelica, Z., Gougeon, R.D., Fekete, A., Kanawati, B., Harir, M., Gebefuegi, I., Eckel, G., Hertkorn, N., 2010. High molecular diversity of extraterrestrial organic matter in Murchison meteorite revealed 40 years after its fall. *Proc. Natl. Acad. Sci.* **107**, 2763–2768.

Schrader, D.L., Cloutis, E. A., Applin, D. M., Davidson, J., Torrano, Z. A., Foustoukos, D., ... & Render, J. (2024). Tarda and Tagish Lake: Samples from the same outer Solar System asteroid and implications for D-and P-type asteroids. *Geochimica et Cosmochimica Acta*, *380*, 48-70.

Schulte, M., Shock, E., 2004. Coupled organic synthesis and mineral alteration on meteorite parent bodies. *Meteorit. Planet. Sci.* **39**, 1577–1590.

Seewald, J.S., Zolotov, M.Y., McCollom, T., 2006. Experimental investigation of single carbon compounds under hydrothermal conditions. *Geochimica et Cosmochimica Acta*, 70, 446–460.

Shibuya, T., Sekine, Y., Kikuchi, S., Kurokawa, H., 2024. Aqueous alteration in icy planetesimals: The effect of outward transport of gaseous hydrogen. *Geochimica et Cosmochimica Acta* **374**, 264–283.

Singerling, S.A., Brearley, A.J., 2020. Altered primary iron sulfides in CM 2 and CR 2 carbonaceous chondrites: Insights into parent body processes. *Meteoritics & Planetary Science* 55: 496–523.

Singerling, S.A., Corrigan, C.M., Brearley, A.J., 2024. The fate of primary iron sulfides in the CM1 carbonaceous chondrites: Effects of advanced aqueous alteration on primary components. *Meteoritics & Planetary Science*, **59**, 475–501.

Smith, E.J., Davison, W., Hamilton-Taylor, J., 2002. Methods for preparing synthetic freshwaters. *Water research* 36: 1286–1296.

Sridhar, S., Bryson, J.F., King, A.J., Harrison, R.J., 2021. Constraints on the ice composition of carbonaceous chondrites from their magnetic mineralogy. *Earth and Planetary Science Letters*, **576**, 117243.

Suttle, M.D., Daly, L., Jones, R.H., Jenkins, L., Van Ginneken, M., et al., 2024. The Winchcombe meteorite—A regolith breccia from a rubble pile CM chondrite asteroid. *Meteoritics & Planetary Science* **59**, 1043–1067.

Suttle, M.D., Genge, M.J., Salge, T., Lee, M.R., Folco, L., et al., 2019. A microchondrule-bearing micrometeorite and comparison with microchondrules in CM chondrites. *Meteoritics & Planetary Science*, **54**, 1303–1324.

Suttle, M.D., King, A.J., Ramkissoon, N.K., Bonato, E., Franchi, I.A., Malley, J., Schofield, P.F., Najorka, J., Salge, T., Russell, S.S., 2022. Alteration conditions on the CM and CV parent bodies–Insights from hydrothermal experiments with the CO chondrite Kainsaz. *Geochimica et Cosmochimica Acta* **318**, 83–111.

Suttle, M.D., King, A.J., Schofield, P.F., Bates, H., Russell, S.S., 2021. The aqueous alteration of CM chondrites, a review. *Geochimica et Cosmochimica Acta* **299**, 219–256.

Takir, D., Emery, J.P., McSween Jr, H.Y., Hibbitts, C.A., Clark, R.N., Pearson, N., Wang, A., 2013. Nature and degree of aqueous alteration in CM and CI carbonaceous chondrites. *Meteoritics & Planetary Science*, **48**, 1618–1637.

Takir, D., Neumann, W., Raymond, S.N., Emery, J.P., Trieloff, M., 2023. Late accretion of Ceres-like asteroids and their implantation into the outer Main belt. *Nature Astronomy*, **7**, 524–533.

Telus, M., Hauri, E.H., Wang, J., 2019. Calcite and dolomite formation in the CM parent body: Insight from in situ C and O isotope analyses. *Geochimica et Cosmochimica Acta* **260**, 275–291.

Travis, B.J., Bland, P.A., Feldman, W.C., Sykes, M.V., 2018. Hydrothermal dynamics in a CM-based model of Ceres. *Meteoritics & Planetary Science*, **53**, 2008–2032.

Tsuchiyama, A., Miyake, A., Okuzumi, S., Kitayama, A., Kawano, J., Uesugi, K., et al., 2021. Discovery of primitive CO2-bearing fluid in an aqueously altered carbonaceous chondrite. *Science Advances*, **7**, eabg9707.

Tsuda, Y., Yoshikawa, M., Saiki, T., Nakazawa, S., Watanabe, S.I., 2019. Hayabusa2–Sample return and kinetic impact mission to near-earth asteroid Ryugu. *Acta Astronautica*, **156**, 387–393.

Tyra, M.A., Farquhar, J., Guan, Y., Leshin, L.A., 2012. An oxygen isotope dichotomy in CM2 chondritic carbonates-A SIMS approach. *Geochimica et Cosmochimica Acta* **77**, 383–395.

Tyra, M., Brearley, A., Guan, Y., 2016. Episodic carbonate precipitation in the CM chondrite ALH 84049: An ion microprobe analysis of O and C isotopes. *Geochimica et Cosmochimica Acta* **175**, 195–207.

Vaccaro, E., Wozniakiewicz, P., Franchi, I.A., Starkey, N., Russell, S.S., 2023. The grain size distribution of matrix in primitive chondrites. *Meteoritics & Planetary Science*, **58**, 688–704.

Vacher, L.G., Marrocchi, Y., Villeneuve, J., Verdier-Paoletti, M.J., Gounelle, M., 2017. Petrographic and C & O isotopic characteristics of the earliest stages of aqueous alteration of CM chondrites. *Geochim. Cosmochim. Acta* **213**, 271–290.

Vacher, L.G., Marrocchi, Y., Villeneuve, J., Verdier-Paoletti, M.J., Gounelle, M., 2018. Collisional and alteration history of the CM parent body. *Geochim. Cosmochim. Acta* **239**, 213–234.

Vacher, L.G., Truche, L., Faure, F., Tissandier, L., Mosser-Ruck, R., Marrocchi, Y., 2019. Deciphering the conditions of tochilinite and cronstedtite formation in CM chondrites from low temperature hydrothermal experiments. *Meteoritics & Planetary Science* **54**, 1870–1889.

Van Schmus, W.R., Wood, J.A., 1967. A chemical-petrologic classification for the chondritic meteorites. *Geochim. Cosmochim. Acta* **31**, 747–765.

Velbel M.A., 1988. The distribution and significance of evaporitic weathering products on Antarctic meteorites. *Meteoritics* 23: 151–159.

Velbel, M.A., Long, D.T., Gooding, J.L., 1991. Terrestrial weathering of Antarctic stone meteorites: Formation of Mg-carbonates on ordinary chondrites. *Geochimica et Cosmochimica Acta* 55: 67–76. Velbel, M.A., Tonui, E.K., Zolensky, M.E., 2012. Replacement of olivine by serpentine in the carbonaceous chondrite Nogoya (CM2). *Geochimica et Cosmochimica Acta*, **87**, 117-135.

Verdier-Paoletti, M.J., Marrocchi, Y., Avice, G., Roskosz, M., Gurenko, A., Gounelle M., 2017. Oxygen isotope constraints on the alteration temperatures of CM chondrites. *Earth Planet. Sci. Lett.* **458**, 273–281.

Verdier-Paoletti, M.J., Marrocchi, Y., Vacher, L.G., Gattacceca, J., Gurenko, A., Sonzogni, C., Gounelle, M., 2019. Testing the genetic relationship between fluid alteration and brecciation in CM chondrites. *Meteoritics & Planetary Science* **54**, 1692–1709.

Visser, R., John, T., Whitehouse, M.J., Patzek, M., Bischoff, A., 2020. A short-lived 26Al induced hydrothermal alteration event in the outer solar system: Constraints from Mn/Cr ages of carbonates. *Earth and Planetary Science Letters*, **547**, 116440.

Walsh, J.N., 1997. "Inductively coupled plasma-atomic emission spectrometry (ICP-AES)." In *Modern Analytical Geochemistry: An Introduction to Quantitative Chemical Analysis Techniques for Earth, Environment and Materials Scientists*, edited by R. Gill, 41–66. Longman Geochemistry Series.

Walsh, K.J., Morbidelli, A., Raymond, S.N., O'Brien, D.P., Mandell, A.M., 2011. A low mass for Mars from Jupiter's early gas-driven migration. *Nature*, **475**, 206–209.

Wegner, W.W., Ernst, W.G., 1983. Experimentally determined hydration and dehydration reaction rates in the system MgO-SiO2-H2O. *American Journal of Science*, **283**, 151–180.

Weisberg, M.K., McCoy, T.J., Krot, A.N., 2006. Systematics and evaluation of meteorite classification. *Meteorites and the early solar system II*, **19** 19–52.

Wilson, L., Keil, K., Browning, L.B., Krot, A.N., Bourcier, W., 1999. Early aqueous alteration, explosive disruption, and reprocessing of asteroids. *Meteoritics & Planetary Science* **34**, 541–557.

Wlotzka F. 1993. A weathering scale for the ordinary chondrites (abstract). *Meteoritics* 28: 460.

Xu, Y., Lin, Y., Hao, J., Kimura, M., Hu, S., Yang, W., et al., 2022. Abundant presolar silicates of the CM chondrite Asuka 12169: Implications for the thermal and aqueous alteration of the CM parent body. *Geochimica et Cosmochimica Acta*, **334**, 45–64.

Young, E.D., Ash, R.D., England, P., Rumble, D., 1999. Fluid flow in chondritic parent bodies: Deciphering the compositions of planetesimals. *Science* **286**, 1331–1335.

Young, E.D., 2001. The hydrology of carbonaceous chondrite parent bodies and the evolution of planet progenitors. *Philosophical Transactions of the Royal Society of London. Series A: Mathematical, Physical and Engineering Sciences*, **359**, 2095–2110.

Zhang, Y., Hu, B., Teng, Y., Tu, K., Zhu, C., 2019. A library of BASIC scripts of reaction rates for geochemical modeling using phreeqc. *Computers & Geosciences* **133**, 104316.

Zhang, G., Lu, P., Zhang, Y., Tu, K., Zhu, C., 2020. SUPPHREEQC: A program for generating customized PHREEQC thermodynamic datasets from SUPCRTBL and extending calculations to elevated pressures and temperatures. *Computers & Geosciences* **143**, 104560.

Zhu, K., Moynier, F., Schiller, M., Alexander, C.M.O.D., Davidson, J., Schrader, D. L., et al., 2021. Chromium isotopic insights into the origin of chondrite parent bodies and the early terrestrial volatile depletion. *Geochimica et Cosmochimica Acta*, **301** 158–186.

Zolensky, M.E., Bodnar, R.J., Yurimoto, H., Itoh, S., Fries, M., Steele, A., et al., 2017. The search for and analysis of direct samples of early Solar System aqueous fluids. *Philosophical Transactions of the Royal Society A: Mathematical, Physical and Engineering Sciences*, **375**, 20150386.

Zolensky, M.E., Bourcier, W.L., Gooding, J.L., 1989. Aqueous alteration on the hydrous asteroids: Results of EQ3/6 computer simulations. *Icarus* **78**, 411–425.

Zolensky, M.E., Mittlefehldt, D.W., Lipschutz, M.E., Wang, M., Clayton, R.N., Mayeda, T.K., Grady, M.M., Pillinger, C., Barber, D., 1997. CM chondrites exhibit the complete petrologic range from type 2 to 1. *Geochimica et Cosmochimica Acta* **61**, 5099–5115.

Zolensky, M.E., Nakamura, K., Gounelle, M., Mikouchi, T., Kasama, T., Tachikawa, O., Tonui, E., 2002. Mineralogy of Tagish Lake: An ungrouped type 2 carbonaceous chondrite. *Meteorit. Planet. Sci.* **37**, 737–761.

Zolotov, M.Y., Mironenko, M.V., Shock, E.L., 2006. Thermodynamic constraints on fayalite formation on parent bodies of chondrites. *Meteoritics & Planetary Science* **41**, 1775–1796.

Zolotov, M.Y., Mironenko, M.V., 2007. Hydrogen chloride as a source of acid fluids in parent bodies of chondrites. *XXXVIII Lunar and Planet. Sci. Conf*. 2340.

Zolotov, M.Y., Shock, E.L., 2004. A model for low-temperature biogeochemistry of sulfur, carbon, and iron on Europa. *Journal of Geophysical Research: Planets* **109,** E6.

Zolotov, M.Y., 2007. An oceanic composition on early and today's Enceladus. *Geophysical Research Letters* **34**, 23.

Zolotov, M.Y., 2009. On the composition and differentiation of Ceres. *Icarus* **204**, 183–193.

Zolotov, M.Y., 2012. Aqueous fluid composition in CI chondritic materials: Chemical equilibrium assessments in closed systems. *Icarus* **220**, 713–729.

Zolotov, M.Y., 2014. Formation of brucite and cronstedtite-bearing mineral assemblages on Ceres. *Icarus* **228**, 13–26.

Zolotov, M.Y., 2016. Salty Ceres. *Nature Geoscience*, **9**, 476–477.

Zolotov, M.Y., 2017. Aqueous origins of bright salt deposits on Ceres. *Icarus* **296**, 289–304.

Zolotov, M.Y., 2020. The composition and structure of Ceres' interior. *Icarus*, **335**, 113404.

Zurfluh, F.J., Hofmann, B.A., Gnos, E., Eggenberger, U., 2013. “Sweating meteorites”—Water-soluble salts and temperature variation in ordinary chondrites and soil from the hot desert of Oman. *Meteoritics & Planetary Science* 48: 1958–1980.

Zurfluh, F.J., Hofmann, B.A., Gnos, E., Eggenberger, U., Jull, A.T., 2016. Weathering of ordinary chondrites from Oman: Correlation of weathering parameters with 14C terrestrial ages and a refined weathering scale. *Meteoritics & Planetary Science* 51: 1685–1700.